Single step production of nanoporous electrospun poly(ε-caprolactone) fibres

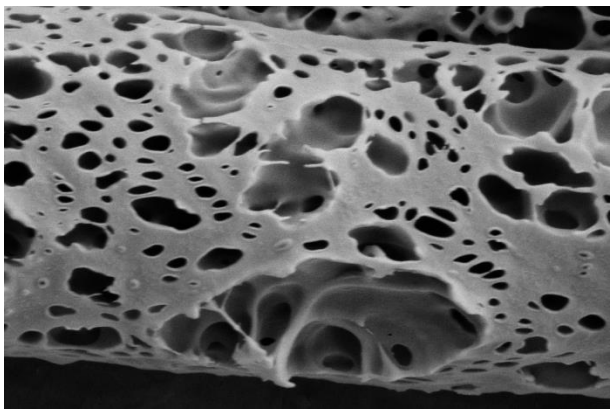

By

Konstantinos Alexandros Katsogiannis

A Doctoral Thesis Submitted as Partial Fullfiiment for The Award of Doctor of Philosophy of Loughborough University

March 2016

Contents

List of Figures

Chapter 2

Chapter 3

Chapter 4

Chapter 5

Chapter 6

Figure 6.5. Contour plots of relative pore covered area as a function of flow rate and voltage at (A) Minimum distance, (B) Maximum distance.

Figure 6.6. Contour plots of relative pore covered area as a function of flow rate and distance at (A) Minimum voltage, (B) Maximum voltage.

Figure 6.7. Contour plots of relative pore covered area as a function of voltage and distance at (A) Minimum flow rate, (B) Maximum flow rate.

Figure 6.8. Relative pore covered area as a function of individual parameters at (A) minimum values, (B) medium values, (C) maximum values.

Figure 6.9. Contour plots of fibre average diameter as a function of voltage and distance at (A) Minimum flow rate, (B) Maximum flow rate.

Figure 6.10. Contour plots of fibre average diameter as a function of flow rate and voltage at (A) Minimum distance, (B) Maximum distance.

Figure 6.11. Contour plots of fibre average diameter as a function of flow rate and distance at (A) Minimum voltage, (B) Maximum voltage.

Figure 6.12. Fibre average diameter as a function of individual parameters at (A) minimum values, (B) medium values, (C) maximum values.

List of Tables

Chapter 6

List of Abbreviations

BET	Brunauer–Emmett–Teller
CA	Cellulose Acetate
CF	Chloroform
DCM	Dichloromethane
DMSO	Dimethyl Sulfoxide
DMT	Derjaguin-Muller-Toporov
FA	Formic Acid
FESEM	Field Emission Scanning Electron Microscope
JKR	Johnson-Kendall-Roberts
MW	Molecular Weight
NIPS	Non-solvent Induced Phase Separation
PCL	Poly(ε-caprolactone)
PEO	Polyethylene oxide
PGA	Poly(glycolic acid)
PLA	Poly(lactic acid)
PLLA	Poly(L- lactic acid)
PMMA	Poly(methyl methacrylate)
PS	Polystyrene
PVA	Poly(vinyl alcohol)
PVP	Polyvinylpyrrolidone
RPCA	Relative Pore Covered Area
RSM	Response Surface Methodology
TBAB	Tetrabutylammonium Benzoate
TFA	Trifluoroacetic Acid
THF	Tetrahydrofuran
VIPS	Vapour Induced Phase Separation

Abstract

Nanoporous polymer fibres are currently attracting increasing interest due to their unique characteristics. Increased specific surface area, improved mechanical properties and improved cellular growth are amongst the advantages that set porous fibres as ideal candidates in applications like catalysis, separation and tissue engineering. This work explores the single step production of porous poly(ε-caprolactone) (PCL) fibres through combinative electrospinning and Non-solvent Induced Phase Separation (NIPS) technique. Theoretical models, based on three different contact models (Hertzian, DMT, JKR), correlating the fibrous network specific surface area to material properties (density, surface tension, Young's modulus, Poisson's ratio) and network physical properties (density) and geometrical characteristics (fibre radius, fibre aspect ratio, network thickness) were developed in order to calculate the surface area increase caused by pore induction. Experimental results proved that a specific surface area increase of up to 56% could be achieved, compared to networks composed of smooth surfaced fibres. The good solvent effect on electrospun fibre surface morphology and size was examined through experimental investigation of four different good solvent (chloroform, dichloromethane, tetrahydrofuran and formic acid) based solutions at various good/poor solvent ratios. Chloroform was proven to be the most suitable solvent for good /poor solvent ratios varying from 75-90% v/v, whereas alternative mechanisms leading to different fibre morphologies were identified, interpreted and discussed. Evaporation rate of the good solvent was identified as the key parameter of the process. Second order polynomial equations, derived from the experimental data, correlating the feed solution physical parameters (viscosity, conductivity, surface tension) to the fibre average diameter produced were developed and validated. Response surface methodology was implemented for the design and conduction of electrospinning experiments on a 12.5 % w/v Chloroform/DMSO solution 90/10 % v/v in order to determine the individual process parameters (spinning distance, applied voltage, solution flow rate) effect in fibre surface morphology and size. The increase in any of these parameters results in increase of both the fibre size and the tendency for pore generation, whereas applied voltage was the parameter with the strongest effect. Findings from this thesis expand the knowledge about both phenomena occurring during the production process and end product properties, and can be

used for the production of controlled morphology and size porous poly(ε-caprolactone) (PCL) fibres.

Keywords:

Electrospinning, Polycaprolactone, Porous, Surface Area, Phase Separation.

Loughborough University

Certificate of Originality
Thesis Access Conditions and Deposit Agreement

Students should consult the guidance notes on the electronic thesis deposit and the access conditions in the University's Code of Practice on Research Degree Programmes

Author.....Konstantinos Alexandros Katsogiannis.....

Title... Single step production of nanoporous electrospun poly(ε-caprolactone) fibres.....

I [Konstantinos Alexandros Katsogiannis], "the Depositor",
would like to deposit [Single step production of nanoporous electrospun poly(ε-caprolactone) fibres], hereafter referred to as the "Work", once it has successfully been examined in Loughborough University Institutional Repository

Status of access OPEN / RESTRICTED / CONFIDENTIAL

Moratorium Period.....years, ending...../.....20.....

Status of access approved by (CAPITALS):.....

Supervisor (Signature).....

School of.....AA CME.....

Author's Declaration *I confirm the following :*

CERTIFICATE OF ORIGINALITY
This is to certify that I am responsible for the work submitted in this thesis, that the original work is my own except as specified in acknowledgements or in footnotes, and that neither the thesis nor the original work therein has been submitted to this or any other institution for a degree

NON-EXCLUSIVE RIGHTS
The licence rights granted to Loughborough University Institutional Repository through this agreement are entirely non-exclusive and royalty free. I am free to publish the Work in its present version or future versions elsewhere. I agree that Loughborough University Institutional Repository administrators or any third party with whom Loughborough University Institutional Repository has an agreement to do so may, without changing content, convert the Work to any medium or format for the purpose of future preservation and accessibility.

DEPOSIT IN LOUGHBOROUGH UNIVERSITY INSTITUTIONAL REPOSITORY
I understand that open access work deposited in Loughborough University Institutional Repository will be accessible to a wide variety of people and institutions - including automated agents - via the World Wide Web. An electronic copy of my thesis may also be included in the British Library Electronic Theses On-line System (EThOS). I understand that once the Work is deposited, a citation to the Work will always remain visible. Removal of the Work can be made after discussion with Loughborough University Institutional Repository, who shall make best efforts to ensure removal of the Work from any third party with whom Loughborough University Institutional Repository has an agreement. Restricted or Confidential access material will not be available on the World Wide Web until the moratorium period has expired.

- That I am the author of the Work and have the authority to make this agreement and to hereby give Loughborough University Institutional Repository administrators the right to make available the Work in the way described above.

- That I have exercised reasonable care to ensure that the Work is original, and does not to the best of my knowledge break any UK law or infringe any third party's copyright or other Intellectual Property Right. I have read the University's guidance on third party copyright material in theses.
- The administrators of Loughborough University Institutional Repository do not hold any obligation to take legal action on behalf of the Depositor, or other rights holders, in the event of breach of Intellectual Property Rights, or any other right, in the material deposited.

*The statement below shall apply to **ALL** copies:*

This copy has been supplied on the understanding that it is copyright material and that no quotation from the thesis may be published without proper acknowledgement.

Restricted/confidential work: All access and any copying shall be strictly subject to written permission from the University Dean of School and any external sponsor, if any.

Author's signature.....Date 30/3/2016

user's declaration: for signature during any Moratorium period (Not Open work): ***I undertake to uphold the above conditions:***			
Date	Name (CAPITALS)	Signature	Address

Acknowledgements

The completion of this work wouldn’t have been possible without the help of several individuals, to whom I would to express my gratitude. First of all, I would like to thank my supervisors, Dr Stella Georgiadou and Dr Goran Vladisavljevic, for providing me the opportunity to work in such a supporting environment. I am no less indebted to the members of staff Sean Creedon, Tony Eyre, Monika Pietrzak and Terry Neal for their invaluable help in the experimental part of the project. Special mention goes to Dr Ramin Rahmani for his guidance through the theoretical part of the project. I would also like to thank my friends Dinos, Vasilis, Giorgos, Ilias, Ilia, Dimitris and Apostolis, who, besides their friendship, contributed to different part of this study. Last but not least, a huge thanks to my family for their endless love and support throughout this work.

List of Publications

Parts of the work presented in this thesis have been published in peer-reviewed journals.

Chapter 4 is based on the published journal article

Katsogiannis K.A.G, Vladisavljević G.T, Georgiadou S, Ramin Rahmani. Assessing the Increase in Specific Surface Area for Electrospun Fibrous Network due to Pore Induction. *ACS Applied Materials & Interfaces* **2016**, DOI**:** 10.1021/acsami.6b09627.

Chapter 5 is based on the published journal article

Katsogiannis K.A.G, Vladisavljević G.T, Georgiadou S. Production of porous electrospun PCL fibres by phase separation. *European Polymer Journal* **2015**, 69, 284-295.

Chapter 6 is based on the published journal article

Katsogiannis K.A.G, Vladisavljević G.T, Georgiadou S. Porous Electrospun Polycaprolactone Fibers: Effect of Process Parameters. *Journal of Polymer Science, Part B: Polymer Physics* **2016**, 54, 1878-1888.

1. Introduction

1.1. Introduction

Starting from the late 20th century, the demand for continuous improvement in the polymer materials field seems to have found the ideal ally in nanotechnology. The dimensions of the materials involved in nanotechnology are usually up to 100nm. At that scale, the materials demonstrate properties unachievable by materials at the macro scale. Electrospinning is a perfect example of the nanotechnology advances. Even though it has been patented in 1934 (Formhals, 1934), it has attracted great interest during the 90s after the work by Doshi and Reneker (1995), demonstrating its successful implementation in various polymer solutions. Electrospinning provides a simple method for the production of polymer fibres with diameters down to 1.6nm (Huang et al., 2006).

The electrospinning capability, however, is not limited to the production of small diameter polymer fibres. Through method variations several special fibre morphologies such as aligned (Kiselev P and Rosell-Llompart, 2012), hollow (Li and Xia, 2004), porous (Yu et al., 2010), etc. have been produced. The latter especially are of great interest due to the number of properties improved by pore introduction into electrospun fibres. Fibrous network specific surface area increase (Casper et al., 2004), improvement of fibre mechanical properties (Kim et al., 2005) and enhancement of cellular growth on scaffolds in tissue engineering (Moroni et al., 2006, Yamaguchi et al., 2004) are amongst the main advantages derived from nanoporosity induction.

Combinations of phase separation and electrospinning are amongst the most effective methods that have been proposed for pore formation on the surface of electrospun fibres (Nayani et al., 2012). An understudied version of that technique is Non-solvent Induced Phase Separation (NIPS), where the addition of non-solvent takes place prior to electrospinning. Previous studies (Qi et al., 2009, Lubasova and Martinova, 2011, Wei et al., 2013, Laiva et al., 2014) have verified the success of the technique. However, given the complexity and the number of factors affecting the overall process, the effect of a number of factors has yet to be explored. Acquiring knowledge on issues like correlation of electrospun mat specific surface area to easily measurable properties, the quantification of its increase due to pore induction, the identification of suitable solvent systems for the process and, finally, the

investigation of the electrospinning process parameters' effect on the size and morphology of the fibres produced, can enhance control over the process and, subsequently, improve both, the end product quality and the simplicity of its production.

1.2. Thesis objectives

The major objectives of the thesis can be summarised as follows:

1.2.1 Chapter 4

- Development of theoretical models predicting electrospun network specific surface area as a function of material properties (density, surface tension, Young's modulus, Poisson's ratio) and network physical properties (density) and geometrical characteristics (fibre radius, fibre aspect ratio, network thickness).
- Theoretical model validation through comparison of predicted values to experimentally obtained values for networks composed of non-porous fibres.
- Determination of the process efficiency through comparison of theoretically predicted surface area of non-porous network to experimentally measured surface area of porous network.

1.2.2 Chapter 5

- Investigation of the good solvent and good/poor solvent ratio effect on the combinative electrospinning- Non-solvent Induced Phase Separation (NIPS) process.
- Elucidation of alternative mechanisms leading to fibre morphologies other than porous.
- Setting criteria for the production of porous, bead free polycaprolactone fibres.
- Identification of suitable ternary system (solvent, non-solvent, polymer) region suitable for the production of porous, bead free fibres.

1.2.3 Chapter 6

- Investigation of individual parameter effect on electrospun fibre size and morphology.
- Comparison between individual parameter effects in order to determine the most influential.
- Overall optimization of the process.

1.3. Thesis methodology

During the course of this project the diverse nature of the research questions that had to be answered dictated the implementation of different methodologies.

In Chapter 4, it was decided that the appropriate method for the quantification of the specific area increase following the pore induction would be the development and subsequent validation of theoretical models, correlating the network specific area to the geometrical and physical characteristics of the smooth surface fibres composing it. After the selection of the most accurate model, the comparison of the experimentally measured specific surface area of networks composed by porous fibres to that theoretically predicted for smooth surface fibres can facilitate the quantification of the pore induction efficiency.

In Chapter 5, a different approach was implemented. One-factor-at-the-time methodology was considered suitable to correlate the initial solution physical properties to the fibre morphology and size. Polymer solutions, based on four different good solvents (Chloroform, Dichloromethane, THF, Formic Acid), under several good/poor solvent ratios were prepared, electrospun and analysed. The main reason for this selection was the inability to simultaneously control all the initial solution physical properties.

In Chapter 6, Response Surface Methodology (RSM) was implemented on the best performing ternary system (selected from the results of Chapter 5) for the optimization of the fibre surface morphology and size, in terms of the electrospinning process parameters. The limitations encountered in Chapter 5 were not applicable in

that case, since electrospinning process parameters are continuous variables and are not interrelated.

2.Literature Review

2.1. Introduction

A critical review of the work that has been previously published in the field of production of nanoporous polymer fibres is presented in this chapter. Fibre formation is based on electrosponning, thus, initially, a general description of the phenomena occurring throughout its duration is provided. That facilitates the understanding of the analysis of individual parameter effect on the process and provides the necessary tools for interpretation of contradicting results often reported in the literature. Different research methodologies for the investigation of the individual parameter effect are presented and compared. Subsequently, the advantages and disadvantages of existing pore generating techniques are analysed. Finally, the chapter reviews the main gaps in the current literature.

2.2. Electrospinning process

Experimentally, a typical electrospinning set up consists of a high voltage power supply, a capillary/spinneret through which the solution is forced, an electrode connecting the above two and a grounded collector. A polymer solution is charged at the capillary, and, when the electrostatic forces prevail over the surface tension of the solution, a jet is ejected (**Figure 2.1**).

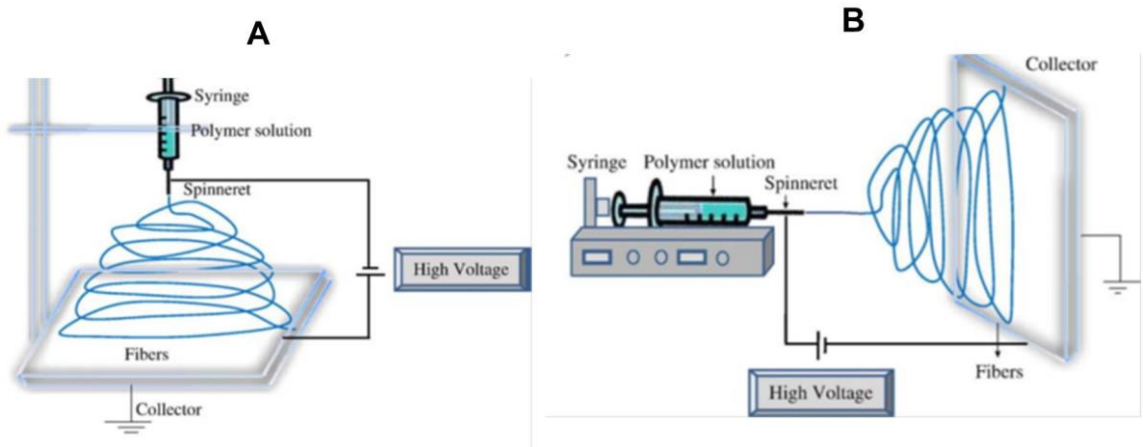

Figure 2.1. Typical electrospinning set up. (A) vertical set up, (B) horizontal set up (Bhardwaj and Kundu 2010).

During its trajectory towards the collector, the macromolecular chain entanglements form the fibrous polymer structures which are simultaneously stretched due to the repulsive forces of the like charges. The solvent evaporation, occurring at the same time, leads to the deposit of solid fibres on the collector.

Even though the process seems simple at a first glance, the several phenomena occurring simultaneously throughout its duration increase its complexity. Wannatong et al. (2004) identified four different forces acting within the electrospinning jet.

Viscoelastic forces within the electrospinning jet, which oppose to the jet stretching.

Surface tension of the electrospinning jet, having similar effect to the viscoelastic forces.

Gravitational force, whose effect depends on the experimental set-up (vertical or horizontal).

Electrostatic force, applied within the electrospinning jet and causing its stretching.

On top of that, phenomena like solvent evaporation, polymer chain diffusion within the jet and heat transfer throughout the jet increase the overall process complexity.

Deeper understanding of the process can be achieved by its the division into stages. There are four major stages in electrospinning, the jet initiation, the jet thinning, the instability region and the solidification region (Garg and Bowlin, 2011).

Jet initiation is the first stage of electrospinning. Droplets, formed at the tip of a capillary adopt a spherical shape, due to the surface tension. However, the application of an electrical field can induce instability to the droplet. When the electrical forces, caused by the repulsion of like charges, overcome the forces due to the surface tension of the polymer solution, a jet is ejected. Taylor (1969) calculated that critical value (V_c) as:

$$V_c^2 = 4\left(\frac{H^2}{L^2}\right)\left(ln\frac{2L}{R} - 1.5\right)(0.117\pi R\gamma) \quad (2.1)$$

Where H is the air-gap distance, L and R are the length and the radius of the capillary, respectively, and γ is the surface tension of the liquid.

Taylor also determined that the electrospinning droplet forms a cone (which was named after him) with half angle of 49.3^{o}, in order to achieve equilibrium between electrostatic forces and surface tension. Ejection of a jet follows the cone formation.

Jet thinning is the second stage of electrospinning. After its ejection the electrospinning jet forms a straight tapered segment. At that stage, the repulsive coulombic forces between the like charges and solvent evaporation result in the decreasing of the jet size. The charges at that stage are accumulated at the jet surface (Reneker and Yarin, 2008). Assuming that the charges on the jet and its density remain constant, the decrease of the jet surface area per unit mass increases the repulsive forces caused by the homonymous charges. When these forces become strong enough to cause instability within jet, bending of the jet is observed and the third stage of the process initiates.

The *instability region* is the stage where the biggest part of the jet size reduction takes place. Three types of instabilities might appear at that stage. The first is the axisymmetric Rayleigh instability that is caused by the jet surface tension and tends to minimize the surface area of the jet by its breaking to droplets. The second axisymmetric instability is developed due to the interaction of jet electrical charges with the field. The third instability is non-axisymmetric, known as whipping instability (Shin et al., 2001), and is mainly responsible for the size reduction of the jet. Its occurrence is caused by the interaction of dipoles formed within the jet with the external field, which cause torque, and subsequently bending to the jet. The trajectory of the jet at that stage changes, since the initially linear path is forced to coil into constantly increasing diameter loops. A typical example of the trajectory of an electrospinning jet is shown in **Figure 2.2**.

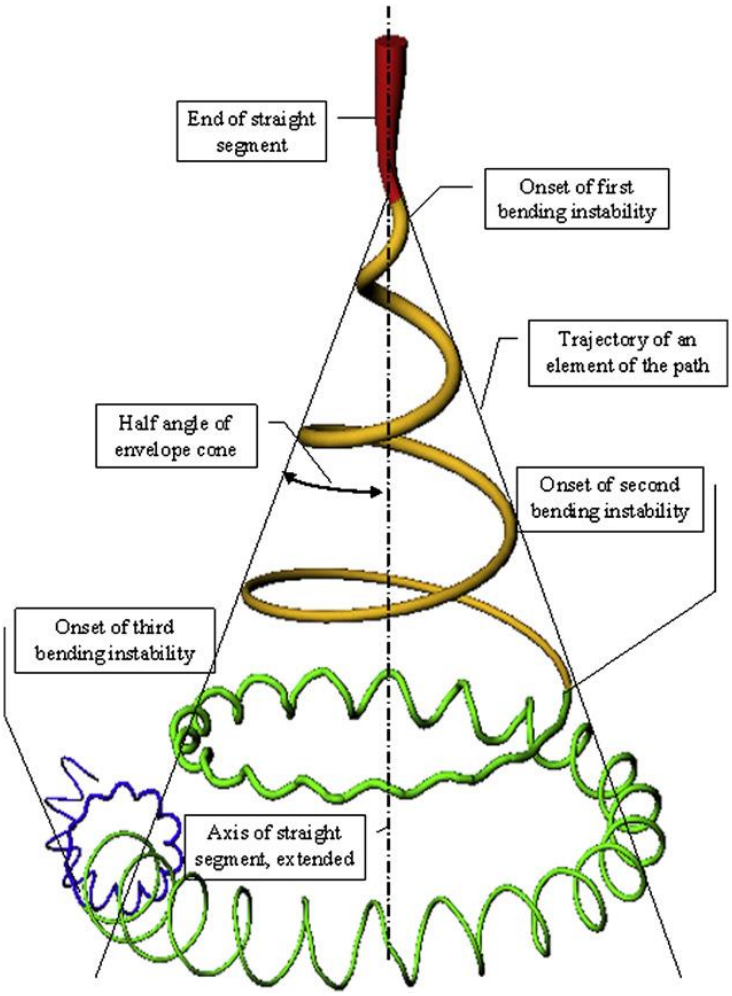

Figure 2.2. Bending instabilities within electrospinning jet (Reneker and Yarin, 2008).

Solidification of the jet is the last stage of electrospinning process. Ideally, the solidification should occur after the third stage of electrospinning, however, it is possible for it to take place at any stage of the process. Parameters that affect the evaporation rate of the solvent during the process, such as its volatility and the available time (through spinning distance), determine the point of the initiation of that stage. The timing of that stage can determine the fibre morphology and/or size, since premature solidification can result in bead presence on electrospun fibres or production of fibres with thick diameters.

2.3. Parameters affecting electrospinning

One's perception of the electrospinning process can be further enriched by the analysis of the effect of individual parameters on it. Prior to that, however, one should bear in mind that the complexity of the process, the number of phenomena occurring simultaneously during the process, the different order of magnitude of individual parameter changes and the interaction between individual parameters can cause misled conclusions about the individual parameter effect on the process.

Individual parameters affecting electrospinning can be classified into three categories, as shown in **Figure 2.3**.

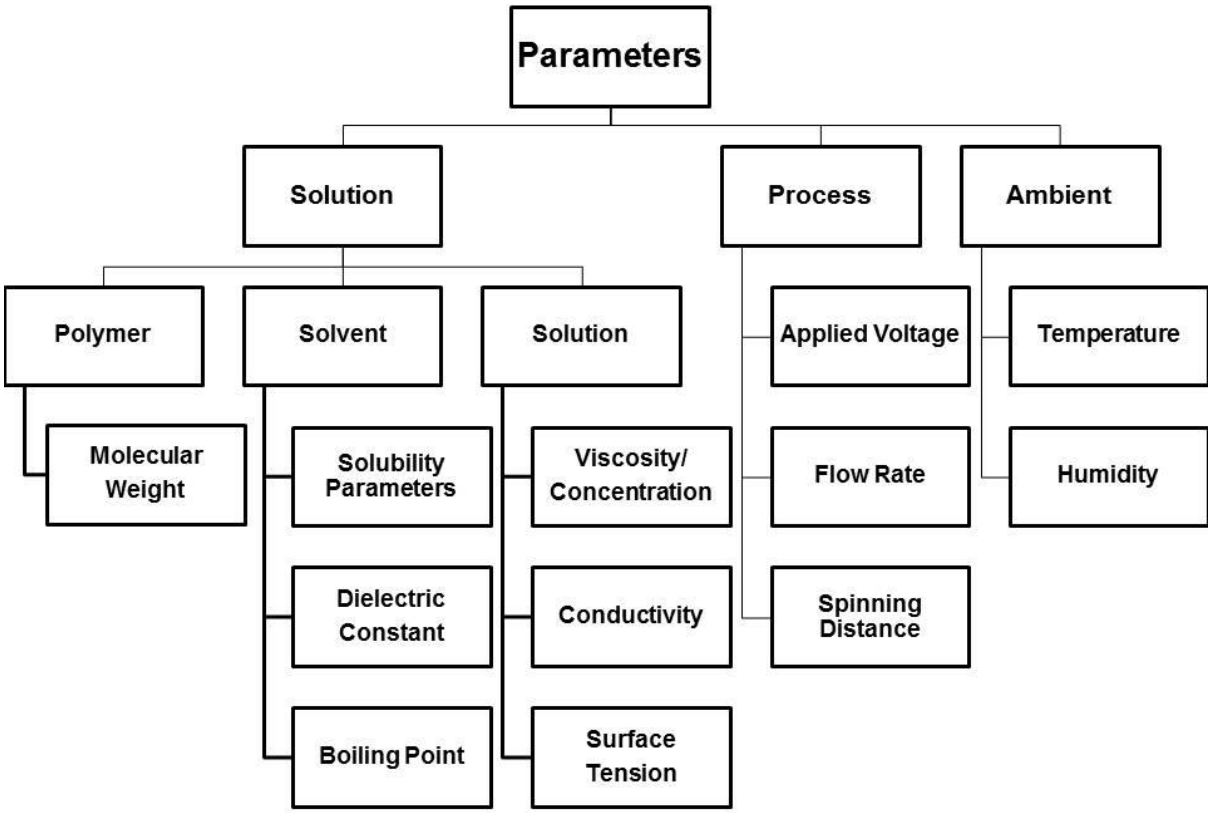

Figure 2.3. Classification of parameters affecting electrospinning.

Solution parameters are the first category of parameters affecting electrospinning. The process is affected by both, individual components' properties and system properties. Polymer Molecular Weight (MW) and solvent dielectric constant and

boiling point are the individual component properties that mainly affect the process, whereas, solution concentration/viscosity, conductivity and surface tension are the system properties that affect the process.

Process parameters are the second category of parameters affecting electrospinning. The category includes the operating variables and the main individual parameters are applied voltage, spinning distance and solution flow rate.

Ambient parameters are the third category of parameters affecting electrospinning. The category includes the environmental conditions under which the process takes place. Ambient temperature and humidity are the main individual parameters in this category.

It should be noted that the electrospinning process is not exclusively affected by the above mentioned parameters. Other parameters, such as the collector set up (Pant et al., 2011, Hsia et al., 2012), the inner capillary diameter (Sencadas et al., 2012), etc can affect the outcome of the process as well. Nonetheless, they are not further analysed, since their effect was not investigated in this study.

2.3.1. Solution parameters

2.3.1.1. Solution concentration/viscosity

Solution concentration and viscosity are often examined together due to their proportional relationship. Solution concentration is one of the most important parameters of electrospinning, since it determines the number of polymer chain entanglements in the solution, and subsequently, whether fibre formation will occur.

Gupta et al. (2005) used the critical chain overlap concentration, C^*, for the investigation of poly(methyl methacrylate) (PMMA) concentration effect in electrospun fibre morphology and size. C^* is the point where no difference is observed between the concentration within a macromolecular chain and the polymer solution and can be defined by equation (2.2):

$$C^* = \frac{3MW}{4\pi(R^2)^{3/2}N_{av}} \quad (2.2)$$

Where MW is the Molecular Weight of the polymer, R is the square root of the distance between the ends of the macromolecular chain and N_{av} is the Avogadro number.

They classified the electrospun polymer solutions into three categories based on the value of C/ C^* (**Figure 2.4**). *Dilute*, where $1<C/ C^*<3$, *Semidilute Unentangled*, where $3<C/ C^*<6$, and *Semidilute Entangled*, where $C/ C^*>6$.

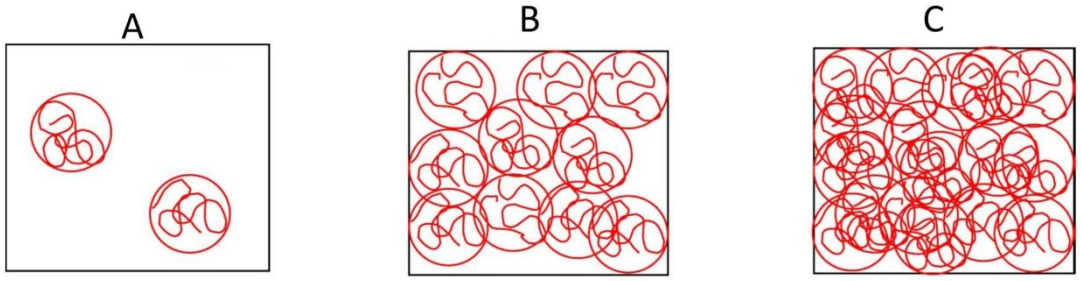

Figure 2.4. Classification of solution regimes based on concentration (A) Dilute, (B) Semidilute Unentangled, (C) Semidilute Entangled (Gupta et al., 2005).

They observed that the use of dilute solutions resulted in the production of droplets, the use of semidilute unentangled solutions resulted in the production of fibres with beads and the use of of semidilute entangled solutions resulted in the production of bead free fibres. The results were attributed to the number of chain entanglements. At the dilute region, the number of entangled polymer chains is too low to oppose the Rayleigh instability and formation of droplets is observed. Gradual increase of solution concentration, and subsequently C/ C^*, increases the tolerance to the instability, and, therefore, fibre formation is observed.

The general conclusions reported from Gupta et al. (2005) are in agreement with findings from several other studies. Too dilute solutions tend to generate droplets rather than fibres (Ojha et al., 2008). At low concentrations formation of beads is observed (Kanani and Bahrami, 2011). When the concentration increases the number and size of the beads is reduced, until their complete elimination (Liu et al., 2008, Kanani and Bahrami, 2011). Above that point the solution concentration or viscosity and the fibre average diameter are proportional (Beachley and Wen, 2009,

Deitzel et al., 2001, Demir et al., 2002). A summary of all the above is presented in **Figure 2.5**.

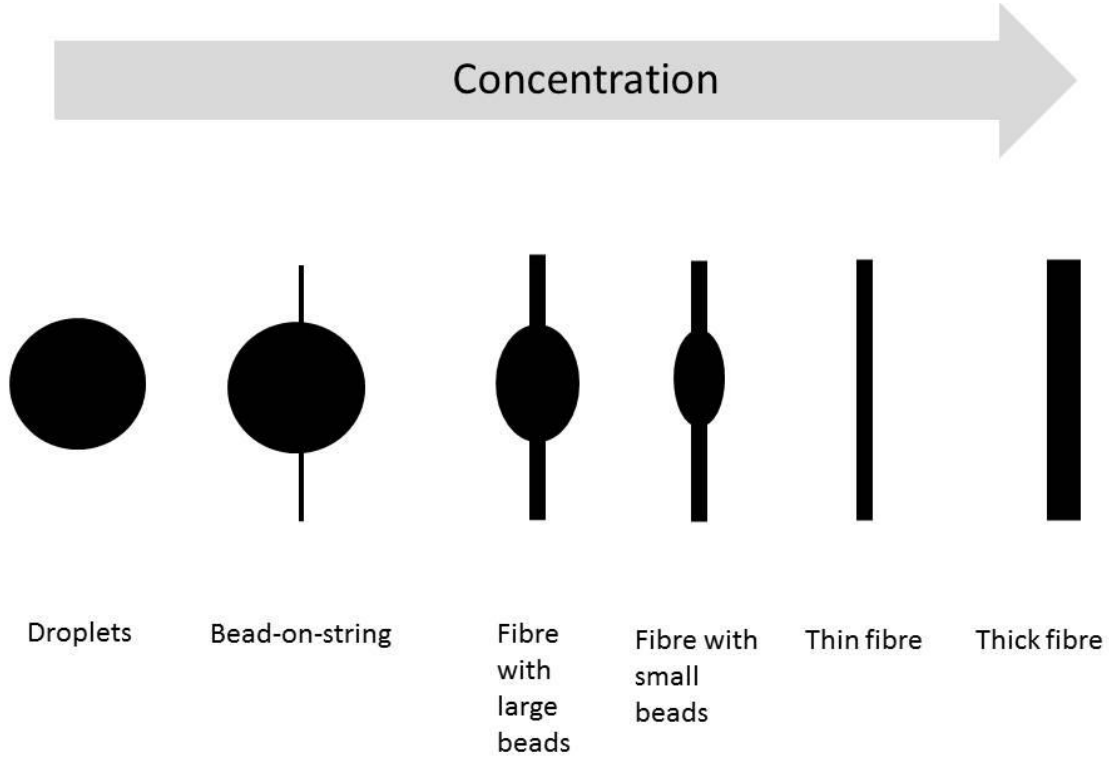

Figure 2.5. Morphological evolution of electrospun fibres under increasing solution concentration.

2.3.1.2. Polymer Molecular Weight

The polymer Molecular Weight (MW) has an effect similar to the solution concentration on electrospinning process. Both parameters determine the macromolecular chain entanglements through different means; the former through the length of the chains and the latter through their number. Hence, a threshold exists, below which, a given concentration polymer solution cannot be electrospun. Above that, the fibre morphology follows the same pattern with increasing MW as with increasing solution concentration (**Figure 2.5)**.

The experimental confirmation of the above has been reported for several polymers, such as polyamide-6 (Mit-uppatham et al., 2004), polycaprolactone (Lavielle et al.,

2013), chitosan (Geng et al., 2005), nylon-6 (Ojha et al., 2007), polyvinylalcohol (Koski et al., 2004).

Gupta et al. (2005) reported similar results for different MW PMMA solutions. In their work, however, their research was expanded to the investigation of the polymer MW distribution effect in the process, as well. They proved that the use of narrow MW distribution polymers can lower the solution concentration necessary for fibre formation. Their theory for their findings is that the presence of short polymer chains within the wide MW distribution polymers can decrease the strength of the chain entanglements and cause their premature breaking within the electrospinning jet.

2.3.1.3. Solution conductivity

Solution conductivity plays an important role in the electrospinning process. The initiation of the process is dependent on solution conductivity, since zero values of the latter would result in no transfer of the electrical charge from the power supply to the solution and, subsequently, no initiation of the process. Besides that, high conductivity values generally facilitate the smooth occurrence of the process and the production of low diameter fibres, since the effective charge distribution within electrospinning jet can prevent bead formation mechanisms and results in more intense stretching of the jet. The latter has been quantified by Baumgarden (1971), whose theoretical and experimental work showed that the cube root of the conductivity is inversely related to the jet radius. Nonetheless, cases where high values of conductivity resulted in the increase of the fibres average diameter have also been reported (Heikkila and Harlin, 2009). The authors attributed that to the increased mass flow rate of the electrospinning jet.

Experimental investigation of conductivity effect in the process can be misleading, since, an attempt to control it can affect other solution parameters as well. Thus, studies where the conductivity is increased by addition of more conductive solvents (Kanani and Bahrami, 2011) or ionic surfactants (Lin et al., 2004) cannot be used for determination of conductivity effect in the process. The best method that has been proposed so far is the use of inorganic salts. Salts, when dissolved in a liquid, dissociate into electrically charged cations and anions. That increases the

conductivity of the solution without significant effect on the other properties of the solution, therefore the observed changes of the fibres produced can be attributed exclusively to conductivity changes. Arayanarakul et al. (2006) investigated the addition of several inorganic salts in the electrospinning of poly(ethylene oxide). The salt addition didn't affect solution viscosity or surface tension as drastically as it did conductivity. The study proved that conductivity increase can eliminate the beads observed at fibres produced by the control solution. Similar results have been reported by other researchers (Liu et al., 2008).

A different perspective, however, should also be considered when investigating the solution conductivity effect in the electrospinning process. Conductivity is the parameter that provides the widest range of values into which it can be set. For example, addition of salt can increase the solution conductivity up to 1000 times (Qin et al., 2007, Moghe et al., 2009). No other electrospinning parameter can be changed over such a wide range. Hence, the possibility that the solution conductivity effect in the process is being magnified by the order of magnitude over which it is set should also be taken into account.

2.3.1.4. Solution surface tension

Generally, high surface tension is an undesirable property for electrospinning solutions, since it opposes both, jet initiation and jet stretching. As seen in equation (2.1) the square root of the critical voltage is proportional to solution surface tension. That means that high surface tension solutions require higher voltage for initiation of electrospinning. Theoretical and experimental work by Fridrikh et al. (2003) predicts that the terminal jet radius, and subsequently the fibre diameter, can be calculated according to equation (2.3):

$$\mathrm{d} = c^{\frac{1}{2}}\left(\gamma\varepsilon\frac{\mathrm{Q}^2}{\mathrm{I}^2}\frac{2}{\pi(2lnx-3)}\right)^{\frac{1}{3}} \quad (2.3)$$

where d is the fibre diameter, c is the solution concentration, γ is the surface tension, ε is the dielectric permittivity, Q is the flow rate, I is the electric current, R is the

radius of curvature and $\chi \sim R/h$ is the dimensionless wavelength of the instability responsible for the normal displacements, which is used to characterize the jet.

In addition to the discussion above, the Rayleigh instability, caused by high solution surface tension, tends to minimize the jet surface area by forcing it to take up a spherical shape. That can result in bead-on-string morphology in the fibres (Fong et al., 1999). Deitzel et al. (2001) concluded that for given process parameters, solution viscosity and surface tension forces within the electrospinning jet determine the operating window.

Similarly to the conductivity effect, it is not easy to accurately experimentally validate the effect of surface tension on electrospinning, since the additives used for surface tension variation can cause changes in other solution properties, such as viscosity and/or conductivity. For example, the use of ionic surfactants, besides lowering of surface tension, simultaneously increases the conductivity of the solutions (Lin et al., 2004, Seo et al., 2009). That obstacle can be surpassed by the addition of non-ionic surfactants in the initial solution. Small amounts of surfactant usually do not significantly alter the viscosity and the non-ionic nature of the surfactant prevents conductivity changes. Yao et al. (2003) were able to electrospin hydrolysed poly(vinyl alcohol) due to the use of the non-ionic surfactant Triton X-100. The surfactant lowered the surface tension of the solution and subsequently, the critical voltage was lowered as well. Bead number and size reduction of electrospun polyvinylidene fluoride fibres was achieved by using the same surfactant by Zheng (2014). Fibre diameter reduction was reported by Zeng et al. (2003) as a result of non-ionic surfactant additions in electrospun poly(l-lactic acid) solutions.

2.3.1.5. Solvent solubility parameters, dielectric constant and boiling point

Given that electrospinning usually involves processing of polymer solutions, the first step of the process is the selection of a suitable solvent/solvent. Even though the Hildebrand solubility parameter (δ) can be used for the prediction of the polymer solubility in a given solvent, in the literature it is more common to follow the methodology proposed by Hansen (1967) who further subdivided the Hildebrand

solubility parameter into hydrogen bonding, polar and dispersive components, as shown in equation (2.4):

$$(\delta_T)^2 = (\delta_H)^2 + (\delta_D)^2 + (\delta_P)^2 (2.4)$$

where subscripts T, H, D and P represent the total, hydrogen bonding, dispersive and polar solubility parameter respectively.

Based on the principle that like dissolves like, the closer the solubility parameter of the polymer to the solubility parameter of the solvent the more likely it is for dissolution to take place. Using Hansen solubility parameters has facilitated the complete solubility mapping and successful prediction of the solubility of various polymers, such as polymethylsilsesquioxane (Luo et al., 2010) and polycaprolactone (Luo et al., 2012). It should be noted that this methodology can also be implemented for solvent mixtures (Haas et al., 2010).

Similarly to the investigation of solution surface tension or conductivity effect in the electrospinning process, the lack of simultaneous control of the solvent properties hinders the isolation and determination of individual property effect in the process. In the case of solvent properties, dielectric constant and boiling point in particular, the experimental validation of the theoretical predictions is more challenging, since the use of additives, such as salts or non-ionic surfactants, is of no use. Nonetheless, some general conclusions can be drawn from the current literature.

Dielectric constant, or relative permittivity, is a measure of the material response to the applied electric field, therefore, solvents with high dielectric constant are generally considered to favour the smooth occurrence of the process and the production of fibres with low diameters. Quite commonly, the use of solvents with low dielectric constant is accompanied by bead presence on the fibres. Examples of this include the use of tetrahydrofuran (dielectric constant 7.6) for electrospinning of polystyrene (Lee et al., 2003) and chloroform (dielectric constant 4.8) for electrospinning of polycaprolactone (Hsu and Shivkumar, 2003). For both cases, the addition of dimethylformamide (dielectric constant 36.7) in the feed solution resulted in the elimination of beads in the fibres. In addition to that, an inversely proportional relationship of solvent dielectric constant to the fibre diameter in electrospinning of

polymethylsilsesquioxane has been reported (Luo et al., 2010), as shown in **Figure 2.6**.

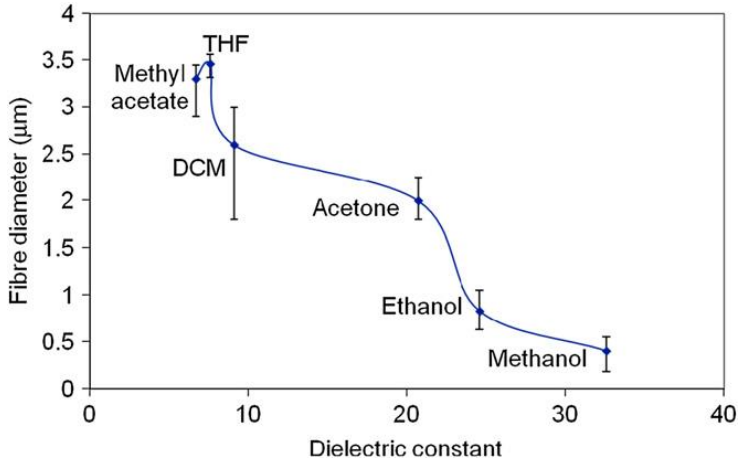

Figure 2.6. Relationship between solvent dielectric constant and fibre diameter in electrospinning of polymethylsilsesquioxane (Luo et al., 2010).

However, even though the above mentioned studies support the theoretical predictions, they cannot prove them, since not all the other solution properties were the same. Up to date, the most accurate work in that field was presented by Luo et al. (2012). They were able to investigate the solvent dielectric constant effect on the fibre size, by electrospinning 7% w/w polycaprolactone solutions in two solvents (acetic acid and formic acid) with comparable properties. Acetic acid solutions (dielectric constant 6.2 at 20 ^{o}C) resulted in the production of droplets, whereas, formic acid solutions (dielectric constant 58 at 20 ^{o}C) resulted in the production of fibres. In addition to that, the use of excess amount of acetic acid in binary solvent systems resulted in bead formation, whereas the use of reverse ratios diminished bead presence, thus, proving the theoretical predictions.

Solvent boiling point is of high importance in electrospinning. The significance of its role in the process is highlighted taking into account that electrospinning is a dynamic process and that the rate of the changes occurring within the electrospinning jet is mainly determined by the evaporation rate of the solvent. During electrospinning the feed solution undergoes composition changes due to solvent loss and difference in the driving force of those changes can lead to different process outcomes. Theoretically, solvent boiling point can affect the process

outcome through several mechanisms. First of all, Wannatong et al. (2004) reported an inversely proportional relationship between electrospun polystyrene fibre diameter and solvent boiling. Even though the feed solutions had the same concentration, the higher evaporation rate of the low boiling point solvent results in an apparent increased polymer concentration in the electrospinning jet, compared to a higher boiling point solution. As discussed earlier, higher solution concentration results in production of thicker fibres, thus, the results presented by Wannatong et al. can be interpreted. Special fibre morphologies have been produced based on solvent boiling point. Koombhongse et al. (2001) reported the production of fibres with ribbon cross sections. They attributed that to the formation, and subsequent collapse, of a solid skin on the surface of the electrospinning jet. The skin formation was caused by the rapid solvent evaporation. Finally, solvent boiling point can be a key characteristic in pore formation through phase separation mechanisms, as will be discussed later in the chapter.

2.3.2. Process parameters

2.3.2.1. Applied voltage

Voltage application is necessary for the occurrence of electrospinning process. As stated in Equation (2.1), a minimum voltage is required for the forces applied from the electric field to overcome the surface tension and, subsequently, the process initiation. Given that higher voltage values result in an increase of the electrical forces within the electrospinning jet, an inversely proportional relationship between voltage and fibre diameter can be expected. That has been experimentally verified in several studies (Geng et al., 2006, Beachley and Wen, 2009, Sencadas et al., 2012). However, a hindering effect of voltage to the electrospinning process has also been reported. Deitzel et al (2001) investigated the voltage effect in the electrospinning of aqueous PEO solutions and reported that, when a certain limit was exceeded, formation of beads was observed. The authors attributed those results to changes of the shape of the Taylor cone at the needle tip. Those changes can cause an excessive solution mass flow and, consequently, induce increased instability in the jet. The same explanation was provided by Zhang et al. (2005), who observed a fibre diameter increase as a result of increased voltage in electrospinning of aqueous

poly(vinyl alcohol) (PVA) solutions. The above observations and interpretation was also reported by Ojha et al. (2008), who investigated the voltage effect for three different MW nylon-6 solutions. For the low MW and the medium MW the increase of voltage from 10 to 20 kV assisted the electrospinning process, since the final product turned from droplets to beaded fibres, while for the high MW solution the same increase resulted in an increase of the fibre diameter.

2.3.2.2. Flow rate

The investigation of solution flow rate effect in electrospinning process has mainly focused in the higher value region, since flow rate is proportional to the amount of fibres that can be collected. Nonetheless, increase of flow rate can cause various phenomena and a wide range of fibre morphologies, depending on the values of the other parameters in the investigated system. Quite commonly, high flow rate can cause change of the shape of the Taylor cone (Zargham et al., 2012). That can cause jet instabilities and, subsequently, bead formation on the electrospun fibres (Zhang et al., 2005, Zuo et al., 2005). However, if the investigated values are able to sustain the shape of the Taylor cone, the increased flow rate will result in an increased amount of polymer within the electrospinning jet. Thus, the increased number of chain entanglements can lead to the production of fibres with increased diameters (Ojha et al., 2008, Park et al., 2008). The excessive amount of solvent used in high flow rate regimes requires more time to completely dry, and if that is not provided merging of the fibres might be observed (Chowdhury and Stylios, 2010). The significance of the setting of the other parameters is highlighted by studies by Sencandas et al. (2011) and Beachley and Wen (2009). They both reported that increased flow rate did not have a significant effect on electrospun chitosan and polycaprolactone fibres respectively. Sencandas et al. attributed that to the use of volatile solvents (dichloromethane and trifluoroacetic acid), which counter-balance the increased flow rate effect. The same explanation could be adapted for the case of Beachley and Wen, who also used volatile solvents (dichloromethane and methanol).

2.3.2.3. Spinning distance

The spinning distance determines the available time for the completion of the process. Thus, longer spinning distances result in an increased time of stretching of the electrospinning jet, and, therefore, production of fibres with smaller diameters(Heikkila and Harlin, 2009, Chowdhury and Stylios, 2010) or reduction of beads (Ojha et al 2008) can be observed. However, cases where spinning distance had no significant effect in the process have also been reported (Zhang et al., 2005). The authors concluded that the fibre solidification process had already been completed at the shorter distance, thus, the longer distance could not make any difference in the process. More interesting, though, are the studies where the increase of distance resulted in an increase of the fibre diameter (Park et al., 2008, Sencandas et al., 2011). In the first study the authors attributed the results to the weakening of the electric field due to the longer distance. In the second study the increased fibre diameter distribution observed at the longer distance experiments lead the authors to the conclusion that secondary jets were ejected from the primary jet surface, due to accumulation of local charge.

2.3.3. Ambient parameters

2.3.3.1. Temperature

Variations in, either ambient or solution temperature, can enhance potentially contradicting phenomena, thus making temperature the parameter with the least predictable effect. On one hand, it is well established that an increase of temperature results in a decrease of solution viscosity. On the other hand, a temperature increase causes the increase of the solvent evaporation rate, which indirectly causes the increase of the solution viscosity. An indication of the irregularities in the temperature effect is discussed in the work by De Vrieze et al. (2009). The authors investigated the effect of temperature on electrospinning of two different polymer solutions, cellulose acetate (CA) and poly(vinylpyrrolidone) (PVP), at various conditions. In both cases, an increase of the fibre diameter was observed when the temperature was elevated from 283 to 293 K, whereas, a further increase of temperature to 303 K resulted a decrease in fibre diameter. The authors attributed

that trend to the prevalence of the viscosity increase effect in the region from 283 to 293 K and the opposite effect in the region from 293 to 303 K. The ambient temperature cannot only affect the fibre size, but the morphology as well as shown by Amiraliyan et al. (2008). The authors reported the production of fibres with ribbon cross sections when the experiments were conducted at elevated temperature. The fibre formation mechanism was discussed earlier and that proves that the same outcome (ribbon fibres) can be achieved through different means (use of volatile solvent or use of high temperature). Mit-uppatham et al. (2004) investigated the solution temperature effect rather than the ambient temperature for polyamide-6 fibres. The authors reported an inversely proportional relationship between solution temperature and fibre diameter, which was attributed to the solution viscosity decrease at higher temperatures.

2.3.3.2. Humidity

Humidity can affect electrospinning process through different mechanisms. It has been extensively used for pore generation, which will be further analysed later in this chapter. The humidity effect in the process depends highly on the other parameters of the investigated system. De Vrieze et al. (2009) investigated the effect of humidity on two different polymer solutions, CA and PVP, at various conditions. It was observed that for the PVP solution a humidity increase resulted in a decrease of fibre diameter, while for the CA solution a humidity increase resulted in an increase in fibre diameter. The authors attributed that to the different chemical interaction of the solvents used in each case with water. In particular, in the case of PVP is water soluble, thus, the absorption of water from atmosphere only causes dilution of the solution. On the other hand, CA is not water soluble, thus, absorption of water from atmosphere causes the precipitation of the polymer before the completion of electrospinning process.

2.3.4. Response Surface Methodology for investigation of individual parameter effect

So far, all the work that has been presented in this study has used linear methodology as an investigating technique. The basic principle of that methodology is keeping all but one factor constant, while the remaining factor varies. The measurement of the variation that is caused facilitates the identification of the correlation between the investigated parameter (independent variable) and the measured property (dependent variable). Although not erroneous in principle, this methodology is subject to certain limitations, especially when applied to processes affected by multiple variables.

The main limitation is that the effect of the investigated parameter cannot be isolated, since the outcome of the process is dependent on the setting of the other variables. Especially in the case that the other variables have a stronger effect on the process, that can hide or distort the effect of the investigated parameter, leading to misleading conclusions. The examples provided earlier, where given parameters appeared to have opposite effects under different investigation conditions are in support of this theory. Large number of experiments (i.e. conduction of experiments at varying levels of all the independent variables) is necessary to overcome that issue.

Response Surface Methodology (RSM) offers an alternative approach. **Figure 2.7** summarizes the basic steps of the process.

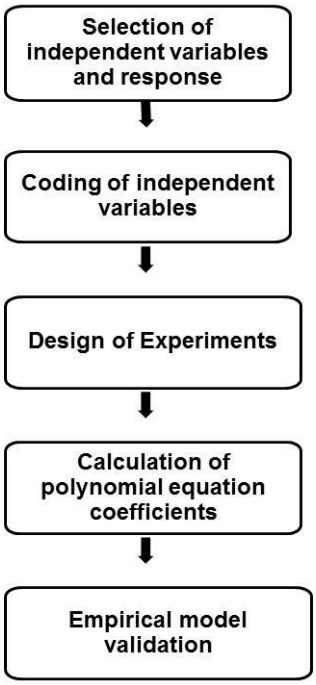

Figure 2.7. Response Surface Methodology fundamental steps (Sukigara et al., 2004).

The basic principle of RSM is the simultaneous variations of the independent variable values, as determined by experimental design and the subsequent development of polynomial equations, correlating the independent and dependent (response) variables, through experimental data fitting (Sukigara et al., 2004).

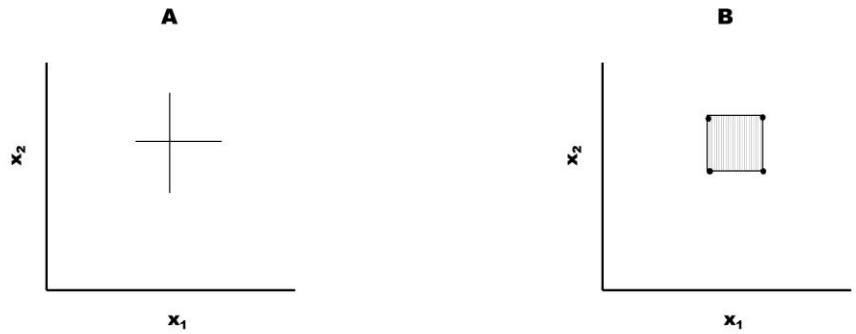

Figure 2.8. Comparison between the independent variable regions covered in a set of experiments by linear methods (A) and Response Surface Methodology (B).

Figure 2.8 demonstrates two different approaches for an experiment, whose outcome (response) depends on two independent variables (x_1 and x_2). In the linear method (**Figure 2.8.A**), where one independent variable is held constant while the other vary, conclusion can be drawn only for the points covered by the trendlines, whereas, in the case of RSM (**Figure 2.8.B**), where both independent variables change simultaneously, that area is expanded to the whole shaded area in the graph.

In addition to that, RSM can be used for the determination of interactions between the independent variables and for optimization (maximum or minimum value of the response) of the overall process (Box and Draper, 2007). All the above make RSM an extremely useful tool for investigating processes affected by numerous variables, such as electrospinning.

Sukigara et al. (2004) investigated the effect of solution concentration and electric field at two different spinning distances on the electrospinning of Bombyx mori silk using Response Surface Methodology. They were able to plot contour plots sufficiently predicting the experimental diameter and were able to identify the values of electric field and solution concentration (8.3 kV/cm and 7.3%, respectively) that lead to the production of the thinnest fibres for their system.

Similar methodology and independent variables were used by other researchers (Gu et al., Yordem et al., 2008), who, both reported that the solution concentration has a strong effect on the fibre average diameter, whereas, the applied voltage is less significant.

Kong and Ziegler (2013) used four independent variables (solution concentration, applied voltage, spinning distance and solution flow rate) in their research for optimization of electrospun starch diameter. They concluded that the solution flow rate didn’t have a significant effect on the response and identified the values that can optimize the process (production of fibres with the smallest possible diameter) within the investigated region.

In all the above cases the polynomial equations developed provided a more detailed picture about the response variation in the region investigated. In addition to that, RSM enables the investigation of independent variable interaction effect on the process, which is hard to be achieved through linear methodology. In summary, it

could be said that the use of RSM scales up the investigation from one dimensional to multi-dimensional.

2.4. Polymers used in electrospinning

The constantly increasing use of polymer fibres in their application fields has caused a proportional widening of the range of electrospun polymers. Up to date more than 200 polymers have been electrospun (Bhardwaj and Kundu, 2010). **Table 2.1** summarizes some of the most common polymers that have been electrospun up to date and their field of applications.

Table 2.1. Electrospun polymer fibres and their application field.

Polymer	Application	Reference
Poly(ε-caprolactone)	Tissue engineering	Vaz et al., 2005
Carbon nanotubes/polycaprolactone	Sensors	Castro et al., 2009
Collagen	Tissue engineering	Mattheus et al., 2003
PMMA	Filtration	Bae et al., 2013
Cellulose Acetate	Bioseparation	Munaweera et al., 2014
Chitosan	Tissue engineering	Croiser and Jerome, 2014
PLA	Tissue engineering	Wen et al., 2005
Cellulose Acetate	Chromatoghraphy	Dods et al., 2015
PAN/SiO_2	Energy storage	Ji et al., 2009
PAN-AA	Catalysis	Demir et al., 2004
Silk fibroin	Biomaterials	Min et al., 2004

Generally, natural polymers like collagen, silk fibroin etc. are used in biomedical applications due to their biocompatibility. Synthetic polymers, like PMMA, PS etc. are used when enhanced mechanical properties are required for the application.

Nonetheless, polymer blends can be used in electrospinning in order to combine the properties of both polymers. The polymers composing the blend can be natural (collagen – chitosan, Chen et al., 2010), synthetic (PGA-PLA, You et al., 2005) or both (PVA – chitosan, Jia et al., 2007).

2.4.1. Poly(ε-caprolactone)

The polymer that was selected for this project was poly(ε-caprolactone) (PCL). PCL is a linear aliphatic polyester having a glass transition temperature of -60 ^{o}C and melting point between 59 – 64 ^{o}C. The chemical formula of PCL is shown in **Figure 2.9**.

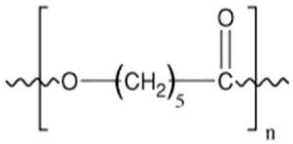

Figure 2.9. Chemical formula of PCL.

The main characteristic of PCL is its hydrophobic nature. Compared to other aliphatic polyesters that are used in electrospinning, such as polyglycolic acid (PGA) and polylactic acid (PLA), the PCL molecule consists of more –CH_2- units, which increases its hydrophobicity. In addition to this, even though PCL can be degraded by outdoor living organisms, it cannot be enzymatically degraded inside the human body due to the lack of the suitable enzymes (Vert 2009). Those two characteristics of PCL result in a reduction of the hydrolytic degradation rate of PCL in the human body, which makes PCL an excellent candidate for applications requiring low degradation rates, such as bone tissue engineering.

This selection of PCL was based on the following criteria:

Applicability. Recently PCL has drawn increasing attention due to the numerous fields it can be used into (Woodruff and Hutmacher, 2010). Its slow degradation rate, its biocompatibility, its bioresorbability and non-toxicity make it an ideal candidate for biomedical applications such as tissue engineering (**Table 2.2**).

Table 2.2. Tissue engineering fields where polycaprolactone has been used.

Polymer	Application	Reference
PCL	bone tissue engineering	Yoshimoto et al., 2003
PCL	nerve tissue engineering	Ghasemi-Mobarakeh et al., 2008
PCL	cardiovascular tissue engineering	Heydarkhan-Hagvall et al., 2008
PCL	skin engineering	Powell and Boyce, 2009

Tailored design flexibility. Blends of PCL with other polymers, such as collagen (Schnell et al., 2007, Yogeshwar et al., 2012), gelatin (Chong et al., 2007), chitosan (Shalumon et al., 2010), PLA (Barnes et al., 2007), PGA (Barnes et al 2007), etc, have been successfully electrospun. This increases both, the range of end product properties that can be achieved and the available choices for meeting predetermined targets.

Convenience of production and use. PCL is a common polymer that can be easily produced and doesn't require any special treatment.

2.5. Secondary structures on electrospun fibres

Currently, porous fibres have been attracting increasing interest. The reason for this trend is the superior properties of porous fibres, compared to the equivalent smooth surface fibres. Kim et al. (2005) proved that surface porosity can improve the mechanical properties of single nanofibres. The authors proved that the presence of pores on a fibre changes their deformation mechanism, under tensile stress, from crazing to nanonecking, thus increasing the energy tolerance prior to breaking. They attributed that change to the stress concentration within the pores rather than the main fibre body. In the field of tissue engineering, it has been proved that porous

surfaces improve cell attachment, proliferation and spreading on the scaffold (Moroni et al., 2006, Yamaguchi et al., 2004).

Porosity induction is generally considered an effective method to increase the material surface area. In the case of conventional materials, at the macro scale, the calculation of the size of that increase can be easily performed, through the comparison of the surface area of porous to non-porous materials. In the case of electrospun fibres, though, the calculation is subjected to several limitations.

First of all, it should be noted that in general all the measurements are conducted on the fibrous network rather than individual fibres. That means that the network properties, such as its density, also affect its specific area. In addition to that, there are limitations on the extent of control that can be applied over the network properties. All the above hinder the calculation of specific surface area increase due to pore formation, since direct comparison of networks with different properties would be inaccurate.

In the literature, the measurement of the specific surface area of fibrous networks composed of porous fibres is quite common (Touny and Bhaduri, 2010, Seo et al., 2004), however, it cannot be used be used for the calculation of specific area increase, since the surface area of fibrous networks composed by non-porous fibres was not measured. Another approach was presented by Yu et al. (2010), who compared the surface area of porous and non-porous fibres, prepared under the same experimental conditions, besides the pore generating mechanism. The results showed that the surface area of the networks composed by porous fibres was up to three times higher than that of non-porous, however, since the network properties and geometrical characteristics were not the same, the above results can be used for calculating the surface area increase caused by the pore generating mechanism and not by the actual pores. Similar approach was followed by Huang et al., (2011), who investigated the use of humidity for pore formation.

All the above highlight the necessity for the development of theoretical models, predicting the network specific surface area. That task, however, faces a challenge. The network specific surface area depends on the number of fibre-to-fibre contacts within it, since they subtract a part of the available surface area provided by the fibre bodies. A statistical approach has been implemented for that calculation

(Bagherzadeh et al., 2013, Eichhorn and Sampson, 2005), nonetheless, the focus of those studies was on the calculation of interfibre pores. That aspect is crucial when the networks are used as scaffolds for tissue engineering application, since it can determine cellular growth and migration. In terms of specific surface area modelling, Sampson (2005) was able to successfully correlate the overall network surface area lost due to contacts to fibrous network porosity. Eichhorn and Sampson (2010) further extended that research to include fibres of different cross sectional morphologies and correlated directly the specific area to the interfibre void size. Nonetheless, none of the above mentioned models has been used to date for the calculation of network specific surface area increase due to pore formation on electrospun fibres.

2.5.1. Pore generating mechanisms

Various methods have been proposed in order to induce pores on electrospun fibres. Pore generation can occur either simultaneously with electrospinning, in a single-step process, or after electrospinning, in a two-step process. An example of the latter is the work presented by Bognitzki et al (2001), where the pore generating mechanism was the selective dialysis from an electrospun polymer blend. In their work the first step involved the production of fibres from a PLA and PVP blend solution. In the second step the use of a selective solvent (for example water, which is a solvent for PVP and a non-solvent for PLA) on the fibres removed the soluble polymer and generated pores on the remaining one. Nonetheless, those methods will not be further discussed due to their complexity compared to single step processes. The two major single-step methods that have been proposed for pore generation are Phase Separation (Megelski et al., 2002) and Breath Figures (Casper et al., 2004).

Phase separation is the most common method for pore induction on electrospun fibres. The key stage of that method is the induction of thermodynamic instability in the polymer solution, which causes its separation to two phases, the polymer poor phase and the polymer rich phase. The precipitation of the polymer from the polymer-rich phase forms the matrix, whereas the pores are formed from the polymer poor phase.

The driving force for phase separation induction can be more easily perceived considering the Flory–Huggins theory. According to that, the Gibbs free energy of mixing for a polymer solution at constant temperature and pressure is given by Equation (2.5):

$$\Delta G_{mix} = \mathrm{RT}(n_1 \ln \varphi_1 + n_2 ln \varphi_2 + n_1 \varphi_2 \chi_{12}) (2.5)$$

Where ΔG_{mix} is the Gibbs energy, R is the universal gas constant, T is the temperature, n is the number of moles, φ is the volume fraction and χ is the interaction parameter. Subscripts 1 and 2 represent the solvent and polymer, respectively.

It should be emphasized that the polymer solution prior to electrospinning is thermodynamically stable and the instability is caused by the changes occurring during the process. Even though only the use of volatile solvents can cause phase separation (Celebioglu and Uyar, 2011), usually other means are employed for that purpose. The most common include the use of a non-solvent either prior, during or after electrospinning (Seo et al., 2012) and the use of temperature.

2.5.1.1. Non-solvent Induced Phase Separation

Non-solvent Induced Phase Separation (NIPS) refers to the addition of non-solvent in the polymer solution prior to electrospinning. The non-solvent must have a higher boiling point than the solvent and must be miscible with it. **Figure 2.10** shows the composition changes occurring during the combined NIPS-electrospinning process.

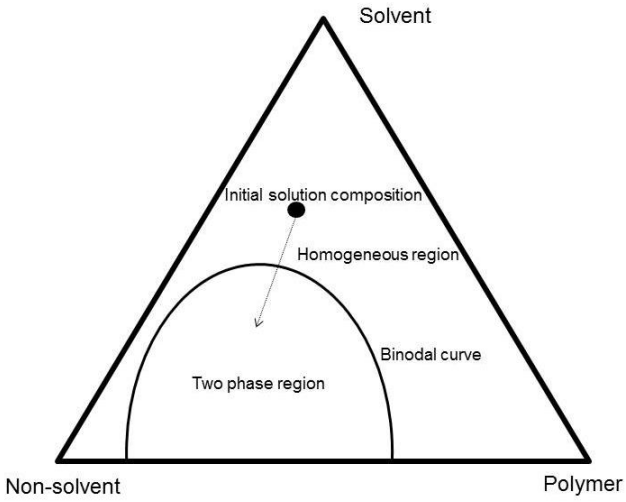

Figure 2.10. Composition changes of the electrospinning jet, after its ejection, during a combined NIPS-electrospinning process.

Initially the electrospinning solution is thermodynamically stable, at the one phase region. Non-solvent is present in the polymer solution, however, its amount does not suffice to cause thermodynamic instability. After its ejection, the electrospinning jet is subjected to composition changes. The polymer solvent is more volatile than the non-solvent, therefore the solvent/non-solvent ratio is constantly decreasing, due to the evaporation of a larger amount of solvent. The jet composition moves from the homogeneous, one phase region, to the two phase region (**Figure 2.10**), where phase separation initiates.

That combinative technique has been successfully implemented for the single-step production of porous polymer fibres. Qi et al. (2009) produced porous poly(L- lactic acid) (PLLA) fibres by using a binary solvent system of dichloromethane (solvent) and butanol (non-solvent). In their findings they also reported an increased tendency for pore generation accompanying the increase of the non-solvent amount in the polymer solution.

Lubasova and Martinova (2011) investigated that method on Polyvinyl butyral fibres. They used various solvent systems in several solvent/non-solvent ratios and they identified the presence of a non-solvent in the polymer solution, the discrete

difference between the evaporation rates of the solvent and non-solvent and the use of appropriate solvent/non-solvent ratios as requirements for pore generation.

Porous Polyethersulfone fibres were produced by Wei et al. (2013) through NIPS. Similarly to Qi et al. (2009) the proportional relationship between high non-solvent/ solvent ratios and pore generation is reported. In addition to that, increased average diameters in porous fibres, compared to non-porous, were observed.

Laiva et al. (2014) investigated the suitability of several binary solvent systems to produce porous poly(ε-caprolactone) fibres. All the solvent systems were composed of chloroform (good solvent) and, diethylether, ethyl acetate and dichloromethane were identified as appropriate solvents for pore formation on the fibres. Since dichloromethane is a solvent for poly(ε-caprolactone), the presence of a non-solvent in the solution as a requirement for initiation of phase separation, reported by Lubasova and Martinova (2011), doesn't generally stand. The phenomenon of increased diameters of porous fibres was reported in this study, as well.

2.5.1.2. Vapour Induced Phase Separation/Humidity

Vapour Induced Phase Separation (VIPS) is examined together with humidity, since the use of the latter can cause the former. Water is a non-solvent for most of the polymers and its absorption from air humidity can initiate phase separation in the electrospinning jet. Nonetheless, humidity can cause pore formation through an alternative mechanism, 'breath figures'.

In terms of the phase separation mechanism, VIPS is similar to NIPS, differing only at the stage of the non-solvent addition. In particular, at NIPS the non-solvent is added in the solution prior to electrospinning, whereas, at VIPS, the non-solvent is added during electrospinning.

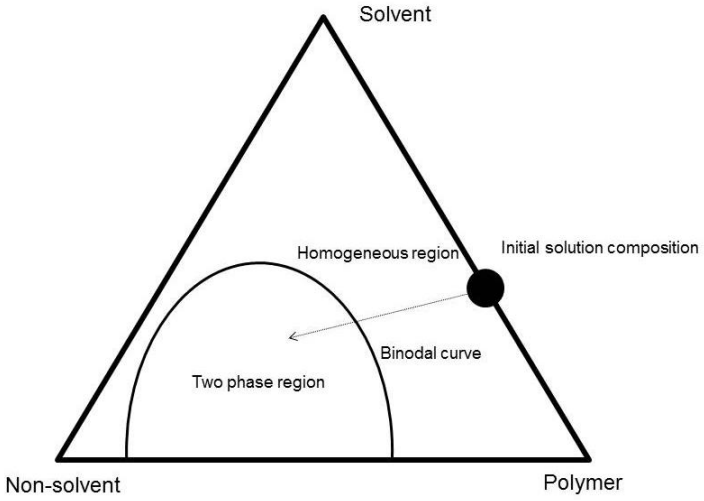

Figure 2.11. Composition changes of the electrospinning jet, after its ejection, during a combined VIPS-electrospinning process.

The composition path of the process is similar to NIPS, since the overall outcome is the constant decrease of the solvent/non-solvent ratio (**Figure 2.11**). However, the main difference can be spotted in the molecular diffusion within the jet. In NIPS the non-solvent molecules pre-exist in the jet, thus, a more uniform distribution of them can be expected, whereas, in VIPS the molecules are absorbed during electrospinning, thus, local accumulation of non-solvent at the jet surface is more possible (Pai et al., 2009).

Pore formation in a humid environment can also occur through the breath figures mechanism (Srinivasarao et al., 2001). This involves the formation of pores on a polystyrene (PS) film in a humid environment. In this case the solvent evaporation caused a lowering of the temperature on the surface of the film. Water vapour from the atmosphere was condensed on the film surface, leaving an imprint on the film. Finally, the pores were created by the evaporation of the water molecules from the surface (**Figure 2.12**).

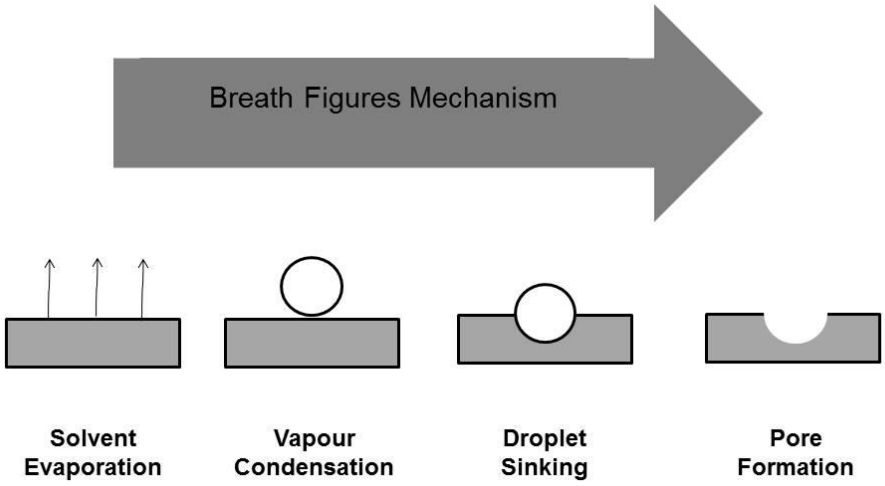

Figure 2.12. Steps for pore formation through breath figures mechanism.

The breath figures mechanism has been extensively implemented during electrospinning in order to generate circular pores. Casper et al (2004) was able to induce surface porosity during electrospinning of a 35% wt Polystyrene solution in THF. The increase of humidity didn't seem to affect the pore size (pore diameter ranges 60-190nm and 50-280 nm for humidity ranges between 31-38 and 66-72%, respectively), however, a massive increase of the pore number in a given area was observed (26 to 466 for the above mentioned humidity ranges).

It should be noted that the occurrence of one of the mechanisms doesn't prevent the occurrence of the other. The contribution of each mechanism in pore formation can be evaluated by the shape of the pores, since VIPS generates irregularly shaped pores, whereas the breath figures mechanism tend to generate circular pores. Nonetheless, that technique has been successfully implemented for pore generation on several polymers (Huang et al., 2011, Nezarati et al., 2013).

2.5.1.3. Thermally Induced Phase Separation

Thermally Induced Phase Separation (TIPS) is the third mechanism through which thermodynamic instability can be induced. In this case the shifting of the binodal curve (which separates the one and two phase regions) due to reduction of

temperature (Megelski et al., 2002) rather than compositional changes is the key for phase separation induction (**Figure 2.13**).

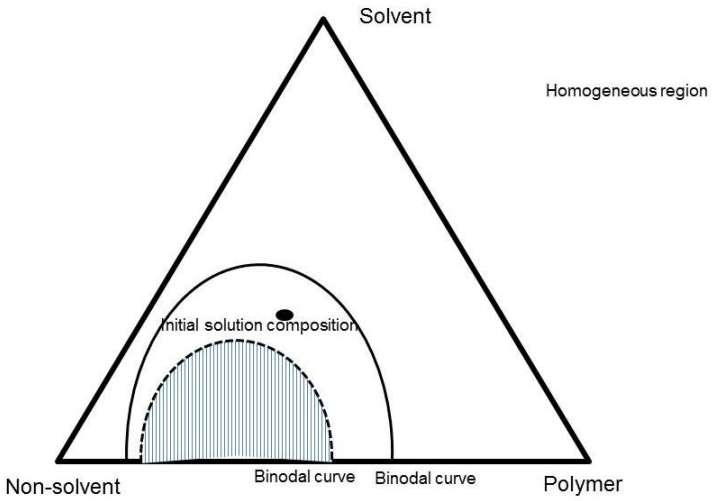

Figure 2.13. Binodal curve changes during TIPS. The dashed line and region represent the binodal curve and two phase region for high temperature, whereas the solid black line and the area below it represent the binodal curve and two phase region for low temperature.

During electrospinning solvent evaporation causes local temperature reduction, thus, that mechanism can occur at any electrospinning process. Experimental validation of the method has been reported by Fashadi and Karimi (2012) for ternary system of PS/THF/H_2O.

2.6. Discussion

This chapter has attempted to summarize the work that has been done so far in the field of production of porous polymer electrospun fibres. It is evident though, that the work presented up to date has not shed light to all aspects of the subject.

The first issue that remains not completely investigated is the quantification of the network specific surface area increase due to pore induction. Even though the theoretical models that have been developed so far provide satisfactory results, there is still space for further improvement through a different approach.

Combination of the statistical approach, which has been implemented so far, with contact mechanics, can lead to the development of theoretical models correlating the network specific surface area to material properties and network physical properties and geometrical characteristics. This can advance the understanding of the level of contribution of individual factors in the configuration of the overall network specific surface area and facilitate the calculation of the pore induction efficiency in terms of network specific surface area increase.

In the literature several models have been developed predicting the contact area of two bodies for several geometries. Three of the most widely applicable models are the Hertzian (Hertz, 1882), the DMT (Derjaguin et al., 1971, Muller et al., 1983) and the JKR (Johnson et al., 1971). The Hertzian model doesn't take into account adhesive forces between the two bodies in contact, the DMT considers only forces acting outside the contact area and the JKR considers only adhesive forces acting in the contact area (Shi and Zao, 2003). Thus, the identification of the contact mode between the electrospun fibres in the fibrous network can provide further information about their physical state.

In terms of the pore generation technique, the combinative electrospinning-NIPS method seems to top the other proposed methods in terms of:

Decreased sensitivity. The key parameter in electrospinning-NIPS technique is the solvent system, thus making the method less sensitive to humidity or temperature variations.

Controllability of fibre morphology. A common limitation in electrospinning is that the solvents of a given polymer, such as chloroform for polycaprolactone, have low dielectric constant, thus resulting in production of defective fibres. That limitation can be overcome with NIPS by the selection of a non-solvent with high dielectric constant.

Universal applicability. There are no limitations to the polymers that NIPS can be applied, in contrast to VIPS (the polymer can't be water soluble) or TIPS (not applicable to low melting polymers).

Given the new elements that are introduced in the standard electrospinning process, though, due to the non-solvent addition, the necessity for the complete investigation of the combinative technique is emphasized. In particular, the effect of the initial

solution physical properties and the electrospinning process parameter effect on the electrospun fibre surface morphology and size for a combinative electrospinning-NIPS technique hasn't been studied before. Such studies have been completed for other pore generating mechanisms, such as breath figures (Megelski et al., 2002) and reactive electrospinning (Touny and Bhaduri, 2010). The work that has been published up to date in the field of electrospinning-NIPS was mainly focused in the establishment of the method and the investigation of the solvent/non-solvent ratio effect on the fibre morphology.

Having identified the gaps in the current literature, the current study aims to shed more light on them by quantifying the network specific area increase due to pore induction and investigating the initial solution physical properties and process parameter effect on electrospun poly(ε-caprolactone) fibre surface morphology and size.

3. Materials and Methods

3.1. Materials

The glassware used in this project was the standard laboratory equipment. All the chemicals in this project were purchased from Sigma-Aldrich and used as delivered. PCL of two different MW (45000 and 80000) was used in this project. CF was ACS reagent, had purity ≥ 99.8% and contained ethanol as a stabilizer. DCM was ACS reagent, with ≥ 99.5% purity and contained amylene as a stabilizer. THF was ACS reagent, had purity ≥ 99.0% and contained BHT as an inhibitor. DMSO was ACS reagent, had purity ≥ 99.9%. FA was reagent grade and had purity ≥ 95.0 %. TBAB had purity ≥ 99.0%.

3.2. Methods

3.2.1. Solution preparation

All the solutions were prepared at room temperature. Solution concentrations were based on equation (3.1)

$$\%\frac{w}{v} = \frac{m_{polymer}}{V_{solvent}} x100 \quad (3.1)$$

Where $m_{polymer}$ is the mass of PCL (g)

$V_{solvent}$ is the volume of the solvent (ml) prior to mixing

The solutions were prepared by the weighing of the appropriate amount of polymer within a jar, the addition of the appropriate amount of solvent/solvent mixture and stirring until complete dissolution. The duration of the procedure depended on the solvent used (typically around 2 hrs). The jar remained covered during the preparation procedure in order to avoid solvent evaporation.

3.2.2. Electrospinning experiments

A horizontal electrospinning set-up was used, as shown in **Figure 3.1**.

Figure 3.1. Pictures of the electrospinning set-up used for the experiments. The numbers in the pictures represent parts of the rig. 1) High voltage power supply, 2) Pump, 3) Syringe, 4) Ventilated chamber, 5) Metallic needle, 6) Collector.

20 ml of the solution was loaded to a plastic syringe and the syringe was placed on a syringe pump (PHD ULTRA, Harvard Apparatus). The electric potential was applied to the metallic needle (18 gauge, 1.270 mm outer diameter, 0.838 mm inner diameter, 3.2 cm length, Fisher Scientific) by the high voltage power supply (Series FC, Glassman High Voltage Inc). The fibres were collected on a flat copper plate covered with aluminium foil. All the experiments were conducted at room temperature (17-22 ^{o}C) and relative humidity of 30-40% within a closed chamber. Typically, each experiment lasted 10 minutes, unless special requirement for the production of large amount of fibres existed. In that case the duration of the experiment was prolonged up to 2 hrs.

3.2.3. Solution characterization

3.2.3.1. Conductivity

JENWAY 4071 conductivity meter was used for the measurement of the conductivity of the solutions. The probe of the conductivity meter was immersed in the solution and held still. Special care was taken to avoid contact between the probe and the glass wall. Sufficient time was given for the setting of the screen reading, which was subsequently recorded.

3.2.3.2. Surface tension

The surface tension was measured using the Du Noüy ring method (White Elec Inst balance, model DB2kS). All the comparative measurements were performed within 4 hrs in order to minimize the temperature change effect. Approximately 40 ml of solution were poured in a container large enough, so as its walls would not affect the measurement. The container was stabilized on its standard position on the equipment. The platinum ring of the balance was immersed within the solution and, subsequently, was removed. The force required for that removal was automatically converted to surface tension and the reading was recorded. Washes with acetone, distilled water and aqua regia (mixture of 1 part HNO_3 and 3 parts of HCl) and burning of the platinum ring ensured that the ring was sufficiently clean prior using it on a different sample. At least three measurements were performed on each sample and their average value was considered as the surface tension of the solution.

3.2.3.3. Viscosity

A rotational viscometer (Thermo Haake VT550) was used for the viscosity measurements. 9 ml of the solution were placed in the instrument vessel and the cup sensor was adapted. The measuring principle of the instrument is based on the torque required to maintain the speed of the rotating cup. The viscosity was measured at shear rates ranging from 0-400 s^{-1} for 120 sec. The average value of the measured viscosities was considered as the viscosity of the solution.

3.2.4. Individual fibre characterization

3.2.4.1. Fibre diameter

Field emission scanning electron microscopy (FESEM, Carl Zeiss (Leo) 1530VP) was used for the characterisation of the surface morphology of the fibres. All the samples were sputter coated with gold (Q150T ES, Quorum) for 120 sec prior to their observation under the microscope. Various instrument settings (magnification, working distance, brightness, contrast) were used for image taking, depending on the characteristics of individual samples. The diameters of the fibres were measured

by AxioVision software. Unless stated otherwise, at least 100 fibre diameters were measured per sample, in order to ensure the accuracy of the measurements.

3.2.4.2. Fibre length

The main fibre mat was removed from the collector and the length measurement was performed on the fibres remaining on the collector. That minimised the probability of measuring segmented fibres. The fibres were manually uncoiled prior to their measuring. A 30 cm ruler (increments of 1mm) was used for the measurements. A minimum of 5 measurements was completed for each sample.

3.2.5. Fibrous network characterization

3.2.5.1. Network specific surface area

Gas adsorption (ASAP 2020, Micrometrics) was used for the measurement of the electrospun mat specific surface area. The sample was left overnight in a vacuum oven at room temperature for the complete removal of any residual solvent from its production. Potential gases or vapours absorbed at the sample surface were removed by outgassing the samples. Liquid nitrogen was adsorbed from the sample. The specific surface area was calculated by the Brunauer–Emmett–Teller (BET) equation (3.2):

$$\frac{1}{\left[V_a\left(\frac{P_0}{P}-1\right)\right]} = \frac{C-1}{V_m C}\frac{P}{P_0} + \frac{1}{V_m C} \quad (3.2)$$

Where P is the pressure of the adsorbed gas, P_0 is the pressure of the saturated gas, V_a is the volume of the absorbed gas, V_m is the volume of the absorbed gas to create a monolayer and C is a constant.

The BET value was plotted against P/P_0 and from the slope and intercept of the linear trendline V_m and C were calculated. The specific area was calculated from equation (3.3):

$$S = \frac{V_m N a}{22400 m} (3.3)$$

Where N is the Avogadro number, a is the effective cross sectional area of one absorbate molecule (0.162 nm^2 for N_2), m is the mass of the sample and 22400 is the volume (ml) occupied by 1 mole of the absorbate at standard conditions

3.2.5.2. Network density

Gas pycnometry (9200 Helium Pycnometer, Micrometrics) was used for the measurement of the electrospun mat density. The mat was left overnight in a vacuum oven at room temperature for the complete removal of any residual solvent from its production. After its weighing, the mat was placed within the pycnometer chamber (5 cc). Helium was inserted within the chamber and the pressure was recorded before and after the expansion. The sample volume was calculated using equation (3.4):

$$V_{samp} = V_{cell} - V_{exp} / \left[\left(\frac{P_1}{P_2} \right) - 1 \right] (3.4)$$

Where V_{samp} is the sample volume, V_{cell} is the volume of the cell (7.75569 cm^3), V_{exp} is the expansion volume (6.15523 cm^3),P_1 and P_2 are the pressures before and after expansion, respectively.

Finally, the mat density was calculated from equation (3.5):

$$\rho_{mat} = \frac{m_{mat}}{V_{mat}} (3.5)$$

3.2.5.3. Network thickness

A digital calliper (ABSOLUTE AOS, Mitutoyo) was used for the thickness measurements of electrospun mats, as shown in **Figure 3.2**. At least 5 measurements were performed on each mat, in order to obtain an average.

Figure 3.2. Measurement of electrospun mat thickness.

3.3. Material and experimental condition selection

The large number of parameters affecting the electrospinning process is evident and has been analysed earlier in this study. Thus, certain experimental conditions had to be set. In particular, those conditions were the molecular weight of the polycaprolactone and the solution concentration range. Although the literature review can provide general guidelines, the sensitivity of the process to changes of any parameter and the different experimental set-up used in this study required the conduction of initial experiments for the determination of the values of the above mentioned parameters.

3.3.1. Molecular Weight of polycaprolactone

In terms of PCL MW selection, it was decided the work to be performed on commercially supplied polymer, in order to eliminate potential variability due to in-house production and to maintain the ability for comparison of the results derived from this study to those obtained from the literature. Within the literature, two commercial products had been used for the vast majority of the studies, PCL with average MW of either 45 or 80 kDa, both supplied by Sigma Aldrich (Cipitria et al.,

2011). As discussed earlier, a lower MW favours the production of small diameter fibres, and, since reports had claimed that PCL with a low MW could be successfully electrospun (Hsu and Shivkumar., 2004), that was the initial choice for this study. However, after several trials (**Table 3.1**), it was found that the low MW weight PCL could not be electrospun, by using the solvents intended to be used in this study.

Table 3.1. Experimental conditions used for electrospinning of low MW PCL.

Experimental conditions	1	2	3	4	5
Solvent system	CF	CF	CF	CF	CF
Solution concentration (% w/v)	10	12.5	15	20	30
Voltage (kV)	25	15	15	20	20
Spinning distance (cm)	15	10	15	10	15
Flow rate (ml/h)	2	1	0.5	3	1

No or limited fibre collection was observed in all the cases. Apparently, the chain entanglements did not suffice for fibre formation under the investigated conditions. In addition to this, partial clogging of the metallic needle might have occurred, due to the high concentration of the polymer solutions. Even when a small amount of product seemed to have been collected, it had the shape of elongated droplets not fibres (**Figure 3.3**). All the above factors led to the selection of the high molecular weight PCL for the conduction of the experiments.

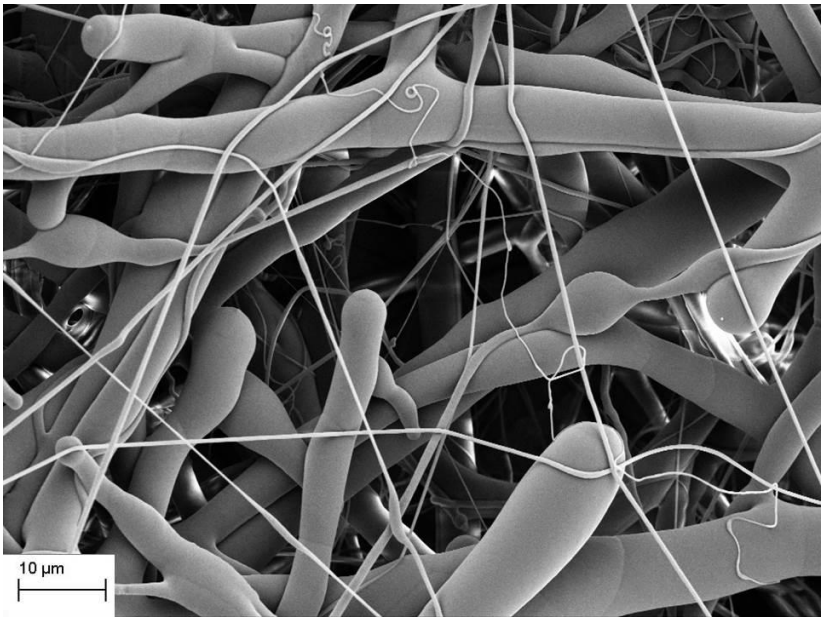

Figure3.3. SEM image of electrospinning product of low MW PCL solution.

3.3.2. Solution concentration range

In terms of solution concentration, the range that has been used in the literature is extremely wide. Solution concentrations varying from 5% wt (Hsu and Shivkumar., 2004) to 40% wt (Piskin et al., 2009) have been reported. The most common range, though, lay between 10-20% w/v, and that was the range tested initially. The solvent used for that testing was chloroform, since that solvent was intended to be used in this study, and the exact experimental conditions are summarized in **Table 3.2**.

Table 3.2. Experimental conditions used for selection of solution concentration range.

Experimental conditions	1	2	3	4	5
Solvent	CF	CF	CF	CF	CF
Solution concentration (% w/v)	10	12.5	15	20	25
Voltage (kV)	20	15	15	20	20
Spinning distance (cm)	15	15	20	15	20
Flow rate (ml/h)	2	1	2	1	2

Figure 3.4 shows the fibres produced from experimental runs 1 and 4. The presence of beads on the fibres produced from the low concentration solution (**Figure 3.4 A**) indicated that a solution of higher viscosity was required. On the other hand, excessive increase of the solution concentration can lead to branching of the fibres **(Figure 3.4 B**). Branching has been observed on viscous solutions (Reneker and Yarin, 2008) and is attributed to the excessive surface charge density on the jet. In addition to that, partial clogging of the needle was observed, especially when a number of experiments were run successively.

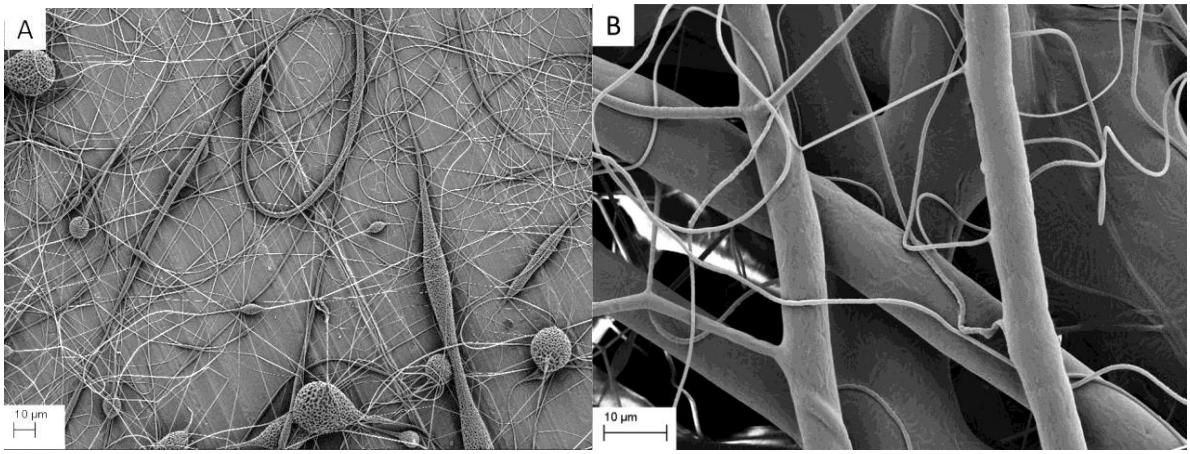

Figure 3.4. SEM images of electrospun PCL fibres from different concentration solutions (A) 10% w/v, (B) 20% w/v.

The needle clogging wasn't completely eliminated by the reduction of solution concentration to 15% w/v, therefore, the use of 12.5% w/v solutions seemed to provide the best compromise.

4.Fibrous Network Specific Surface Area

4.1. Abstract

The effect of pore formation on electrospun fibrous network specific surface area is investigated in this chapter. Three different models, based on the available surface area due to fibre body and excluding the surface lost due to fibre-to fibre contacts, were developed. The models for calculation of the excluded area were based on Hertzian, DMT, JKR models. Overall, the theoretical models correlated the network surface area to the material properties (density, surface tension, Young's modulus, Poisson's ratio) and network physical properties (density) and geometrical characteristics (fibre radius, fibre aspect ratio, network thickness). Pore induction proved to increase the network specific surface area up to 52%, compared to the maximum surface area that could be achieved by non-porous fibre network with the same physical properties and geometrical characteristics. The model based on JKR contact model describes accurately the fibre-to-fibre contact area under the experimental conditions used for pore generation. The experimental results and the theoretical model based on Johnson-Kendall-Roberts contact model show that the increase in network surface area due to pore induction can reach to up to 58%.

4.2. Introduction

Specific surface area of any material is one of its most important properties in terms of industrial applicability. Essentially, the increased interest that electrospinning, and nanotechnology in general, attract is due to the massive increase of specific surface area that can be achieved because of the reduced size scale of nanomaterials. On top of size reduction, other techniques, such as the surface modification of fibres composing the network, can further increase the end product specific surface area.

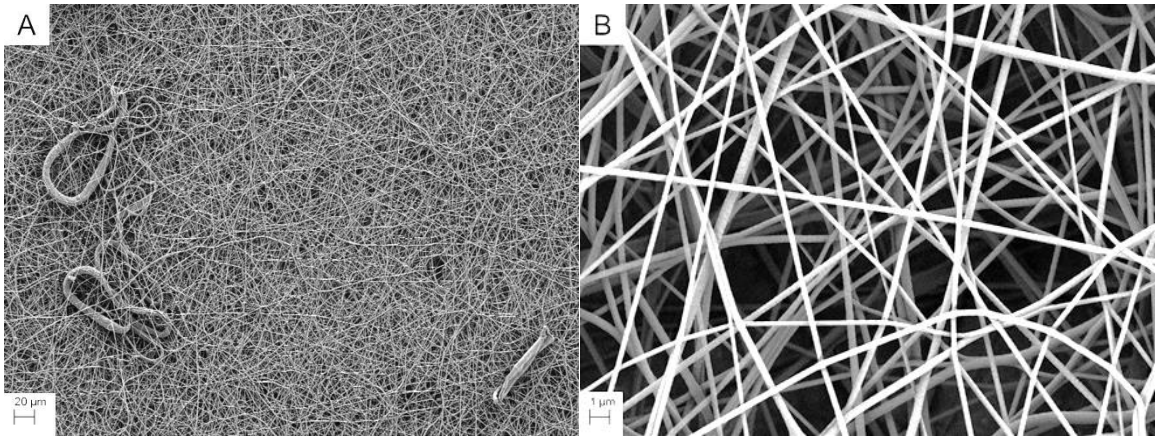

Figure 4.1. SEM pictures of a fibrous network produced by electrospun polycaprolactone fibres at different magnifications. (A) x500 (B) x10000.

Figure 4.1 shows SEM images of a typical network composed by electrospun fibres. Since eventually fibrous networks rather than individual fibres are used in any kind of application, the calculation of the network specific surface area must involve the scaling up from individual fibre to fibrous network. An important aspect that has to be considered in that case is the numerous fibre-to-fibre contacts occurring within the network and subsequently, the network specific surface area decrease due to those contacts. Once that is accomplished, the calculation of the network specific surface area increase due to pore induction can be achieved through comparison of experimentally measured specific surface area of networks composed by porous fibres to the theoretically predicted surface area of smooth surface networks with the same geometrical and physical characteristics.

4.3. Theoretical Analysis

4.3.1. Introduction

The development of the theoretical models is based on the assumption that the fibrous network specific area depends on two parameters:

- The maximum available network specific surface area. That parameter is determined by the size and the material properties of the fibres in the network.

- The excluded area due to fibre-to-fibre contacts. That parameter can be further subdivided to the number of the fibre-to-fibre contacts and the contact area at any contact point.

All the above can be summarised in equation (4.1):

$$S_{net} = S_{max} - N_{con}\, S_{excl} (4.1)$$

Where S_{net} is the specific surface area of the network

S_{max} is the maximum available surface area

N_{con} is the number of fibre-to-fibre contacts within the network and

S_{excl} is the area excluded from each contact

4.3.2. Maximum available surface area of the fibrous network

The first step to develop the theoretical model is to calculate the maximum available network specific surface area. This can be achieved based on the assumption that all the fibres composing the network are cylinders of equal radius R and length L_i. In that case, the maximum specific area of the network can be calculated by using equation (4.2):

$$S_{max} = 2\pi R \sum_{i=1}^{n_f} L_i + 2\pi R^2 n_f \ (4.2)$$

Where n_f is the number of fibres composing the network.

The length of the fibres is significantly larger than their radius (typically $L_i/R>1000$ (Beachley and Wen, 2009)), therefore equation (4.2) can be simplified to equation (4.3):

$$S_{max} = 2\pi RL \ (4.3)$$

Where L is the sum of the length of the fibres consisting the network.

The specific area per unit mass is:

$$\frac{S_{max}}{m} = \frac{2\pi RL}{m} \quad (4.4)$$

The mass can be obtained based on the density of fibre material and the volume of a cylinder.

$$\rho_{material} = \frac{m}{V} \quad (4.5)$$

$$V = \pi R^2 L \quad (4.6)$$

Equation (4.4) can then be written as:

$$\frac{S_{max}}{m} = \frac{2}{\rho_{material} R} \quad (4.7)$$

Equation (4.7) demonstrates that the maximum specific surface area of a fibrous network (achievable when no fibre-to-fibre contacts occurring within the network), composed by smooth surface fibres, is inversely proportional to the fibre radius and material density.

4.3.3. Number of fibre-to-fibre contacts

The next step is to calculate the number of fibre-to-fibre contact within the network. Within literature some studies had already investigated the issue (Eichhorn and Sampson, 2005, Bagherzadeh et al., 2013). The work of the latter was selected for adaptation in this study, since they take into consideration and exclude the fibre length occupied by previous contacts prior to calculating the probability for any further contact. Their work is based on four assumptions:

- All the fibres are cylinders of equal diameter and length.
- The coverage of any point of space within the network by fibre is given by the Poisson distribution.
- Fibres are located within a two dimensional plane.
- Fibre positioning follows a line Poisson process.

Overall, their calculated average number of contacts, per fibre unit length in a single layer fibrous network is:

$$N_{per\ length} = \frac{4\pi \log\left(\frac{1}{\varepsilon}\right)}{2\pi R + 16R\lambda \log\left(\frac{1}{\varepsilon}\right)} \quad (4.8)$$

In a multi layered mat, the number of contacts is given by equation (4.9):

$$N_{per\ length} = (2n-1)\frac{4\pi \log\left(\frac{1}{\varepsilon}\right)}{2\pi R + 16R\lambda \log\left(\frac{1}{\varepsilon}\right)} \quad (4.9)$$

Considering equations (4.5) and (4.6), equation (4.9) can be modified to:

$$N_{per\ mass} = (2n-1)\frac{4\pi \log\left(\frac{1}{\varepsilon}\right)}{2\pi R + 16R\lambda \log\left(\frac{1}{\varepsilon}\right)}\frac{1}{\pi \rho_{material} R^2} \quad (4.10)$$

Where ε is the porosity of the fibrous network, λ is the fibre aspect ratio, d is the fibre diameter, n is the number of layers in the network and t is the thickness of the fibrous mat.

$$\varepsilon = 1 - \frac{\rho_{mats}}{\rho_{material}} \quad (4.11)$$

$$\lambda = \frac{L}{d} \quad (4.12)$$

$$n = \frac{t}{2R} \quad (4.13)$$

4.3.4. Contact area based on Hertzian model

The determination of the individual fibre-to-fibre contact area is the final step for the theoretical model development. Nonetheless, the geometrical characteristics of the network elements complicate the study. When the contact area to be calculated is between two bodies with nominally smooth and flat surfaces, the issue is simple and independent of any variables. The contact area is determined only by the size of the bodies, and in particular the size of the smaller body (**Figure 4.2**). Parameters like the deformation on the bodies are usually negligible considering the contact area.

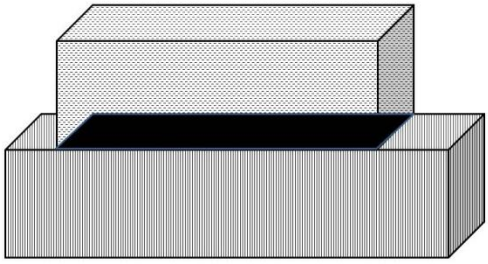

Figure 4.2. Contact area between cuboids. The rectangular shaped contact area is shaded with a darker colour.

When the bodies in contact have curved surfaces though, such as spheres or cylinders, the calculation of the contact area becomes more complex. The contact area is significantly smaller compared to their size, therefore, the deformation of bodies at contact foot print becomes important. In the case of cylindrical bodies, depending on the alignment of the cylindrical bodies with respect to each other the contact foot print can be considered to be a line (more precisely, a very narrow rectangle), circle or ellipse. (**Figure 4.3**).

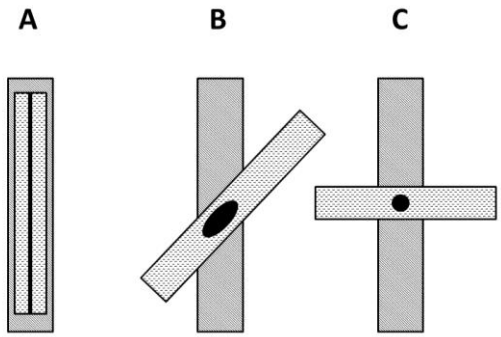

Figure 4.3. Overview of contact area (black shaded area) between cylinders at different angles. (A) At 0^o (parallel axes cylinders) the area is a rectangular, (B) between 0^o and 90^o it becomes an ellipsis and at (C) 90^o it is a circle.

Even though in the case of fibrous network the contact occurs between cylinders, it is simpler if the investigation starts considering the contact between two spheres. Hertz (1882) was the first to investigate such a problem and determined the

displacement and the radius of the circular contact area between two spheres with equal radii Rs (**Figure 4.4**), which were subjected to an assumed pressing load.

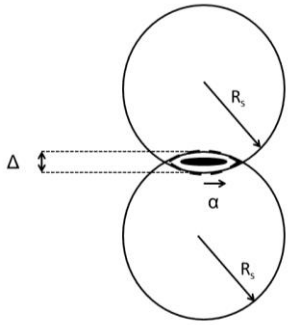

Figure 4.4. Contact between two spheres with equal radii. The contact area is the black shaded area.

The displacement of the spheres is given by equation (4.14)

$$\Delta = \frac{\alpha^2}{R_{rc}} (4.14)$$

Where α is the radius of the circular contact area and R_{rc} is the reduced radius of curvature, given by equation (4.15) for the contact of spheres of equal radius R_S:

$$\frac{1}{R_{rc}} = \frac{2}{R_s} (4.15)$$

The radius of the circular contact area (α) can be calculated by equation (4.16):

$$\alpha = (\frac{3PR_{rc}}{4E})^{1/3} (4.16)$$

Where P is the applied force and E* is the contact modulus given by equation (4.17) for spheres made of the same material.

$$\frac{1}{\mathrm{E}*} = 2\frac{1-v^2}{E} (4.17)$$

Where E and v in the equation above are Young's modulus of elasticity and Poisson's ratio of the sphere material respectively.

In the case of the fibrous network though, the contact occurs between randomly oriented cylinders. The issue, however, can be simplified by the equation of the cylinders to spheres (Bhushan, 2001). The basis for that is the change of the coordinates of set of axes formed by the cylinders. The new set of axes has to meet the requirement of:

$$A + B = \frac{1}{R} \quad (4.18)$$

$$B - A = \frac{1}{2R}(2 + 2cos2\theta)^{\frac{1}{2}} \quad (4.19)$$

Where R is the radius of the cylinders and θ is the angle formed by them.

From the solution of equations (4.18), (4.19), the parameters A and B are obtained as follows:

$$A = \frac{2 - (2 + 2cos2\theta)^{1/2}}{4R} \quad (4.20)$$

$$B = \frac{2 + (2 + 2cos2\theta)^{1/2}}{4R} \quad (4.21)$$

The radius of curvature (R_e) is given by equation (4.22) and can be used in equation (4.16) for the calculation of the circular contact area:

$$R_e = \frac{1}{2}(AB)^{-\frac{1}{2}} \quad (4.22)$$

The displacement of the equated spheres can be found by using equation (4.14) with the R_{rc} replaced by $2R_e$.

Finally, it is necessary to calculate the normal load applied on each point of contact by utilising the equated sphere displacement concept. This is based on the assumption that no external force is applied on the network, thus, only network mass was considered as force. The network was considered to be composed of n layers of equal mass, the weight of each can be calculated by using equation (4.23):

$$m_{layer} = \frac{m_{overall}}{n} \quad (4.23)$$

The force that applied on each layer, though, is not the same throughout the network. The force applied on any layer will depend on the weight of the layers above it. For instance, the bottom layer receives the weight of n-1 layers, the second layer of n-2 and so on, until the top layer, which receives no force (**Figure 4.5**).

Figure 4.5. Forces applied on individual fibre layers in a fibrous network.

The average force that is applied in any layer within the network is:

$$F_{av} = \frac{(n-1)}{n} mg \quad (4.24)$$

The total applied force on the layer is then equally distributed to all the contacts occurring on the latter (**Figure 4.6**), therefore the force applied on each contact, per unit mass, can be found by dividing the total weight experienced in that layer by the number of contacts occurring in the same single layer:

$$F_c = \frac{g(n-1)}{\frac{N_{cont}}{n}} \quad (4.25)$$

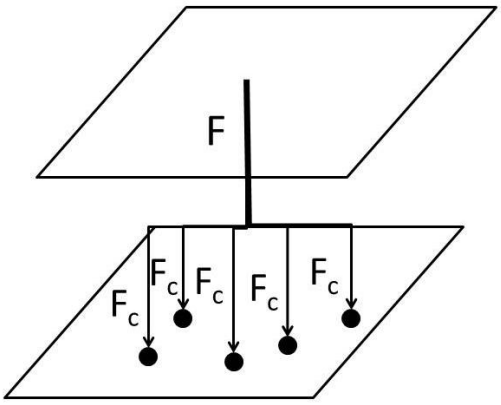

Figure 4.6. Force distribution within a single layer. F represents the overall force applied by the upper layer, whereas F_c is the force applied on individual contacts (black bullet points). The sum of F_c equals to F.

Considering that a contact always occurs between two surfaces, each contact detracts the sum of the two spherical caps in contact. Therefore, the total excluded area at each contact point is:

$$S_{excl} = 2\pi R_e \Delta = \pi a^2 \quad (4.26)$$

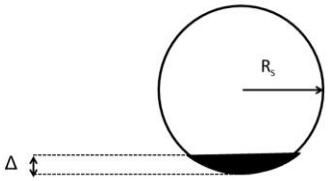

Figure 4.7. Excluded area of a sphere (black shaded area) at a contact.

Combining equations (4.14)-(4.17) and (4.20)-(4.25) the Hertzian contact area of two cylinders inclined at an angle θ is given by equation (4.27):

$$S_{excl} = 2\pi \left[\frac{1.06g(n-1)}{2n-1} \frac{R^4}{\sqrt{1-cos\,2\theta}} \frac{\pi + 8\lambda\, log(1/\varepsilon)}{log(1/\varepsilon)} \rho_m \frac{1-v^2}{E} \right]^{2/3} \quad (4.27)$$

Equation (4.27) can be simplified by the introduction of a new entity, angle factor (Θ), defined by equation (4.28):

$$\Theta = \left(\left(2-(2+2cos2\theta)^{\frac{1}{2}}\right)\left(2+(2+2cos2\theta)^{\frac{1}{2}}\right)\right)^{\frac{1}{2}} \quad (4.28)$$

The fibres are randomly oriented within the fibrous network, therefore, the probability of the contact angle to lie at any value within the range between 0^0 to 90^0 is equal. Based on that, the angle factor value can be calculated based on equation (4.29):

$$\Theta = \frac{\sum_{\theta=0}^{90}\left(\left(2-(2+2cos2\theta)^{\frac{1}{2}}\right)\left(2+(2+2cos2\theta)^{\frac{1}{2}}\right)\right)^{\frac{1}{2}}}{91} \approx 1.27 (4.29)$$

Finally, the average excluded area by any Hertzian contact within a fibrous network is given by equation (4.30):

$$S_{excl} = 2\pi\left\{\frac{1.2(n-1)g}{2n-1}\cdot\frac{[\pi+8\lambda\log(1/\varepsilon)]\rho_m R^4}{\log(1/\varepsilon)}\cdot\frac{1-\upsilon^2}{E}\right\}^{2/3} \quad (4.30)$$

4.3.5. Contact area based on adhesive models

The model developed by Hertz is not universally applicable, since it is subject to certain limitations. In particular it doesn't take into account adhesive forces between the two bodies in contact. Different methodologies, such as DMT model (Derjaguin et al., 1971, Muller et al., 1983) and JKR model (Johnson et al., 1971), have been developed in order to include the adhesion effect in the calculation of the contact area. The difference between the adhesive models is that the DMT model considers only the adhesive forces acting outside the contact area, whereas the JKR model considers only the forces acting in the contact area (Shi and Zhao, 2004).

The radius for the circular contact area predicted by the DMT model is:

$$\alpha = \left[\frac{3R_{rc}}{4E}(F+4\gamma\pi R_{rc})\right]^{1/3} \quad (4.31)$$

The radius for the circular contact area predicted by the JKR model is:

$$\alpha = \left[\frac{3R_{rc}}{4E}\left(F_c+6\gamma\pi R_{rc}+\sqrt{12\gamma\pi R_{rc}F_c+(6\gamma\pi R_{rc})^2}\right)\right]^{1/3} \quad (4.32)$$

Following the same methodology that has been developed for a Hertzian contact, equation (4.30) can be modified as follows in the case of the DMT model:

$$S_{excl} = 2\pi \left[\frac{1.19R^2}{E} \left(\frac{g(n-1)[\pi + 8\lambda \log(1/\varepsilon)]}{2(2n-1)\log(1/\varepsilon)} \rho_m R^2 + 6.36\pi\gamma \right) \right]^{2/3} \quad (4.33)$$

and as follows considering a JKR contact:

$$S_{excl} = 2\pi \left[\frac{1.19R}{E} \left(\frac{g(n-1)[\pi + 8\lambda \log(1/\varepsilon)]\rho_m R^3}{2(2n-1)\log(1/\varepsilon)} + 9.53\pi\gamma R + \sqrt{9.53\pi\gamma R \frac{g(n-1)[\pi + 8\lambda \log(1/\varepsilon)]\rho_m R^3}{(2n-1)\log(1/\varepsilon)} + (9.53\pi\gamma R)^2} \right) \right]^{2/3} \quad (4.34)$$

4.4. Experimental testing of the theoretical models

The design for the experimental testing of the theoretical models involved the production of both, networks composed by porous and non-porous fibres. The latter were to be used for the determination of the contact model that calculates more accurately the contact area between the polymer fibres within the network, and subsequently, the overall network specific surface area. The former were to be used for the quantification of the pore induction efficiency in terms of surface area increase. In total five samples were produced, in two of which the fibres were non-porous and in the remaining three the fibres were porous. The NIPS mechanism that was used for pore generation is examined in detail in Chapter 5. **Table 4.1** summarizes the experimental conditions used for the production of the samples and the images of the produced fibrous networks are shown in **Figure 4.8**.

Table 4.1. Experimental conditions used for the production of fibrous networks.

Sample	1	2	3	4	5
Solvent system	CF	CF/DMSO	CF/DMSO	CF/DMSO	CF/DMSO
Solvent ratio (% v/v)	73	9/1	9/1	9/1	9/1
Additives	0.2% w/v TBAB	1% v/v FA	-	-	-
Solution concentration (% w/v)	12	12	12	12.5	12.5
Voltage (kV)	25	15	15	25	22
Spinning distance (cm)	15	20	20	17.5	22
Flow rate (ml/h)	2	1	1	2.75	1.41

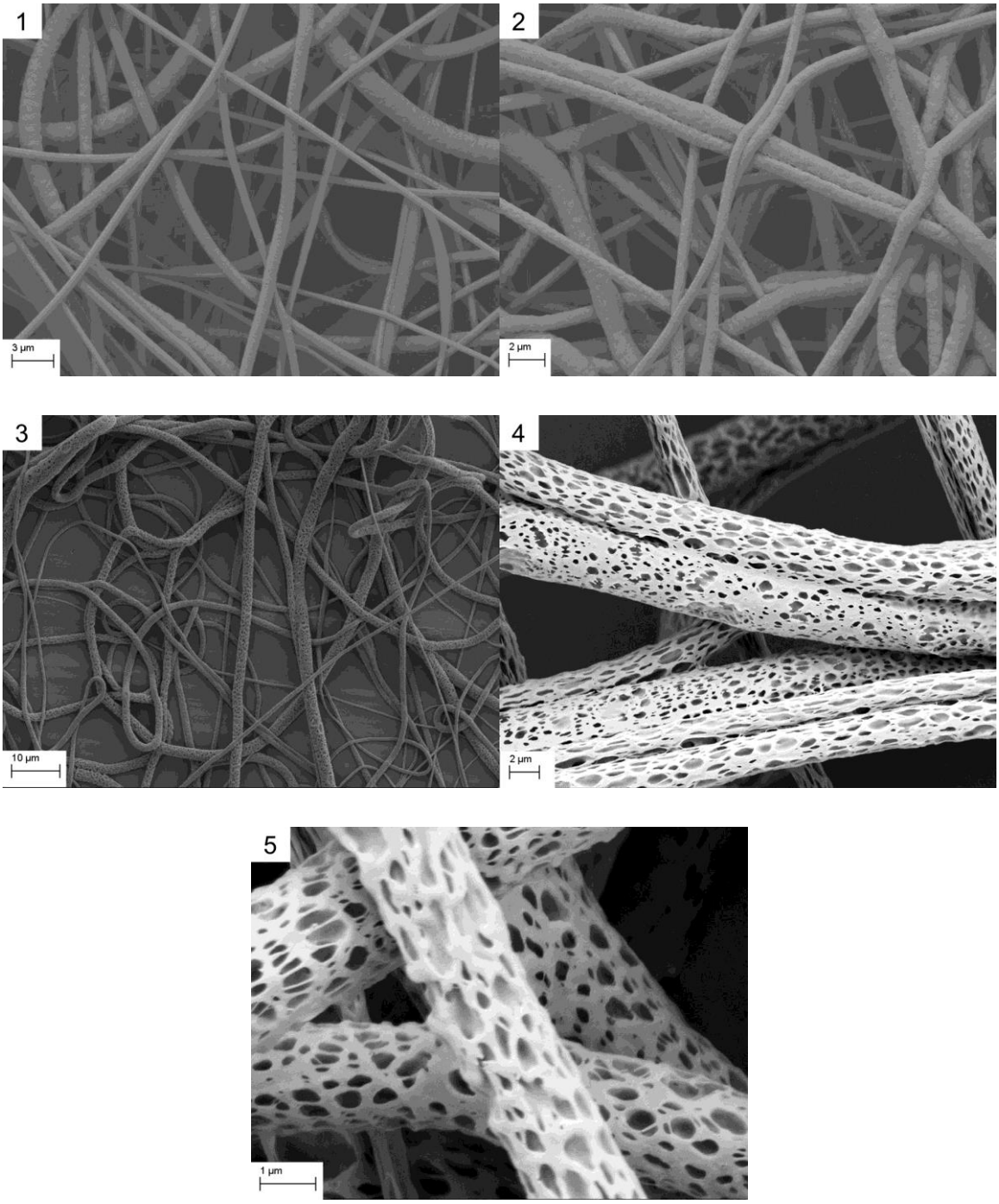

Figure 4.8. SEM images of the fibrous networks. Numbers on the top left corner represent the sample number.

The three necessary values for the calculation of the theoretical specific surface area parameters (Young's modulus, Poisson's ratio and polycaprolactone surface tension) were obtained from the literature. Croisier et al. (2012) determined that the Young's modulus of electrospun PCL fibres to be approximately 3.7 GPa, whereas the a

value of 0.3 was used for Poisson's ratio (Williams et,al., 2005, Eshraghi and Das, 2005). 0.04 J/m^2 was used as surface tension of polycaprolactone (Cava et al., 2007). The experimentally measured geometrical and physical properties of the fibrous network are shown in **Table 4.2**, whereas **Table 4.3** summarizes the results predicted by the three theoretical models and the experimentally obtained values for the specific area of the five electrospun fibrous networks.

Table 4.2. Geometrical and physical properties of the produced fibrous networks (network density, fibre diameter, network thickness, fibre aspect ratio).

Sample	ρ (kg/m^3)	d (nm)	t (mm)	λ
1	987	970	0.47	2110
2	1013	900	0.38	2840
3	1028	1500	0.32	3680
4	910	3310	0.27	2770
5	967	2320	0.41	3130

Table 4.3. Theoretical predictions, based on the three contact models, and experimentally obtained values of the network specific surface area.

Sample	Hertzian model (m^2/g)	DMT model (m^2/g)	JKR model (m^2/g)	Experimental (m^2/g)
1	3.57	2.91	2.19	2.29
2	3.85	3.36	2.84	2.73
3	2.31	2.23	2.14	2.63
4	1.05	1.04	1.02	1.61
5	1.49	1.45	1.41	2.15

Keeping in mind the first objective of the chapter, i.e. the verification of surface area increase due to pore induction, a comparison of surface area of porous and non-porous networks has to be made. An alternative approach is to compare the experimentally measured specific areas to a reference point. That point is the maximum specific area that a fibrous network, composed of smooth surface fibres with a given diameter, can achieve, as defined by equation (4.7). Non-porous fibres

cannot surpass that threshold, therefore, if the porous fibres were able to exceed it, pore induction would be proven to be successful technique in terms of specific surface area increase. Indeed, the experimental results prove that point (**Figure 4.9**).

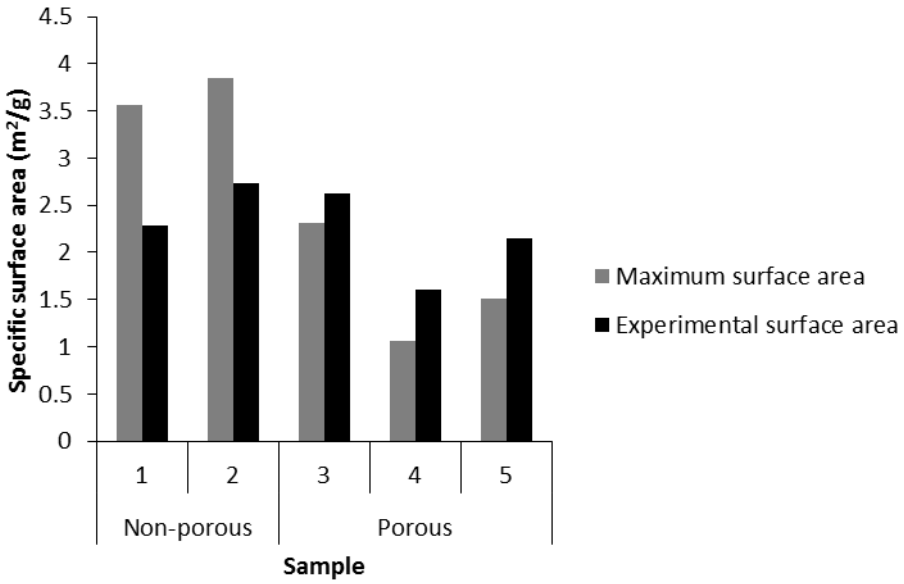

Figure 4.9. Comparison of the theoretical maximum surface area of a fibrous network to the experimentally observed. The left column represents the surface area of a network composed by non-porous fibres with diameters equal to the respective experimental diameters.

In the case of fibres with a smooth surface the experimentally observed network surface area is always lower than the maximum (around 36 and 29% less for samples 1 and 2, respectively), due to the fibre-to-fibre contacts. In the case of porous fibres, however, the maximum surface area is always surpassed (by 14, 52 and 42% for samples 3, 4 and 5, respectively). As shown in equation (4.7) the maximum available specific surface area is inversely proportional to the density of the material composing the fibres. In the case of smooth surface fibres, the fibres are exclusively composed of the polymer, therefore, the fibre density and the polymer density match. On the other hand, in the case of porous fibres, the fibre body is a mixture of polymer and air. Since air is lighter than the polymer, the fibre density is lower compared to smooth surface fibres and subsequently the maximum available specific surface area of the network is increased.

Having verified the increase of the specific surface area following pore induction on electrospun networks, the remaining question was the quantification of that increase. The approach previously presented underestimates the specific area increase, since the excluded surface area due to fibre-to-fibre contacts was not taken into account in the case of the porous network. In order to include that, equations (4.30), (4.33) and (4.34) were used to identify the contact model which calculates the contact area of polycaprolactone fibres more accurately. The theoretical predictions were tested only for the non-porous networks (**Figure 4.10**).

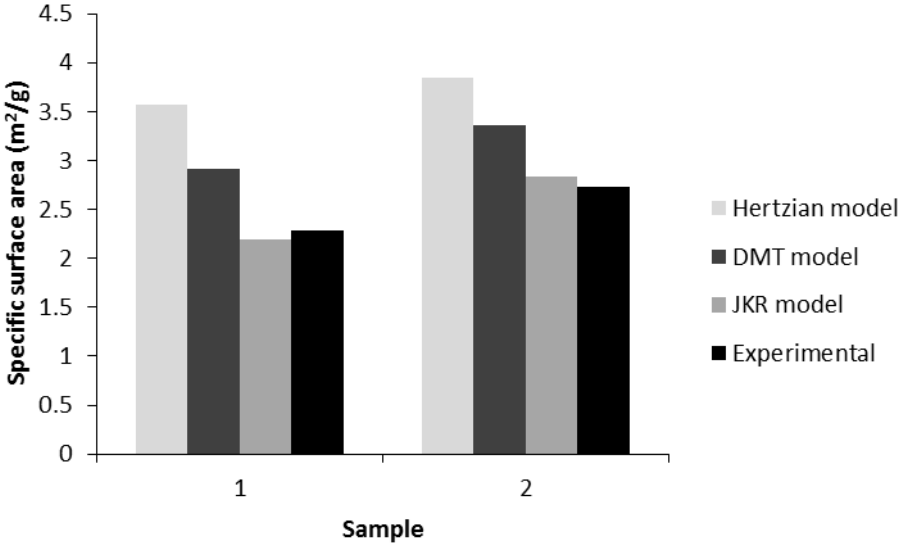

Figure 4.10. Comparison of theoretical model predictions and experimentally observed specific surface area values for networks composed by smooth surface fibres.

In both cases the experimentally obtained values comply with the JKR model. Experimental value of SSA for sample 1 was 2.29 m^2/g (predicted value based on JKR model 2.19 m^2/g), whereas for sample 2 the experimental value was 2.73 m^2/g (predicted value based on JKR model 2.84 m^2/g).

Having verified that the JKR contact model can provide accurate results for the prediction of the polycaprolactone fibrous network SSA, the theoretical values of the SSA for non-porous networks with similar to porous geometrical characteristics were calculated for samples 3, 4 and 5. The results are demonstrated in **Figure 4.11**.

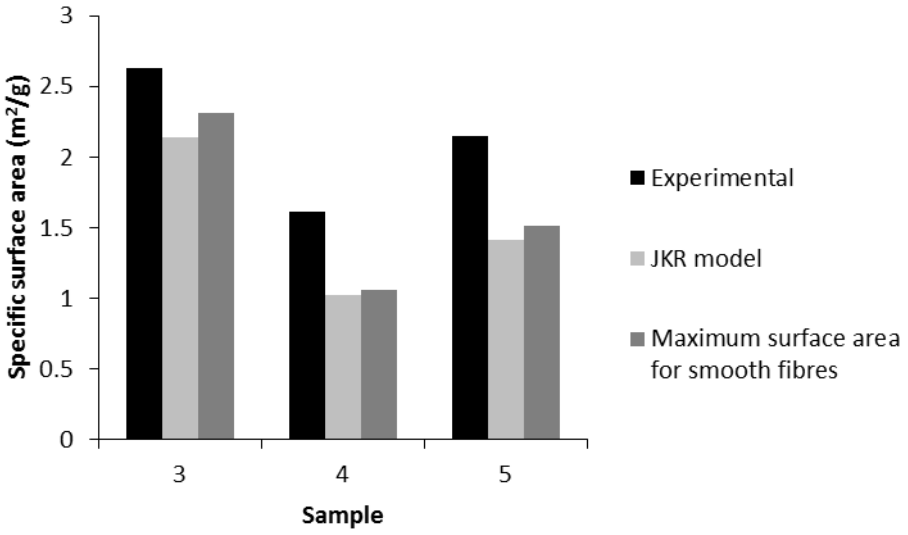

Figure 4.11. Specific surface area increase due to pore induction. The comparison is made against non-porous networks and considering JKR fibre-to-fibre contacts.

Considering the theoretically predicted values, the increase of the network SSA can be calculated as 23, 58 and 52% for samples 3, 4 and 5, respectively. The variance of the SSA increase between samples 3, 4 and 5 can be attributed to the different experimental conditions used for their production and is examined in detail in Chapter 6.

It should be noted that the developed models presented in this study are not expected to be universally applicable in electrospun fibrous networks. Phenomena like bead presence on the fibres, varying fibre cross sections (e.g. ribbon), special fibre orientation (e.g. aligned) or incomplete fibre drying are common in electrospinning and should be taken into account in individual cases.

4.5. Conclusions

Increase in SSA of electrospun fibrous network due to pore induction was investigated in this study. Theoretical contact mechanic models based on Hertz, DMT and JKR, correlating the network SSA to its physical properties as well as geometrical characteristics (such as fibre diameter, fibre aspect ratio, network

density, and network thickness) were developed. The models offer a more detailed analysis of the factors contributing to the configuration of electrospun network SSA. SSA of networks composed by porous fibres is up to 52% higher than the maximum SSA that non-porous fibres could achieve. JKR model describes accurately the fibre-to-fibre contact area under the experimental conditions used for pore generation. Overall, pore induction was proven, both experimentally and theoretically, to increase the network SSA up to 58%, compared with equivalent non-porous networks.

5. Solvent Effect in Electrospinning-NIPS Technique

5.1. Abstract

The effect of different binary solvent systems on the size and surface morphology of electrospun poly(ε-caprolactone) (PCL) fibres is examined in this chapter. Chloroform (CF), dichloromethane (DCM), tetrahydrofuran (THF) and formic acid (FA) were used in mixtures with dimethyl sulfoxide (DMSO) in order to generate pores on the fibre surface, through a combinating electrospinning - Non-solvent Induced Phase Separation (NIPS) mechanism. The production of porous, bead free fibres with an average diameter ranging from 1470 to 2270 nm was achieved using 12.5% w/v PCL in CF/DMSO solution with good/poor solvent ratios varying from 75-90% v/v at the applied voltage of 15 kV, a spinning distance of 20 cm, and the feed flow rate of 1 ml/h. DCM and THF were proven to be less suitable good solvents for the process due to the formation of a solid skin on the jet surface, caused by the limited diffusivity of the polymer molecules from the jet surface to the liquid core and its subsequent collapse. FA was found to be unsuitable due to an evaporation rate similar to DMSO. The pore formation was favoured at high good/poor solvent ratios, whereas, the production of fibres with ribbon cross sections or fibres with beads was more pronounced at low good/poor solvent ratios. Data fitting was used for the development of a second order polynomial equation, correlating the fibre average diameter to the solution parameters (conductivity, surface tension, and viscosity), for the given polymer and solvent systems, under the specific experimental conditions used in this study. The ternary mixture compositions that lead to the formation of porous fibres were mapped on a ternary graph.

5.2. Introduction

The single step production of porous poly(ε-caprolactone) (PCL) fibres through a combinating electrospinning and non-solvent induced phase separation (NIPS) technique is investigated in this chapter. Chapter 2 has presented the work that has been previously done in the field, however, the complexity of the process forces further investigation of the method. The main objectives of this chapter are the identification of solvent systems that can lead to the production of porous, bead free fibres, the investigation of the good solvent's properties and good/poor solvent ratio

effect in the process and the correlation of the feed solution's properties (conductivity, surface tension, and viscosity) to the fibre size.

The lack of ability to simultaneously control all the solvent/solution properties lead to the selection of one-factor-at-a time as the investigating method. Four common PCL solvents (chloroform (CF), dichloromethane (DCM), tetrahydrofuran (THF) and formic acid (FA)) were used for the investigation of the good solvent effect in the process. The first criterion for their selection was the ability of these solvents to produce electrospinnable solutions. The second criterion was the wide range of physical properties and characteristics that these solvents possess. CF was used as a reference solvent, DCM was used due to its comparatively lower boiling point, THF was used due to its miscibility with water and FA has a higher boiling point and dielectric constant compared to the other good solvents. Dimethyl sulfoxide (DMSO) was selected as a poor solvent based on its high dielectric constant, its miscibility with all the good solvents and its high boiling point. The physical properties of the solvents used in this work are summarized in **Table 5.1**.

Table 5.1. Physical properties of the solvents used in this work.

Solvent	Boiling point (^{o}C)	Dielectric constant at 20 ^{o}C	Surface tension at 20 ^{o}C (mN/m)	PCL solubility
CF	61	4.8	27.2	Good
DCM	40	9.1	28.1	Good
THF	66	7.6	28.0	Good
FA	101	58.0	37.7	Partial
DMSO	189	46.6	43.7	Poor

The solvent/non-solvent ratio in the solvent mixture effect in the process is also investigated in this chapter. Polymer solutions based on three of the good solvents (CF, DCM, THF), were prepared with solvent/non-solvent ratios varying from 50-100% v/v, with an interval of 10% v/v. The solution concentration was 12.5% w/v in all

cases and the solutions were electrospun under the same conditions (applied voltage of 15 kV, spinning distance of 20 cm, feed flow rate of 1 ml/h). The morphological evolution of the fibres produced by different solvent/non-solvent ratio solutions can provide additional information for the good solvent effect on the fibre morphology, as well. The particularities of the FA based solutions, however, dictated a variation in the experimental conditions. FA is not as good solvent of PCL as the rest investigated solvents, thus, the complete polymer dissolution requires more time. Given that FA is a catalyst for PCL depolymerisation reaction though, the extended time for polymer dissolution result in simultaneous polymer MW decrease. Nonetheless, the solution concentration reduction to 10% w/v and the use of only one high good/poor solvent ratio (90% v/v) allows a separate investigation of that solvent as well. The experimental conditions used in that case were the same as in all the other experiments.

5.3. Physical properties of feed solutions

Characterization of feed solution properties facilitates the description of the process and can provide the necessary data for the development of an empirical equation correlating the initial state to the end product properties. As analysed in Chapter 2, the three main solution parameters that affect electrospinning are conductivity, surface tension and viscosity. The results from the experimental measurements of the above mentioned properties for the CF, DCM and THF based solutions are shown in **Figure 5.1**. Complete data can be found in Appendices A and B.

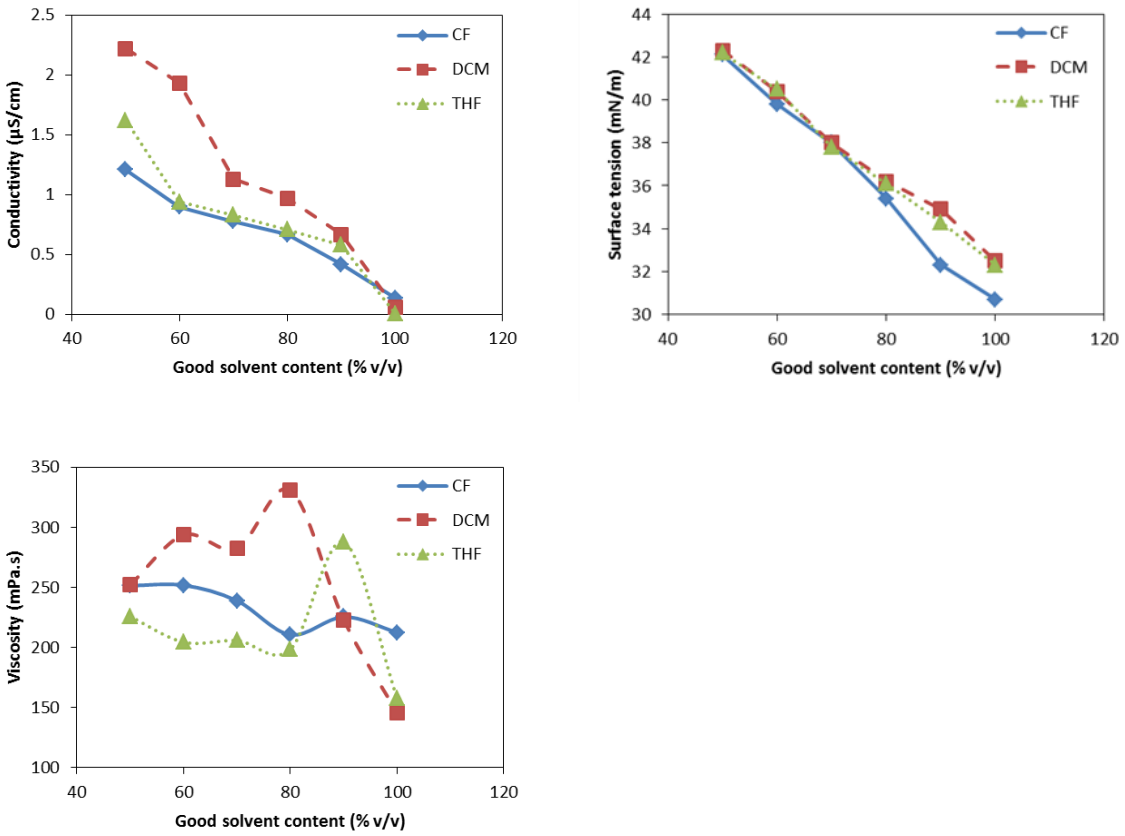

Figure 5.1. Feed solution properties (A) Conductivity, (B) Surface tension, (C) Viscosity. DMSO is the poor solvent in all the cases.

The addition of increasing amounts of DMSO in the feed solutions results in an increase in both, solution conductivity and surface tension regardless of the good solvent of the solution. This was expected, since both the conductivity and surface tension of DMSO are higher than any of the good solvents (**Table 5.1**). On the other hand no relationship between the amount of non-solvent and viscosity of the solution could be established. This may be a result of the complex molecular interactions developed within the solution between polymer, good solvent and poor solvent.

5.4. Chloroform based solutions

Figure 5.2 shows the fibres produced from CF based solutions, with increasing DMSO content in the feed solution.

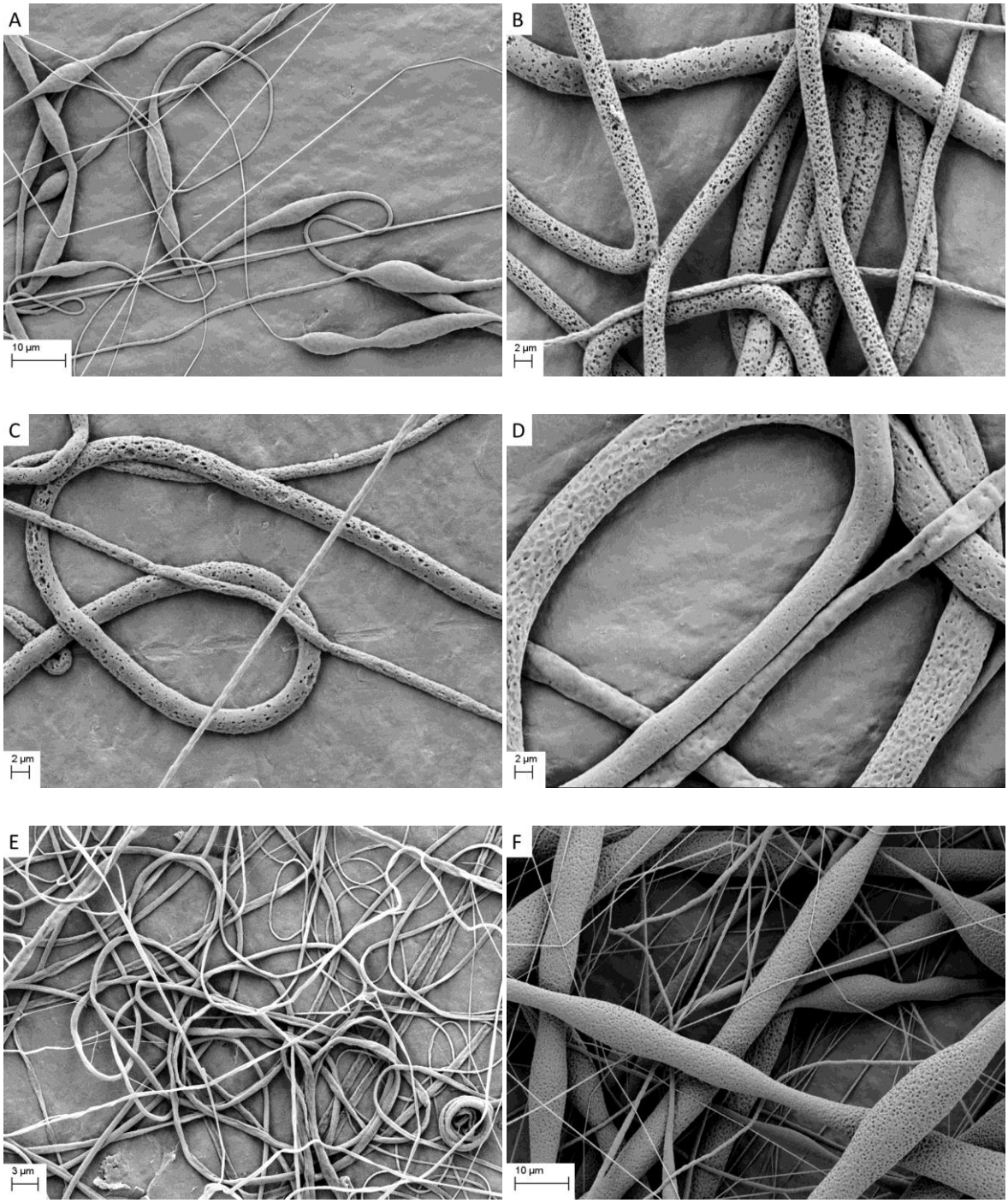

Figure 5.2. SEM pictures of the fibres produced by CF/DMSO solutions. The polymer concentration in the feed solution was 12.5% w/v in all cases and the concentration of good solvent in the good/poor solvent mixture was: (A) 100 % v/v, (B) 90 % v/v, (C) 80% % v/v, (D) 70% v/v, (E) 60% v/v, (F) 50% v/v.

The average diameters of the fibres and their coefficient of variation are summarized in **Table 5.2**.

Table 5.2. Fibre average diameter and coefficient of variation for fibres produced by CF based solutions (* the diameter refers to the width of fibres with ribbon cross sections).

CF amount (% v/v)	Fibre average diameter (nm)	Coefficient of variation (%)
100	600	49
90	2270	35
80	1470	40
70	2120	67
60	650*	52
50	550	54

Initially, the use of CF as a single solvent resulted in the production of non-porous fibres with bead-on-string morphology. This morphology could be caused by the low dielectric constant of chloroform. The addition of small amounts of non-solvent (10 and 20% v/v), however, modified the fibre morphology. The fibres exhibited porous surface and the beads were eliminated due to the higher solution conductivity compared with pure CF. The higher evaporation rate of CF compared to that of DMSO alters the composition of the electrospinning jet during its travel, since the amount of CF that evaporates is greater than the amount of DMSO. The transition of the binary solvent system from the stable, one phase region to the unstable, two phase region causes the initiation of the phase separation mechanism. The surface morphologies of the fibres indicate the successful completion of the mechanism. The pores are irregularly shaped, have varying depth and wide size distribution, which are characteristics that accompany the structures produced by phase separation. The observed reduction of the fibre diameter from 2270 to 1470 nm accompanying the increase of the DMSO concentration in the electrospinning solution from 10% to

20% v/v can be attributed to the increase of the conductivity of the solution from 0.42 to 0.67 μS/cm.

A further increase of the DMSO content in the initial solution, however, results in a different course of events. A tendency for pore elimination and transformation of circular fibre cross sections to elliptical or ribbon is observed when the DMSO concentration in the feed solution is 30% v/v, and this tendency is completed at higher DMSO concentrations (CF 60% v/v) with the production of fibres with smooth surface and ribbon cross sections. Fibres with similar morphologies have been reported previously (Koombhongse et al, 2001) and this morphology is caused by the formation and subsequent collapse of a solid skin on the surface of the electrospinning jet. As mentioned before, the evaporation of the solvents occurs mainly from the surface of the jet. The diffusion of the remaining polymer molecules from the jet surface to the liquid core, however, is hindered by the increased amount of the lower evaporation rate non-solvent. The consequent polymer accumulation on the jet surface is responsible for the skin formation. The evaporation of the solvents from the liquid core continues to occur through the solid skin. When the core isn't able to provide support to the skin, it collapses under forces applied on it by the atmospheric pressure (**Figure 5.3**).

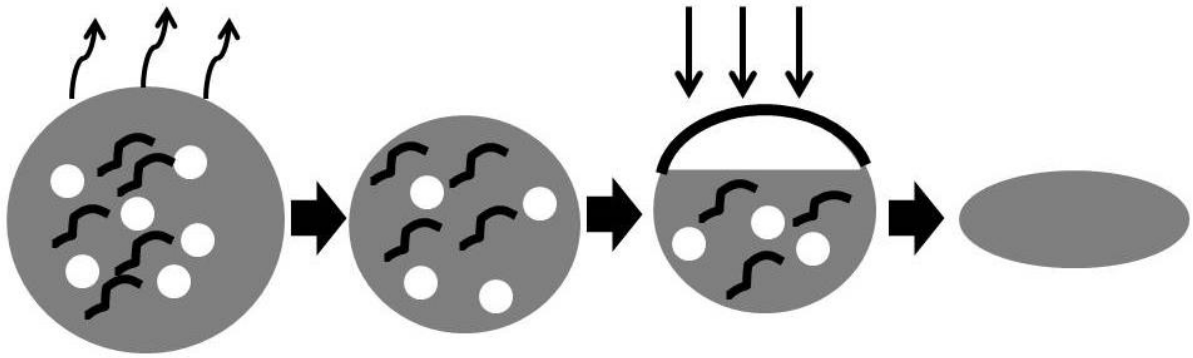

Figure 5.3. Formation of fibres with ribbon cross sections. The white points represent the DMSO molecules, whereas the black lines are the polymer chains.

Another interesting phenomenon is the presence of beads when the amount of DMSO was increased to 50% v/v. There are two possible explanations for this

phenomenon. Wei et al. (2013) adapted the theory that large non-solvent amounts can cause the formation of heterogeneous regions within the electrospinning jet. In this case, this formation is enhanced, since in the existing amount of non-solvent (DMSO) the addition of water by its absorption from the atmosphere should be taken into account. The different viscosities of those regions lead to the formation of fibres with different diameters. The presence of beads can be attributed to the presence of regions with low viscosities. A second explanation involves the subsequent increase of the surface tension after the water absorption. The water contribution can elevate the surface tension of the jet up to the point, where, it can prevail over the forces applied by the electric field, and, therefore, lead to bead formation.

In summary, the morphological evolution of the fibres with increasing amount of non-solvent is shown in **Figure 5.4**.

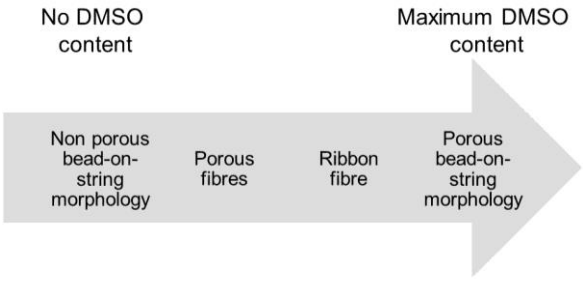

Figure 5.4. Fibre morphology changes with increasing amount of non-solvent.

5.3. Dichloromethane based solutions

Figure 5.5 shows the fibres produced from CF based solutions, with increasing DMSO content in the feed solution. The average diameters of the fibres and their coefficient of variation are summarized in **Table 5.3**.

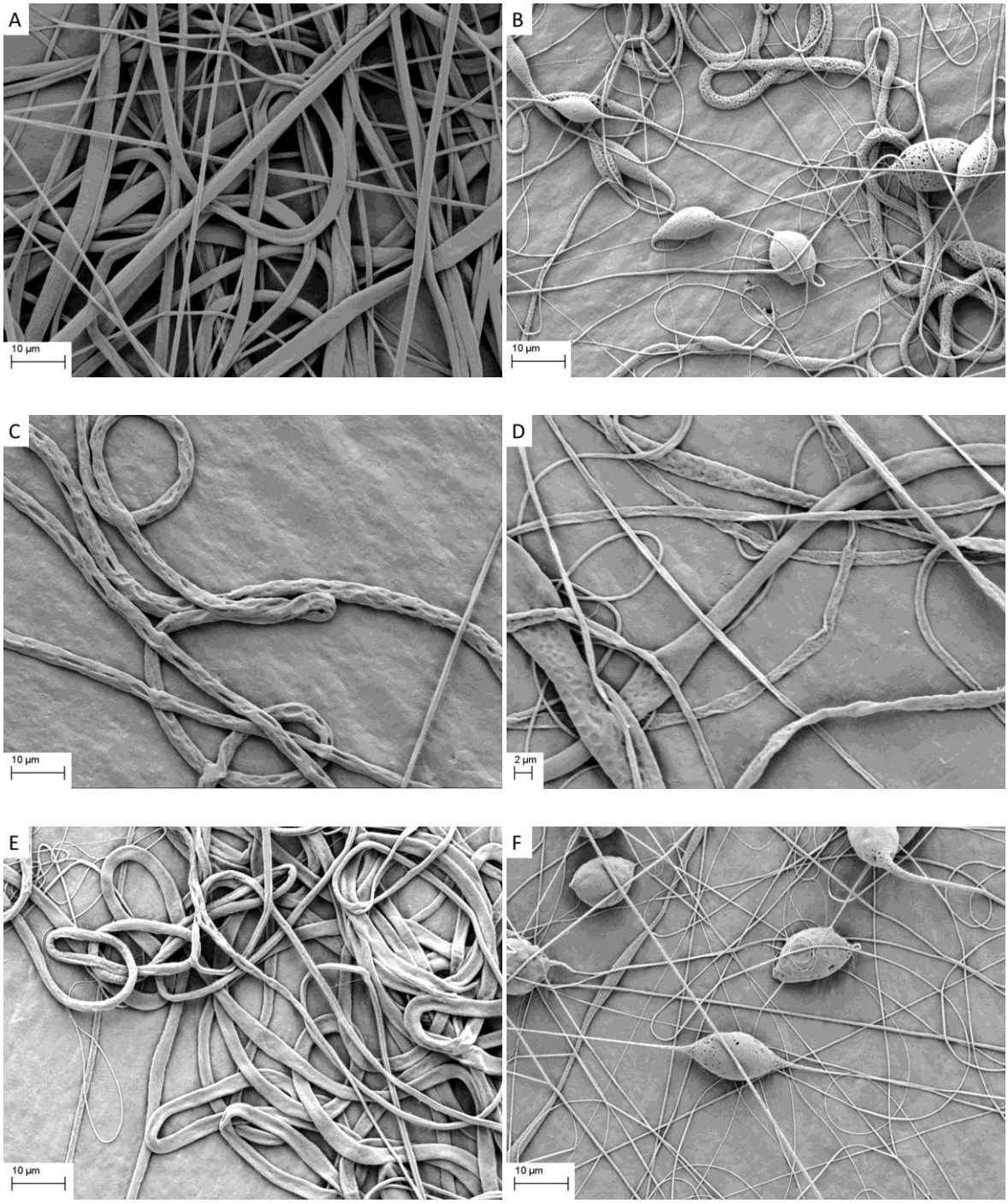

Figure 5.5. SEM pictures of the fibres produced by DCM/DMSO solutions. The polymer concentration in the feed solution was 12.5% w/v in all cases and the concentration of good solvent in the good/poor solvent mixture was: (A) 100 % v/v, (B) 90 % v/v, (C) 80% % v/v, (D) 70% v/v, (E) 60% v/v, (F) 50% v/v.

Table 5.3. Fibre average diameter and coefficient of variation for fibres produced by DCM based solutions (* the diameter refers to the width of fibres with ribbon cross sections).

DCM amount (% v/v)	Fibre average diameter (nm)	Coefficient of variation (%)
100	1550	40
90	600	21
80	2900	26
70	1030*	53
60	2150*	36
50	470	38

DCM and CF based feed solutions possess similar properties in terms of solution conductivity, surface tension and viscosity, therefore, the observed differences in the fibre morphology and size have to be attributed to other parameters. The key parameter is the DCM volatility, which is higher than that of CF. Even though the CF and DCM solutions have the same initial concentration, the higher evaporation rate of DCM results the formation of a more dense jet compared to those found in CF. The increased viscosity of the jet facilitates the formation of a solid skin on the jet surface, due to difficulties that the polymer chains are facing in their migration from the surface to the liquid core (Demir 2010).

When DCM was used as a single solvent (**Figure 5.5.A)**, the fibre morphology was a mixture of fibres with circular and ribbon cross sections. In contrast with the use of chloroform as a single solvent system, no beads were observed on the fibres. The bead absence can be attributed mainly to the higher DCM dielectric constant (9.1), and also to the higher evaporation rate and the subsequent increase of the solution concentration. The circular shape and the comparable sizes and depth of the observed pores on some fibres, indicate that they were produced by the breath figures mechanism.

The variations, which are observed from the CF morphological evolution for the binary solvent systems, can be explained by the difference of CF and DCM evaporation rate as well. Low DMSO concentrations (10% v/v) were proven to be suitable for the formation of pores on the fibre surface, similarly to the CF based solutions. The presence of beads is the feature that differentiates the fibre morphologies in these cases. Two phenomena described above, the formation of heterogeneous regions within the jet and the increase of the jet surface tension following water absorption, could be used as possible explanations for the bead formation. A further increase of the DMSO concentration (20% v/v) in the feed solution caused the formation of fibres with wrinkled surface. It is interesting to note that the diameter of these fibres is 2900 nm, due to higher solution viscosity. In that case a solid skin formed on the surface of the jet, however, since the large diameter of the fibres leads to longer drying time, the drying has not been completed and when their collapsing occurred they were in quasi solid state and, therefore, it was not uniform. The elongated shape of the pores supports this theory, since the stretching of the fibres continues to occur when they are at the quasi solid state. Complete drying of the fibre skin, in the cases where the DMSO amount in the feed solution was 30 and 40% v/v, was a result of the smaller fibre size (diameters 1030 and 2150 nm, respectively), and, hence, its uniform collapsing led to the production of fibres with ribbon cross sections. The beads that were observed when the non-solvent content was increased to 50% v/v could be attributed either to the formation of heterogeneous regions within the jet or to the subsequent increase of the surface tension after the water absorption.

In summary, the morphological evolution of the fibres with increasing amount of non-solvent is shown in **Figure 5.6**.

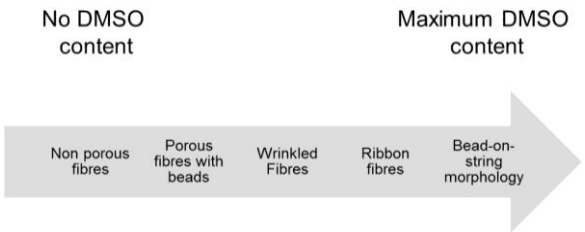

Figure 5.6. Fibre morphology changes with increasing amount of non-solvent.

5.4. Tetrahydrofuran based solutions

Figure 5.7 shows the fibres produced from THF based solutions.

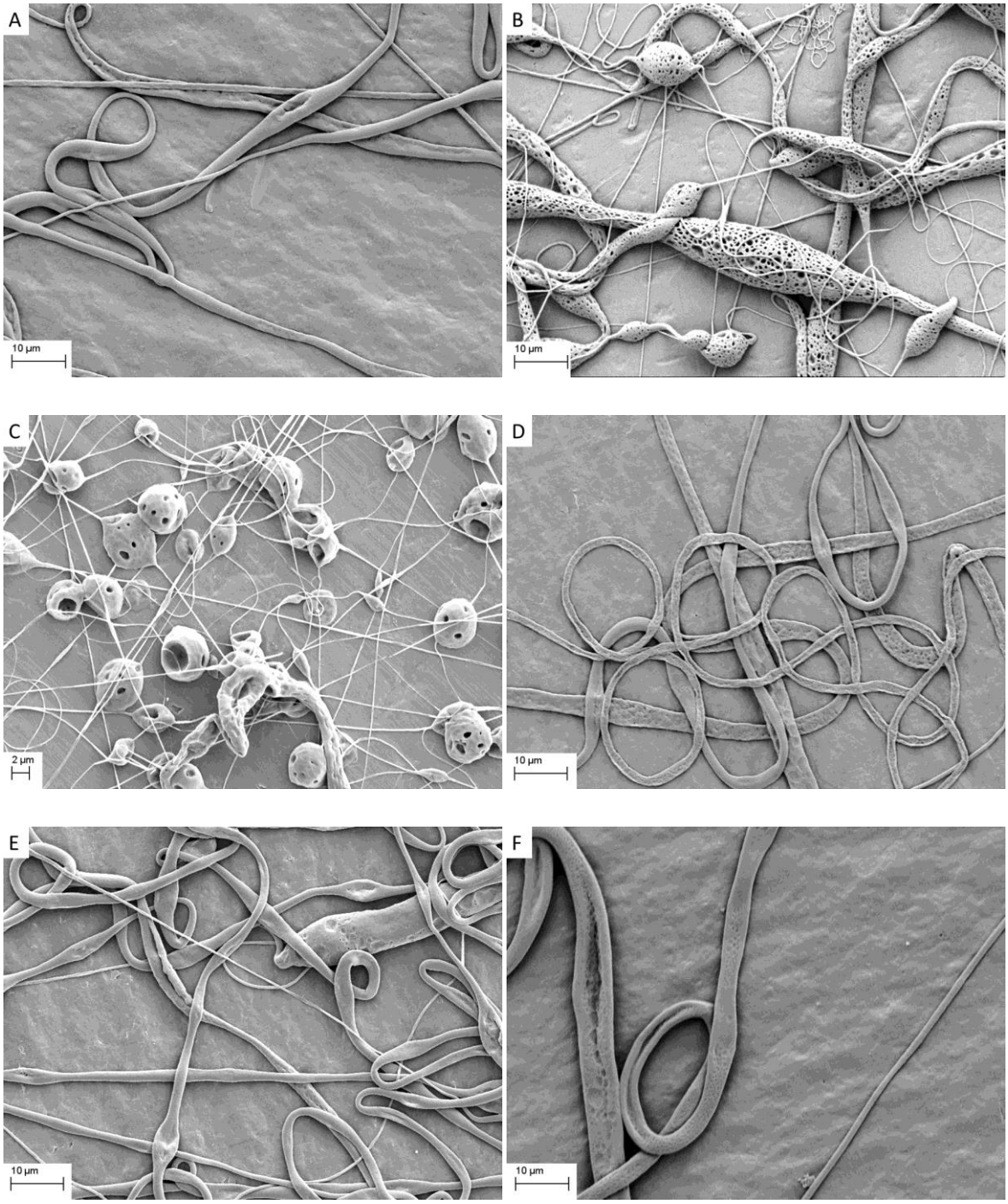

Figure 5.7. SEM pictures of the fibres produced by THF/DMSO solutions. The polymer concentration in the feed solution was 12.5% w/v in all cases and the concentration of good solvent in the good/poor solvent mixture was: (A) 100 % v/v, (B) 90 % v/v, (C) 80% % v/v, (D) 70% v/v, (E) 60% v/v, (F) 50% v/v.

The average diameters of the fibres and their coefficient of variation are summarized in **Table 5.4**

Table 5.4. Fibre average diameter and coefficient of variation for fibres produced by THF based solutions (* the diameter refers to the width of fibres with ribbon cross sections).

THF amount (% v/v)	Fibre average diameter (nm)	Coefficient of variation (%)
100	1460	35
90	900	73
80	280	24
70	1180*	52
60	1390	38
50	2412*	34

THF based feed solutions' properties are similar to those of CF based solutions. In addition to that, THF and CF have similar boiling points (61 and 66 ^{o}C, respectively). The key parameter for the observed differences in the fibres morphology and size is THF's increased miscibility with water. This miscibility enhances the absorption of larger amounts of water from the atmosphere, compared to other solvent systems, and also facilitates the diffusion of the water within the jet.

The lack of beads that is observed when THF was used as a single solvent can be attributed to the relatively high dielectric constant of THF (7.6).

The addition of small amounts of DMSO (10 and 20 % v/v) to the feed solutions resulted in the presence of beads on the fibres. In those cases, the evaporation of THF and, mainly, the simultaneous absorption of larger amounts of water, compared to the CF and DCM based solutions, due to its miscibility with THF, contribute to the formation of heterogeneous regions within the jet, which could cause the bead formation. In support of this theory is the high normalised standard deviation of the fibre diameter (73%) for the solution where 10% v/v DMSO was added.

A further increase of the DMSO amount in the feed solution to 30% v/v or above, however, results in the predominant production of fibres with ribbon-shaped cross section. As mentioned before, the formation of a solid skin is the reason for these morphologies. In those cases the skin formation is favoured due to the presence of large amounts of non-solvent, which hinders the diffusion of the polymer chains from the jet surface to the core. It should be noted that, besides the DMSO which was present in the initial solution, the larger amounts of the absorbed water will also enhance this phenomenon.

The significance of the THF miscibility with water is highlighted by a comparison of the fibre morphologies for the samples where the good solvent concentration was 50% v/v. In the case of THF, no beads are observed (Figure 5.7.F) in contrast to the observed morphologies for the CF and DCM based solutions (Figures 5.2.F and 5.5F, respectively). A possible explanation is that the water, which is absorbed by the atmosphere, is distributed more uniformly within the jet due to its miscibility with THF and the formation of heterogeneous regions, with different viscosities, is avoided. In support of this theory is the lower coefficient of variation of the fibre diameter that is observed for the THF based solution (34%) compared to the CF and DCM based solutions (54 and 38%, respectively).

In summary, the morphological evolution of the fibres with increasing amount of non-solvent is shown in **Figure 5.8**.

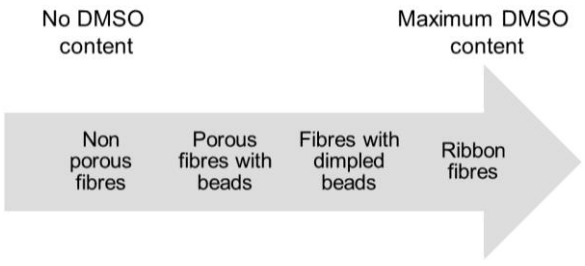

Figure 5.8. Fibre morphology changes with increasing amount of non-solvent.

5.4. Formic acid based solutions

FA based solutions were tested for the production of porous PCL fibres, however, the experiments cannot be directly compared to the other solutions. FA is not as good solvent for PCL as CF, DCM and THF, therefore the preparation of the solutions required longer time. During that time, the depolymerisation reaction of PCL is accelerated due to the presence of the acid, which acts as catalyst. This reaction results in the reduction of the PCL MW to non electrospinnable levels. That issue was partially addressed by the reduction of the solution concentration from 12.5 to 10% w/v and the preparation of solution with high solvent/non-solvent ratio (90% w/v).

The fibres that were produced from FA based solutions are shown in **Figure 5.9** and the properties of the feed solutions are summarized in **Table 5.5**.

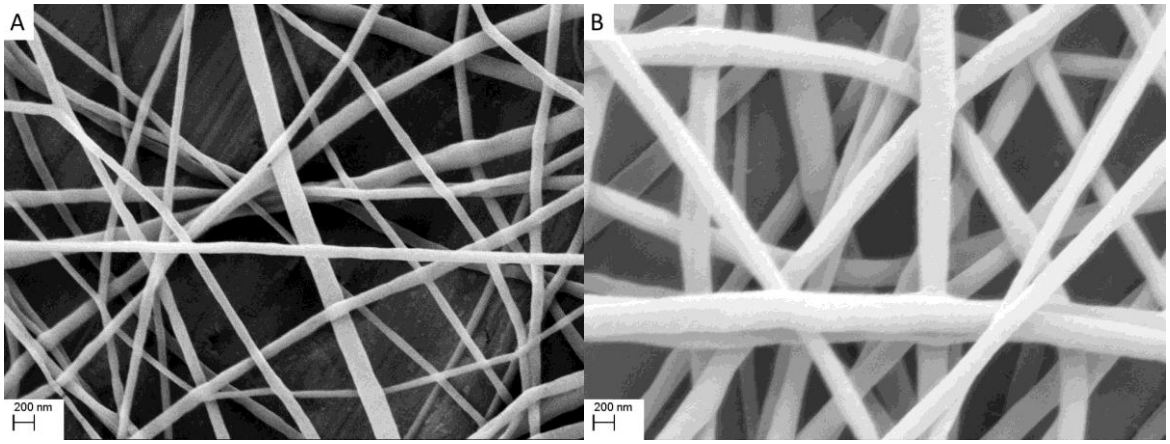

Figure 5.9. SEM pictures of fibres produced by FA based solutions. The polymer concentration in the feed solution was 10% w/v in both cases and the concentration of good solvent in the good/poor solvent mixture was: (A) 100 % v/v, (B) 90 % v/v.

Table 5.5. Feed solution properties and fibre average diameter and coefficient of variation for fibres produced by FA based solutions.

FA concentration (% v/v)	Conductivity (μS/cm)	Surface tension (mN/m)	Viscosity (mPa.s)	Fibre average diameter (nm)	Coefficient of variation (%)
100	9.8	39.7	111.5	100	29.7
90	3.4	40.8	180.9	250	39.0

The use of FA as a single solvent results in the production of fibres with extremely small diameters. The increased conductivity and dielectric constant and the reduced viscosity of the solution can be held responsible for that phenomenon. The addition of small amount of DMSO (10% w/v) in the feed solution, doesn't significantly change the morphology or the size of the fibres. The increase of the fibre diameter can be attributed to the subsequent decrease of conductivity and increase of the viscosity and surface tension of the feed solution. The most interesting observation however is the absence of pores on the surface of the fibres. FA has the highest boiling point, compared to the other good solvents used in this project. Since its evaporation rate is closer to that of DMSO, the composition of the solvent mixture within the electrospinning jet doesn't change enough to cause the instability required for the initiation of phase separation. This requirement for a distinct difference between the evaporation rates of the good and the poor solvent has also been reported by Lubasova and Martinova (2011).

5.5. Development of an empirical equation predicting the fibre diameter

The ability to control or predict the fibre size based on the properties of the feed solution is of high importance. In this study, empirical modelling was implemented for the correlation of the initial solution properties to the fibre average diameter. Numerous parameters affect the outcome of electrospinning process. Out of the parameters that were varied during this study, only three (solution conductivity, surface tension and viscosity) were selected as independent variables of the equation for reasons of simplicity. The criterion for this selection was their importance in fibre formation and the best fitting of the data into an equation. Multiple linear regression analysis was implemented for the development of second order polynomial equations correlating the response variable (fibre average diameter) to the independent variables. Least squares method was used for the determination of the coefficients of the equations. All the above were performed through the use of appropriate software (Design-Expert). Fibres with beaded morphologies were not used as data for the development of the equation, since the presence of beads affects the fibre diameter.

The equation that was developed is

$$D = 8435x_1^2 - 328.0x_1x_2 - 119.5x_1x_3 + 24483x_1 - 58.24x_2^2 + 4.670x_2x_3 + 3339x_2 + 0.2620x_3^2 - 187.8x_3 - 45920 \quad (5.1)$$

where D is the predicted average diameter of the fibres (nm), X_1 is the solution conductivity (μS/cm), X_2 is the solution surface tension (mN/m), and X_3 is the solution viscosity (mPa.s).

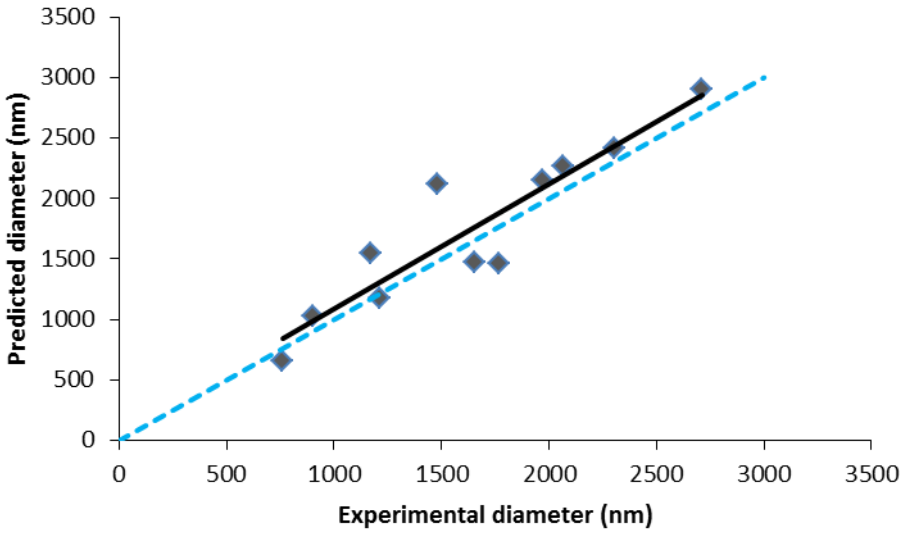

Figure 5.10. Fitting of the experimental data in the empirical equation. The black solid line represents the trendline of the experimental data, whereas the light blue dashed line the ideal fitting.

Equation (5.1) was tested for 5 different samples and the results are demonstrated in **Table 5.6** and **Figure 5.11**. Production of bead free fibres was the main criterion for the selection of the good/poor solvent ratio.

Table 5.6. Properties of the solutions used for equation testing.

Sample number	Good solvent	Good solvent amount (% v/v)	Solution conductivity (μS/cm)	Solution surface tension (mN/m)	Solution viscosity (mPa.s)
1	CF	75	0.73	36.9	228
2	DCM	75	1.01	37.5	285
3	DCM	83	0.79	35.9	252
4	THF	75	0.74	37.3	208
5	THF	83	0.73	35.9	217

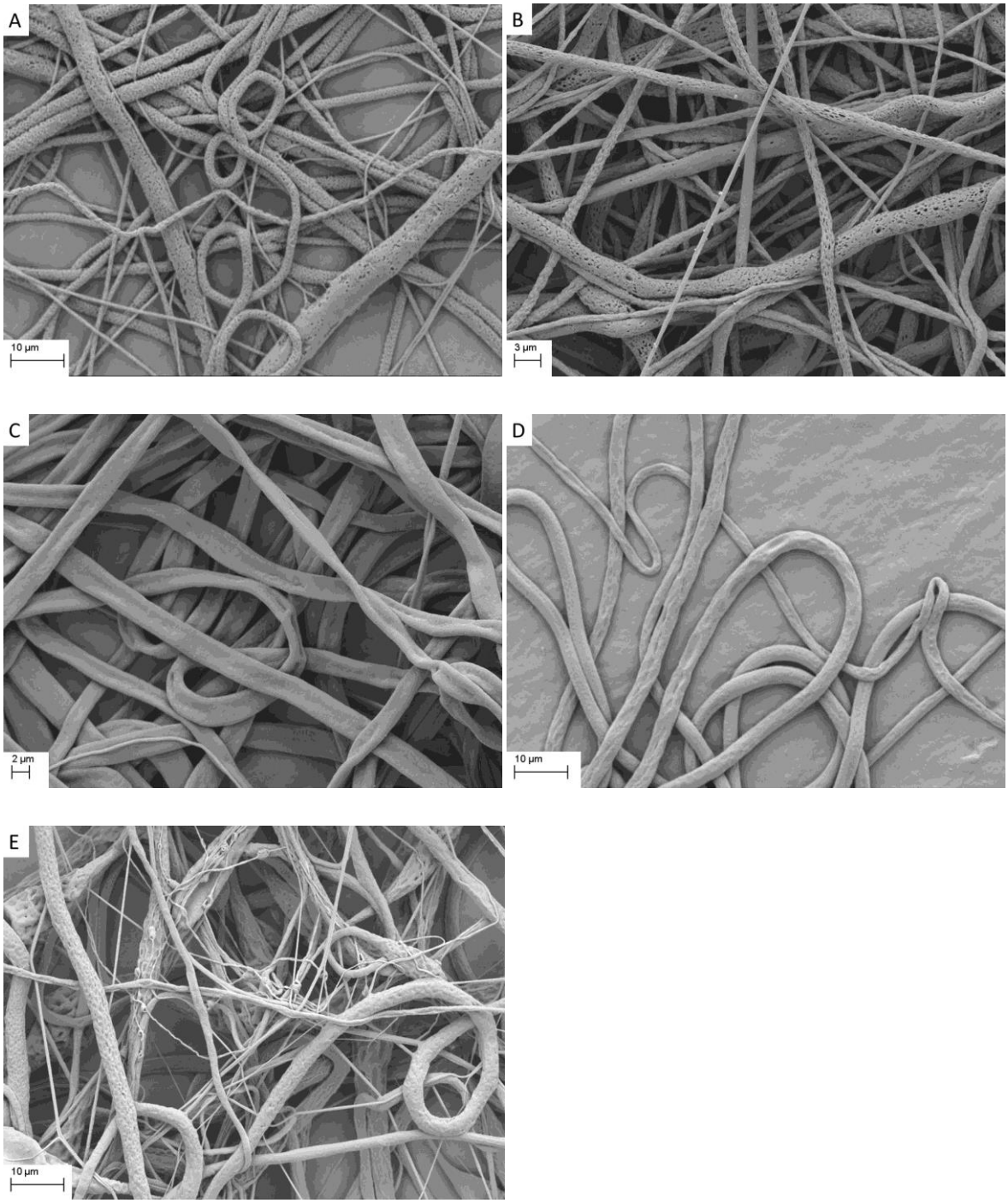

Figure 5.11. SEM pictures of the fibres produced for the testing of the empirical equation. The good solvent and its amount in the solvent mixture was: (A) CF 75% v/v, (B) DCM 75% v/v, (C) DCM 83% v/v, (D) THF 75% v/v, (E) THF 83 % v/v.

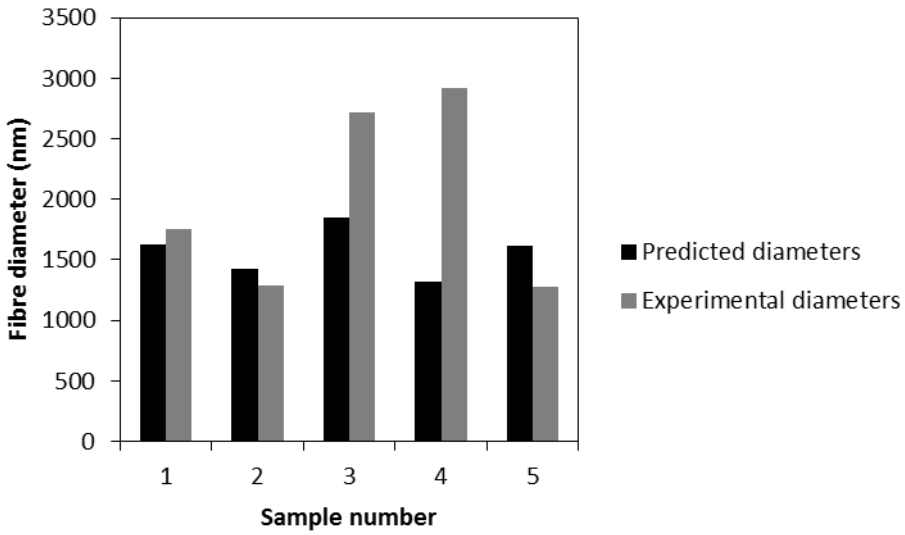

Figure 5.12. Results from testing of the empirical equation.

Figure 5.12 shows the comparison of the theoretically predicted values to the experimentally obtained. The equation predicted quite accurately the fibre diameter for the cases where the amount of good solvent (CF and DCM) was 75% v/v. The predicted diameters were 1630 and 1420 nm respectively, whereas the experimental diameters were 1750 and 1290 nm. Larger deviation was observed between the predicted and experimental diameter (1850 and 2720 nm, respectively) for the case where the amount of DCM was 83% v/v. It should be noted that the fibres had ribbon cross sections and as experimental diameter is characterised the width of the fibre. Considering a complete collapse, the fibre width can be equated to fibres with circular cross sections (Eichhorn and Sampson, 2010) and diameter of 1730 nm, which is closer to the experimentally observed value. The equation failed to predict the diameter of the fibres where the amount of THF was 75% v/v (predicted and experimental diameter 1320 and 2910 nm, respectively) and this could be due to the miscibility of THF with water and the subsequent increase of the surface tension. Finally, for the case where the amount of THF was 75% v/v the equation predicted diameter of 1610 nm, whereas the experimental diameter was 1280 nm.

5.6. Mapping the ternary composition region

The ternary system (polymer, solvent, non-solvent) that can be used for the production of porous, bead free fibres through the combination of electrospinning and phase separation should meet several requirements. The first requirement refers to the identification of the appropriate good solvent. As shown before, CF was proven to be a suitable solvent for the production of porous PCL fibres. CF has a high enough evaporation rate so as to alter significantly the jet composition after its ejection, and low enough, so as not to favour skin formation.

The second requirement refers to the identification of the suitable good/poor solvent ratio. First of all, an amount of poor solvent has to be present in order to initiate the phase separation mechanism. However, it was demonstrated that the decrease of that ratio beyond a certain limit facilitates the formation of fibres with ribbon cross sections, which is in contrast with Qi et al (2009) findings. Qi et al (2009) used a binary solvent mixture of dichloromethane (solvent) and butanol (non-solvent) for the production of porous poly(L-lactic acid) fibres and reported that the increase of the good/poor solvent ratio favours pore formation. The differences can be attributed to the lower solution concentration that Qi used (8% w/w compared to 12.5% w/v), which does not hinder the motion of the polymer from the jet surface to the liquid core as strongly as in this study. In addition to that, Qi et al (2009) used butanol as a poor solvent, which is more volatile compared to DMSO (boiling points 118 and 189 ^{o}C, respectively). Thus, the amount of poor solvent, which also hinders the polymer diffusion to the core, was decreased, and, therefore, the solid skin didn't form. In the case of the 12.5% w/v CF/DMSO system, the good/poor ratio threshold for the skin formation lies at around 70% v/v.

The third requirement refers to the electrospinnability of the ternary system. In order to produce bead free fibres, the polymer concentration must be sufficient for fibre formation. On the other hand, the excessively high polymer concentration will result in production of fibres with large diameters.

The solution concentration effect was investigated by electrospinning of solutions with various concentrations. The 10% w/v solutions were proven to be unsuitable for the production of bead free fibres, regardless of the good/poor solvent ratio (**Figure**

5.13). When the good/poor solvent ratio was 90 or 75% v/v, beads were observed on the fibres, whereas, a further increase of the poor solvent ratio (50% v/v) resulted in the production of droplets.

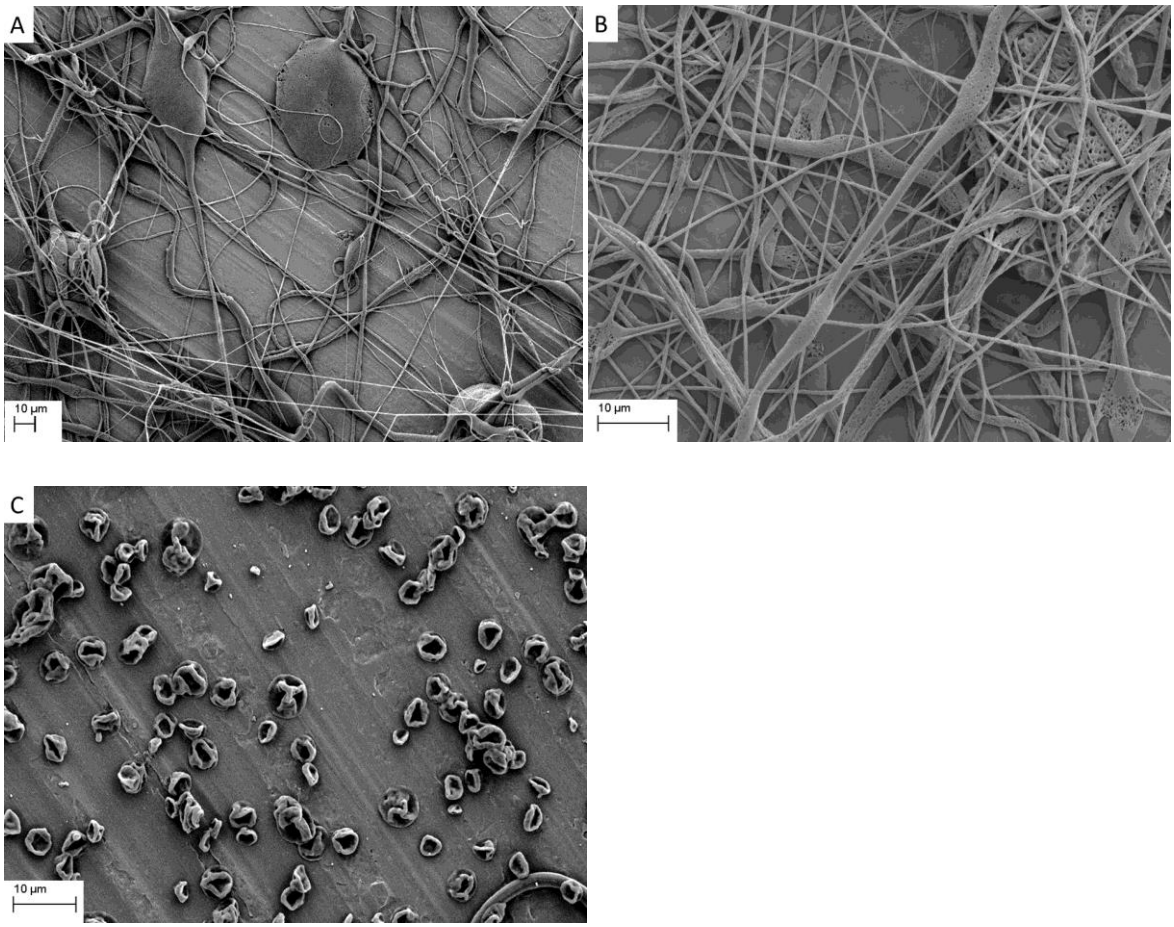

Figure 5.13. SEM pictures of the fibres produced by 10% w/v CF/DMSO solutions. The good/poor solvent ratio was: (A) 90 % v/v, (B) 75 % v/v, (C) 50% % v/v.

12.5% w/v was proven to be a suitable polymer concentration for the production of bead free PCL fibres, as shown above. In this case, the second requirement is met when the good/poor solvent ratio is held within the range of 75 to 90% v/v.

When the solution concentration was further increased (15% w/v) porous, bead free fibres were produced, however, an enormous increase of the fibre average diameter was observed (around 4360 nm) (**Figure 5.14**).

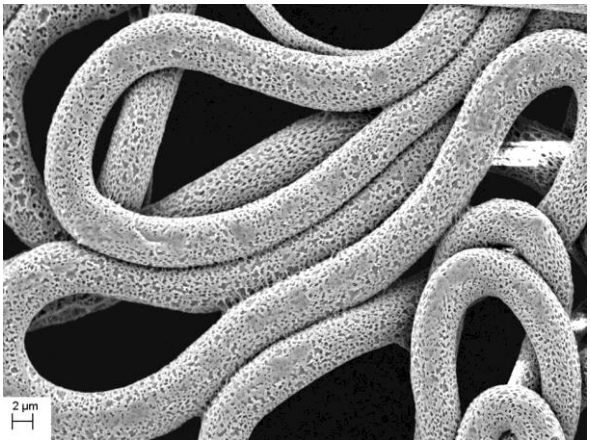

Figure 5.14. SEM picture of fibres produced by 15% w/v CF/DMSO solutions. The good/poor solvent ratio was 90% v/v.

All the above mentioned criteria are summarized in **Figure 5.15**.

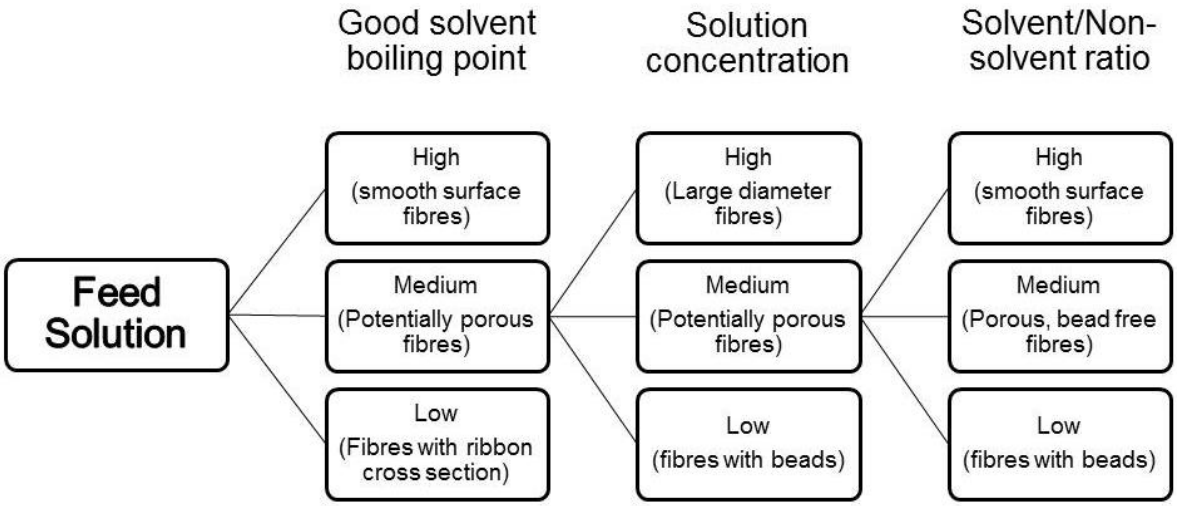

Figure 5.15. Process criteria for the production of porous, bead free fibres.

In summary, a ternary graph, indicating the regions where the process was successful, when CF was used as a good solvent was constructed (Figure **5.16**). All the compound contents of the solution were converted to weight by using their densities (ρ_{PCL}=1.145 gr/ml, ρ_{CF}=1.49 gr/ml, ρ_{DMSO}=1.1 gr/ml) and the data were

normalised. The following graph can be used to identify the regions under which the ternary system can result the production of porous, bead free fibres.

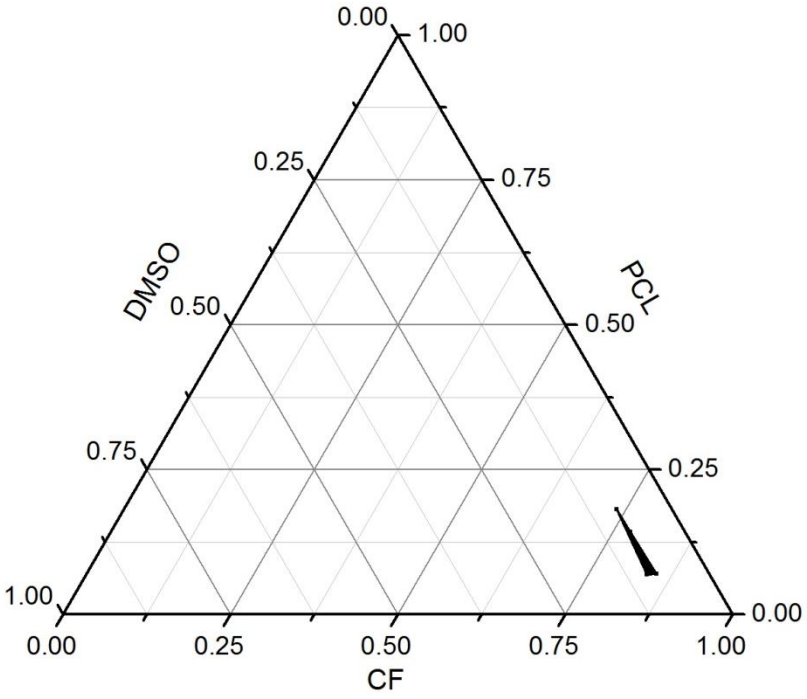

Figure 5.16. Mapping of the region for the production of porous, bead free PCL fibres. The black shaded area indicates the ternary mixture compositions that can lead to the production of porous bead free PCL fibres.

It should be noted that the regions with higher polymer concentration were not investigated, since the concentration would further increase the fibre diameter.

5.7. Conclusions

The production of porous PCL fibres was achieved through a single step process by the addition of non-solvent to the polymer solution prior to electrospinning. The good solvent effect on the fibre morphology was investigated and CF was identified as a suitable solvent for that procedure. The evaporation rate of the good solvent is the parameter that determines its suitability, whereas, other properties, such as its miscibility with water also affects the fibre morphology. The different fibre formation mechanisms that the jet undergoes under varying initial good/poor solvent ratios were explored and the emerging fibre morphologies were explained. An empirical

equation correlating the fibre average diameter to the solution parameters (conductivity, surface tension, viscosity) was developed and tested. The regions, from which the ternary mixture can lead to the production of porous, bead free fibres, were identified.

6. Process Parameter Effect in Electrospinning-NIPS Technique

6.1. Abstract

The effect of electrospinning process parameters (solution flow rate, applied voltage, spinning distance) on the size and surface morphology of porous electrospun poly(ε-caprolactone) was investigated in this chapter. Response surface methodology was implemented for the design of electrospinning experiments. The feed solution was a 12.5% w/v poly(ε-caprolactone) (PCL) in a binary solvent mixture of 90%v/v chloroform/ dimethyl sulfoxide. Spinning distance of 10-25 cm, applied voltage of 10-25 kV and feed flow rate of 0.5-5 ml/h were the range of limiting values of the independent variables used for the development of a central composite design. Second order polynomial equations, correlating electrospinning process parameters to relative pore coverage and fibre average diameter were developed and validated. An increase in any of the electrospinning process parameters favoured pore formation and fibre diameter increase. Under the experimental conditions investigated, the relative pore surface coverage was 15.8-31.9% and the average fibre diameter was in the range of 1.6-3.3 μm. Applied voltage was proven to be the parameter with the strongest impact on both, fibre diameter and surface morphology.

6.2. Introduction

The aim of this chapter is to examine and quantify the effect of electrospinning process parameters (applied voltage, solution flow rate, tip to collector distance) on the single step process of porous electrospun PCL fibres production that was investigated in the previous chapter. The determination of that effect can provide the most convenient method for the optimization of the process in terms of, both, surface morphology and size of the fibres. In particular, the process parameters possess certain characteristics that make them stand out from the rest of the parameters:

- They are part of every experimental set up, therefore the findings of that work could be universally applicable.
- They can be set at any desired value (continuous variables), thus enhancing the control over the procedure outcome.
- They are not interrelated. A change in the value of any of these parameters doesn’t affect the values of the rest.

Response surface methodology (RSM) rather than linear analysis was implemented in this study, in order to increase its applicability. The first step towards the completion of the objectives set in this chapter was the selection of an appropriate solvent system, whose use could lead to the production of porous, bead free fibres. The work presented in the previous chapter had identified such a solvent system (12.5% w/v PCL in 90% v/v CF/DMSO), therefore a similar solution was used in the current study. Since the independent variables had been selected based on the criteria mentioned above, the next step was the determination of the responses. Average fibre diameter was selected as the response for the characterization of the fibre size. In the case of the quantification of the fibre surface morphology, however, the characterization seems to be more complicated. A common technique that has been used (Megelski et al., 2002, Casper et al., 2004) involves the assumption that the pores have circular shapes and the subsequent measurement of the circle radius for the characterization of the surface morphology. That method was considered inadequate in the current study due to three main reasons:

- The pores produced by the method investigated are irregularly shaped. By considering them circular the accuracy of the characterization method is automatically decreased.
- The precision is sensitive to pore merging, a phenomenon often observed on fibres produced by the currently investigated technique.
- Finally, the individual pore size is not sufficient for the universal representation of the tendency for pore formation, which is this study's objective. By measuring just the pore size, the process would appear to be more efficient in cases of fibres with a small amount of large pores compared to fibres with significantly more, but slightly smaller pores.

Taking into account the above observations, a novel characterization method had to be introduced in order to minimize the above mentioned possible sources of error. This method involves the use of the Relative Pore Covered Area (RPCA), calculated by equation (6.1), as the main characterization rather than pore diameter:

$$\mathrm{RPCA} = \frac{\text{Sum of pore covered area}}{\text{Total measured fibre surface area}} x100 \quad (6.1)$$

RPCA was calculated by measuring the individual pore areas within a given area, addition of those areas and division of the sum by the overall area. RPCA takes into account the actual area, without any circularity assumptions that could minimise the accuracy. In addition to that, the use of RPCA provides more information about the overall fibre morphology, since the overall fibre area is also considered. It should be noted, though, that the use of RPCA doesn't exclude the average pore size from the surface morphology characterization, since the latter can provide additional information. The combination of both, RPCA and average pore size, can meet the requirements for the complete fibre characterization, as long as the main method is RPCA.

6.3. Design of Experiments

Since the independent variables of the experiment had been selected, the determination of a suitable range of their values had to follow. The range had to meet the following requirements:

- It had to be as wide as possible, in order to facilitate the identification of possible weak individual parameter effect. That requirement applies to all parameters.
- To allow the collection of sufficient amount of fibres. That requirement mainly means that the distance should not be excessively increased nor the flow rate should be excessively decreased.
- To lead to the production of bead free fibres. That requirement refers to the upper limit of flow rate and lower limit of distance.
- To comply with the safety standards of the equipment (i.e the voltage can't be infinitely increased).

Taking all the above into consideration, the range of values that was used for the design of experiments is summarised in **Table 6.1**.

Table 6.1. The limiting values of process parameters used for the experimental design.

Parameter	Minimum value	Maximum value
Voltage (kV)	10	25
Distance (cm)	10	25
Flow Rate (ml/h)	0.5	5

Central composite designs are generally considered to be the most appropriate designs for RSM. In the current study, where thee independent variables formed the design, a three level factorial design is composed by eight factorial, six star and five (or six) centre points. The role of the factorial points is to provide the fundamental data for the curve fitting, the centre points improve the precision of the fitting and the star points facilitate the estimation of curvature. Data coding was performed in order to simplify its processing. The upper limit of the design was given the value +a, whereas the lower limit was given the value –a. The factorial points had the values +1 and -1 and the star point were set at the point (0,0,0). The experiments were conducted in randomized order, in order to eliminate the probability of systematic error occurrence. The coded values of the process parameters used in the experiments and the actual design are shown in Table 6.2 and Figure 6.1 respectively.

Table 6.2. Coded values of the independent values used in the experimental design.

Run	Distance (cm)	Voltage (kV)	Flow Rate (ml/h)
1	1	1	-1
2	0	0	0
3	1	-1	1
4	0	0	0
5	-1	-1	-1
6	0	1.68	0
7	0	0	0
8	0	0	1.68
9	1	1	1
10	0	0	0
11	-1	1	-1
12	0	-1.68	0
13	-1	1	1
14	1.68	0	0
15	-1.68	0	0
16	0	0	-1.68
17	1	-1	-1
18	0	0	0
19	-1	-1	1

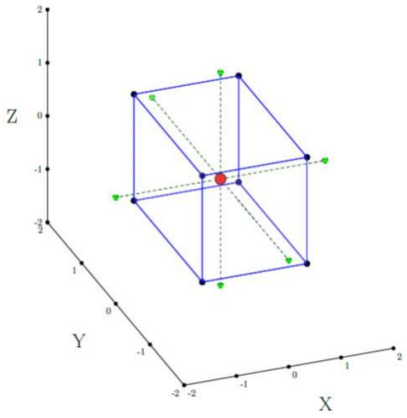

Figure 6.1. Design of experiments used in this study. Blue coloured points represent the factorial points, green coloured the star points and the centre point are coloured red.

6.4. Experimental results

Figure 6.2 shows the SEM images of the fibres produced under different experimental conditions and **Table 6.3** summarises the corresponding experimental conditions and results.

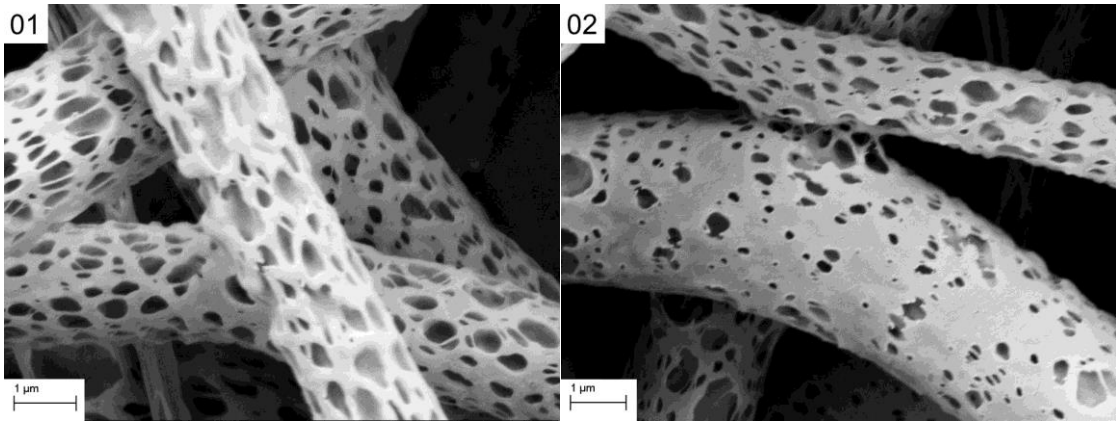

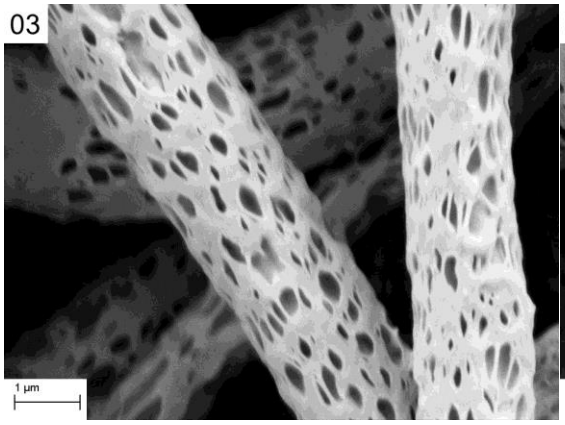
03
1 µm

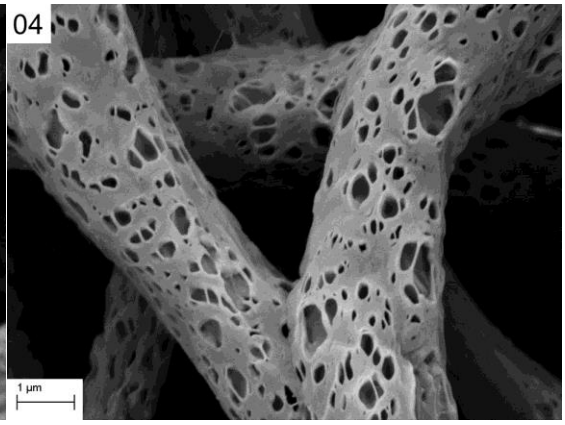
04
1 µm

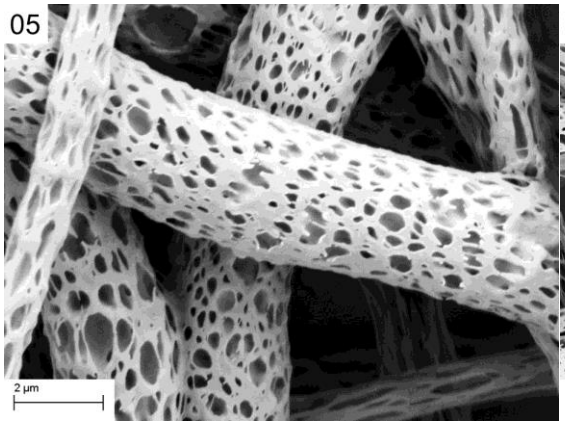
05
2 µm

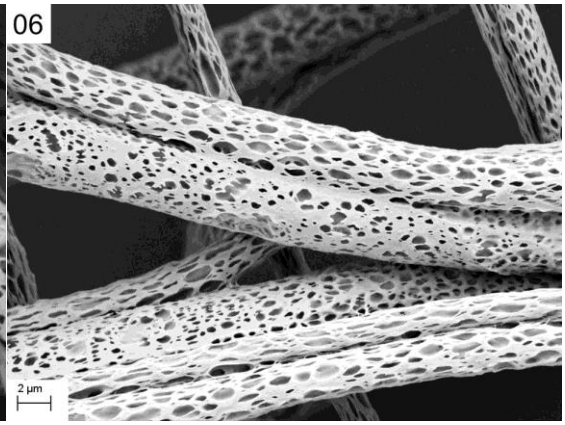
06
2 µm

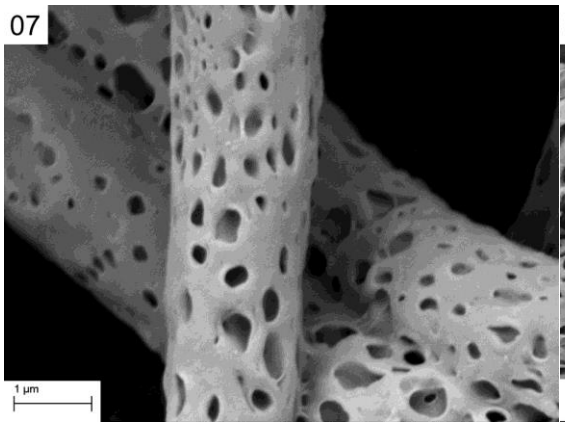
07
1 µm

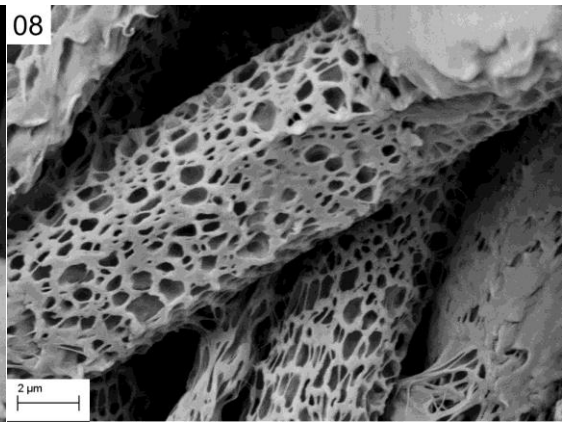
08
2 µm

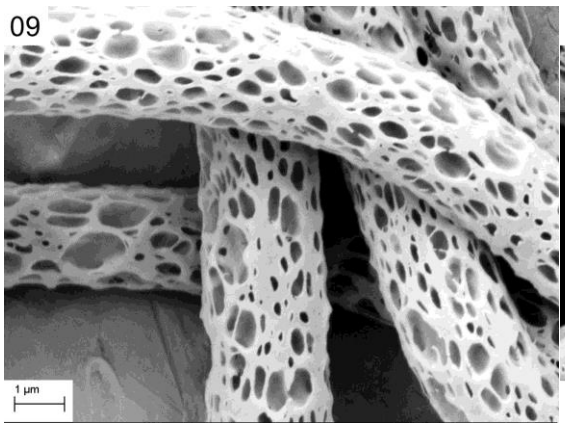
09
1 µm

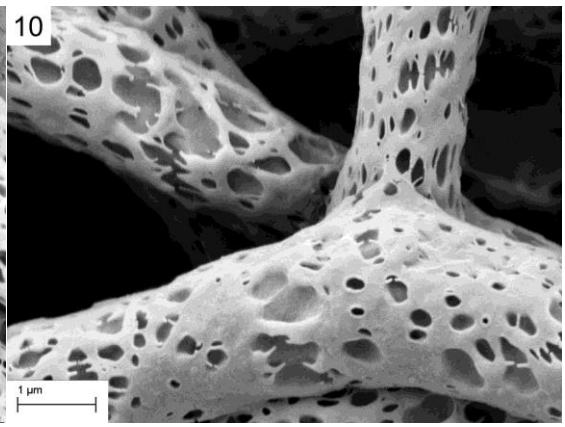
10
1 µm

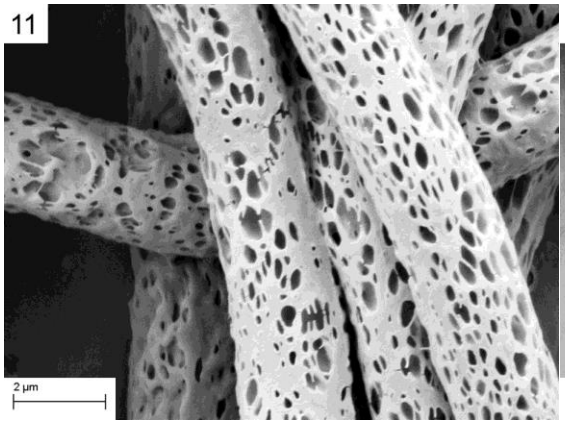
11
2 µm

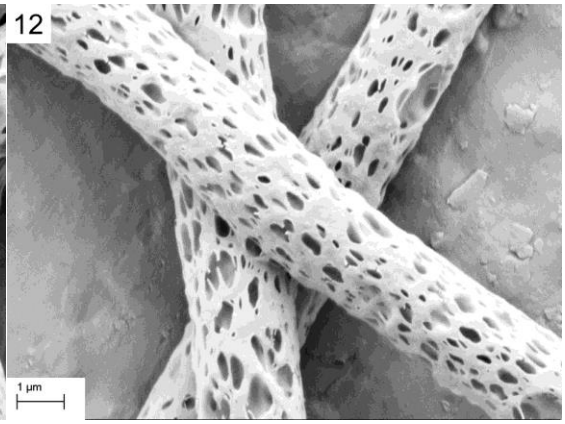
12
1 µm

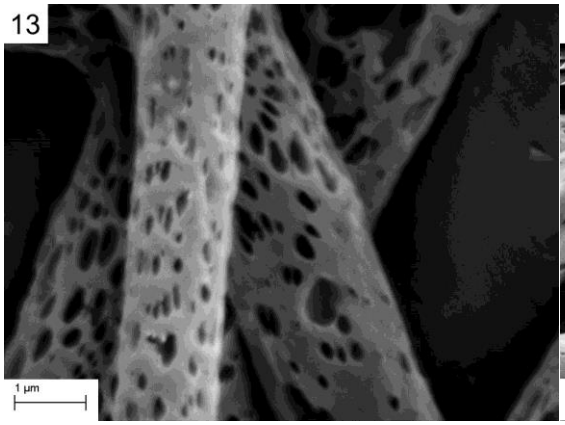
13
1 µm

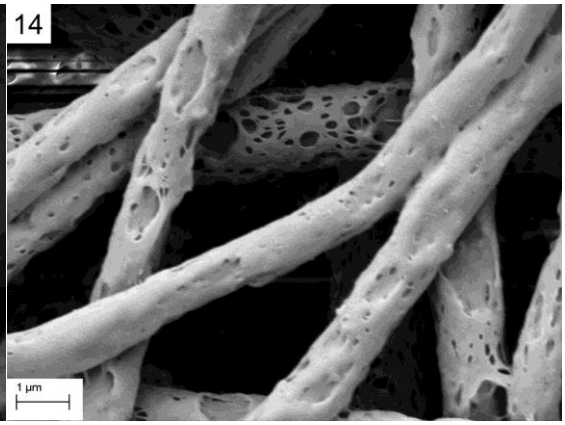
14
1 µm

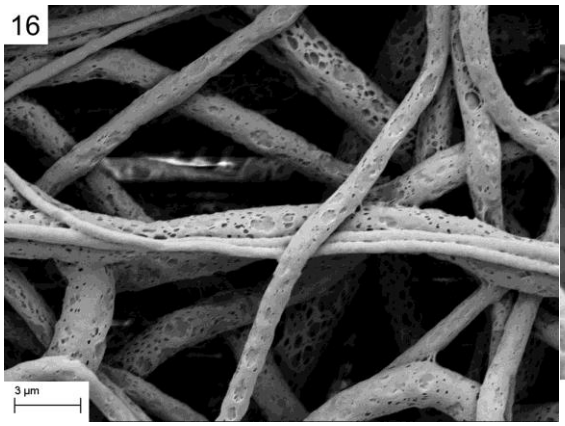
16
3 µm

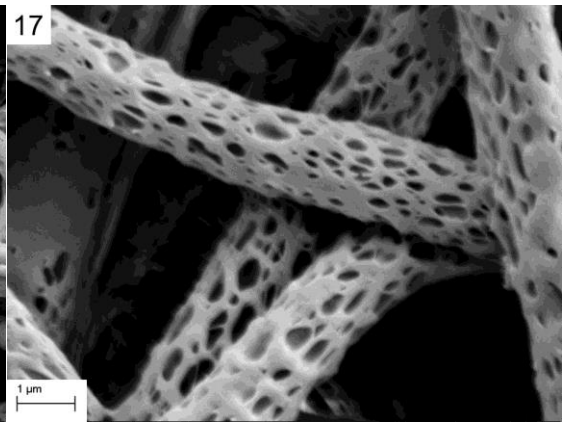
17
1 µm

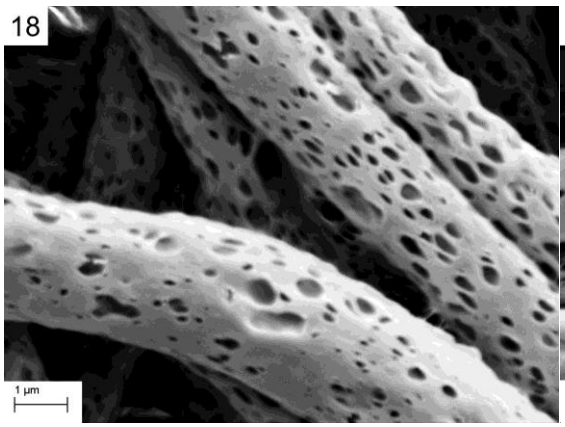
18
1 µm

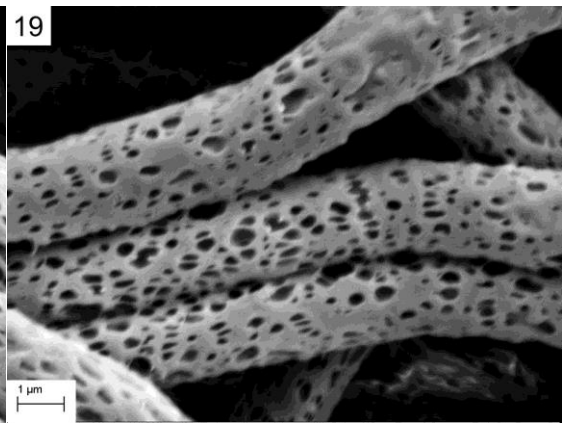
19
1 µm

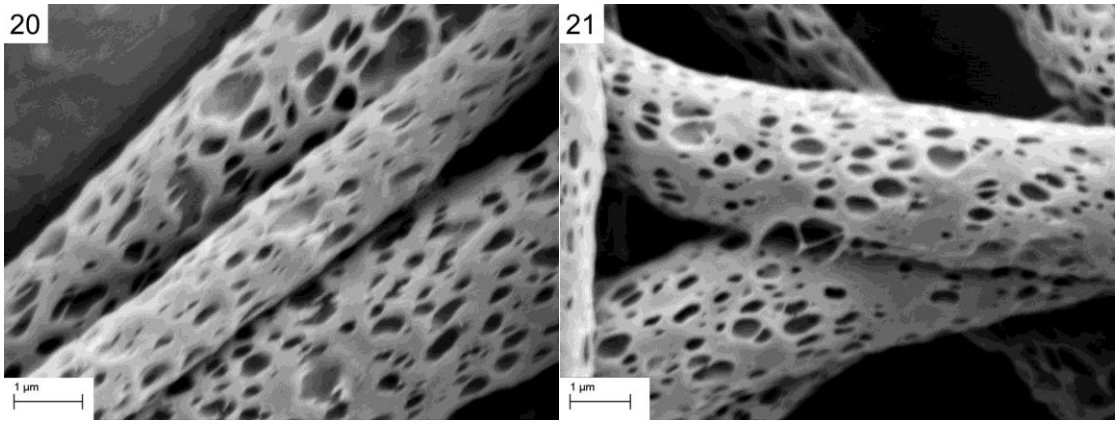

Figure 6.2. SEM images of fibres produced under different experimental conditions. The number at the top left corner represents each experimental run.

Table 6.3. Uncoded values of controlled and response parameters (* validation runs, D stands for Distance, V stands for Voltage, FR stands for Flow Rate, FD stands for Fibre Diameter, CV_{FD} stands for Fibre Diameter Coefficient of Variation, A stands for Average Pore Area, CV_A stands for Average Pore Area Coefficient of Variation, RPCA stands for Relative Pore Covered Area, NA stands for Not Analysed, NFC stands for No Fibre Collection).

Run	D (cm)	V (kV)	FR (ml/h)	FD (μm)	CV_{FD} (%)	A (μm^2)	CV_A (%)	RPCA (%)
1	22	22	1.41	2.32	36.7	0.102	124.3	26.5
2	17.5	17.5	2.75	2.09	23.6	0.037	159.0	18.3
3	22	13	4.09	2.01	28.5	0.036	108.5	15.8
4	17.5	17.5	2.75	2.14	21.1	0.050	87.3	17.0
5	13	13	1.41	2.19	37.0	0.080	117.4	22.7
6	17.5	25	2.75	3.31	34.6	0.299	118.1	31.9
7	17.5	17.5	2.75	2.39	24.9	0.044	106.8	18.0
8	17.5	17.5	5	2.83	45.1	0.154	95.1	28.6
9	22	22	4.09	2.49	20.2	0.062	123.9	23.9
10	17.5	17.5	2.75	2.22	17.3	0.050	128.2	17.6
11	13	22	1.41	2.52	39.6	0.053	153.1	18.3
12	17.5	10	2.75	2.42	32.2	0.059	137.4	18.1
13	13	22	4.09	2.15	20.1	0.044	184.5	17.9
14	10	17.5	2.75	NA	25.5	NA	NA	NA
15	17.5	17.5	0.5	NA	22.5	NA	NA	NA
16	22	13	1.41	1.62	27.2	0.050	92.5	16.9
17	17.5	17.5	2.75	2.04	19.5	0.048	96.9	17.2
18	13	13	4.09	2.04	17.3	0.049	104.7	16.5
19*	15	19	2	2.62	17.4	0.052	155.8	17.0
20*	20	16	3.5	2.20	27.5	0.049	91.4	17.4
21	25	17.5	2.75	NFC	NFC	NFC	NFC	NFC

No fibres were collected when the distance was set at 25 cm (run 15). The fibres produced at the spinning distance of 10 cm (run 14) and when the flow rate was 0.5 ml/h (run 16) were a mixture of porous and non-porous fibres and, therefore, were excluded from the data analysis. In all the other cases, porous, bead free fibres were produced.

The average circularity of the pores for each experimental run was calculated as follows:

$$f_{por} = \frac{4\pi A}{P^2} \quad (6.2)$$

Where A is the area and P is the perimeter of individual pores. In none of the experimental runs the average circularity of the pores exceeded 0.750, thus proving the irregular shapes of the pores and highlighting the necessity for the use of RPCA instead of pore diameter as response. The deviation of the average pore circularity from that of a circle (f_{circ} = 1) proves the irregularity of the shapes of the pores and indicates that the main mechanism responsible for the pore formation was phase separation.

6.4. Models development and validation

Design-Expert software was used for the fitting of the data into second order polynomial equations. The equations correlate the response variables (RPCA and fibre average diameter) to the electrospinning process parameters within the range of values used to produce the equations (tip-to-collector distance from 13 to 22 cm, applied voltage from 10 to 25 kV, feed flow rate from 1.41 to 5 ml/h).

$$\mathrm{RPCA} = -0.253x_1^2 + 0.128x_1x_2 + 0.060x_1x_3 + 6.68x_1 + 0.131x_2^2 + 0.089x_2x_3 - 6.46x_2 + 2.60x_3^2 - 17.9x_3 + 34.3 \quad (6.3)$$

$$\mathrm{D} = -0.024x_1^2 + 0.005x_1x_2 + 0.022x_1x_3 + 0.685x_1 + 0.012x_2^2 - 0.009x_2x_3 - 0.433x_2 + 0.128x_3^2 - 0.930x_3 + 0.910 \quad (6.4)$$

Where x_1 is the tip-to-collector distance, x_2 is the applied voltage and x_3 is the feed solution flow rate. The fitting of the data was satisfactory (R^2 values were 0.93 and 0.96, respectively) as shown in Figure 6.3.

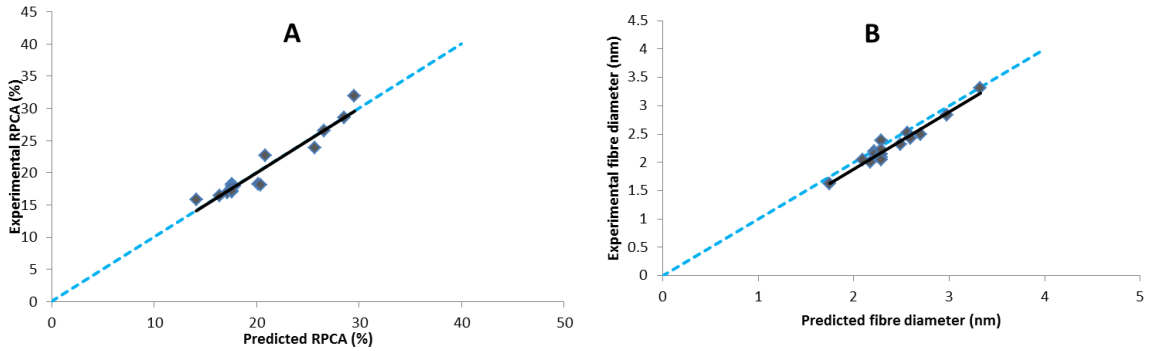

Figure 6.3. Fitting of the experimental data to the empirical equations (A) Relative pore covered area, (B) Average diameter. The black solid lines represent the trendlines of the experimental data, whereas the light blue dashed lines represent the ideal fitting.

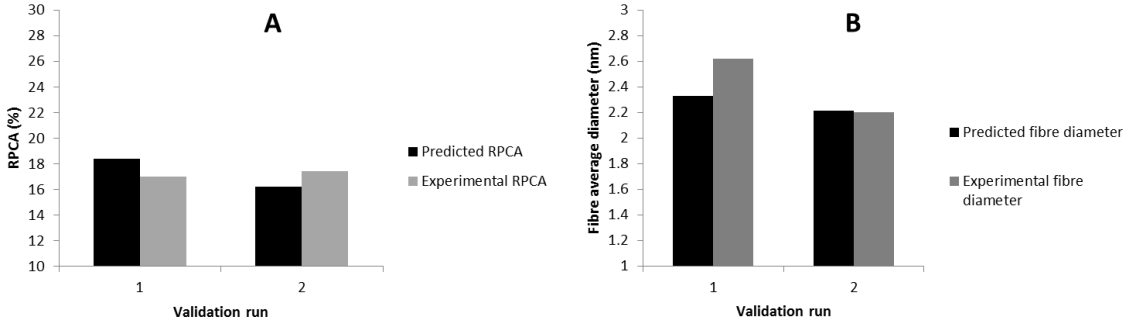

Figure 6.4. Validation of the empirical equations (A) Relative pore covered area, (B) Average diameter.

Two runs, with randomly selected values of process parameters (Table 6.3, runs 20 and 21) were used for the validation of equations (6.3) and (6.4). Equation (6.3) predicts relative pore covered areas of 18.4 and 16.3% for the two validation runs (experimental values 17.0 and 17.4%, respectively) (Figure 6.4A). Equation (6.4) predicts average diameters of 2330 and 2210nm (experimental values were 2620 and 2200nm, respectively) (Figure 6.4B). In all the cases, the differences between the predicted and the experimental values are smaller than the standard deviation of the predicted fibre diameters, thus, validating the empirical equations (Sukigara et al., 2004).

6.5. Electrospinning parameter effect on relative pore covered area

Having established the equation that correlates the RPCA to the electrospinning process parameters (6.3) within the region investigated, the next step is the extraction of conclusions about individual parameter effect on the response. The method that was selected for this was the plotting of contour graphs where a given individual parameter was set at its minimum and maximum value. This method serves a dual purpose; it provides information about the interactions between the other two parameters, but, most importantly, the comparison between the plots reveals the parameter effect on the response.

Theoretically, longer spinning distances could be expected to result in higher values of pore covered areas. At longer distances there is more available time for the solution, either to reach the two phase region or to proceed to areas within the two phase region where the pore formation is favoured. The experimental observations confirm that assumption, as seen in **Figure 6.5**.

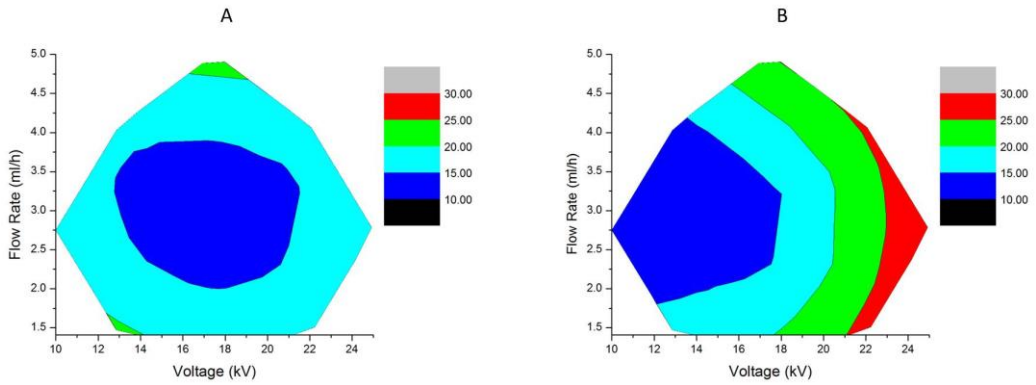

Figure 6.5. Contour plots of relative pore covered area as a function of flow rate and voltage at (A) Minimum distance, (B) Maximum distance.

At the minimum spinning distance, the range of values of the relative pore covered area lies between 10-20%, whereas, at the maximum distance the range is expanded to values up to 30%. This theory is supported by the morphology of the fibres collected at the spinning distance of 10 cm, which were excluded from the equation development. The fibres were a mixture of porous and non-porous fibres due to the lack of time necessary for solution to reach the two phase region. Another

interesting observation is that flow rate and voltage seem to have a similar effect at the minimum distance, whereas voltage has a more dominant role at the maximum distance.

The effect of voltage on the fibre morphology is more complex, since several contradicting phenomena are expected to accompany its change. In terms of solution thermodynamics, one might assume that by increasing the electrostatic input, the mobility of the charged molecules within the electrospinning jet will subsequently increase. The increased mobility enhances the mixing and hinders the initiation of phase separation. This phenomenon can be compared to the increase of temperature (Fashandi and Karimi, 2012). On the other hand, the increased amount of energy would lead to a subsequent increase of the evaporation rates of the solvents, thus resulting to an acceleration of the induction of the phase separation mechanism. In terms of mechanics, the stretching of the jet caused by the voltage during electrospinning can induce phase separation or affect the surface morphology of the fibres. Kulichikhin et al (2014) proved that stretching of entangled polymer solutions can cause phase separation by the formation of a polymer filament surrounded by a liquid shell. In addition to this, the stretching of porous membranes in the uni-axial direction has been proven to increase the pore area at high strains (Morehouse et al, 2006). The effect of stretching is expected to be stronger in electrospun fibres compared to membranes, since the stretching is applied on the fibres before their drying, when they are more vulnerable to external forces. More importantly though, the work by Kim et al. (2005) investigated the deformation of porous fibres under tensile stress. They reported that the fibre undergoes elongation, where the pores are stretched before its deformation by necking. Figure 6.6 shows the contour plots of relative pore covered area as a function of flow rate and distance at the minimum and maximum values of voltage.

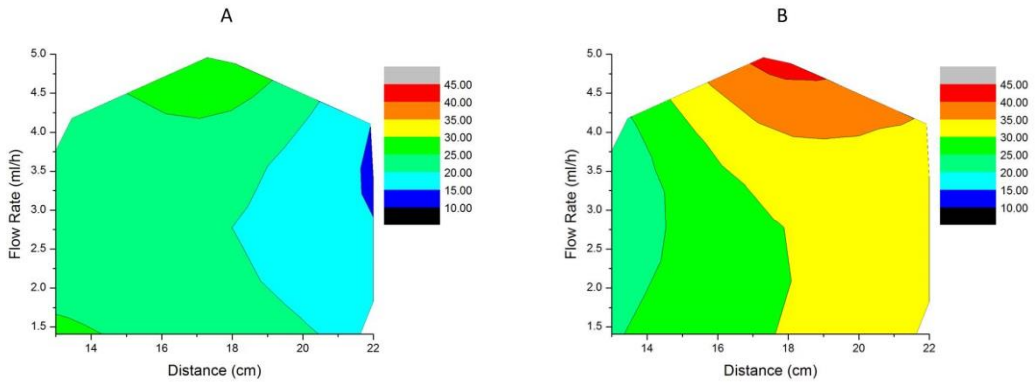

Figure 6.6. Contour plots of relative pore covered area as a function of flow rate and distance at (A) Minimum voltage, (B) Maximum voltage.

The experimental results prove that the phenomena favouring the increase of RPCA, at elevated voltage values, prevail over their antagonists. The contour plots reveal that an increase of voltage from the minimum to the maximum value results in an increase of the relative pore covered area from 10-30% to 20-45%. In addition to this, the elliptical shape of the pores, observed at the experiment of maximum voltage (**Figure 6.3.06**), indicates the importance of the mechanics in the pore size and morphology. The absence of necking suggests that within the investigated limits (voltage up to 25 kV) increase of voltage is an easy method to increase the RPCA, without any side effects.

Figure 6.7 shows the contour plots of relative pore covered area as a function of voltage and distance at the minimum and maximum values of flow rate.

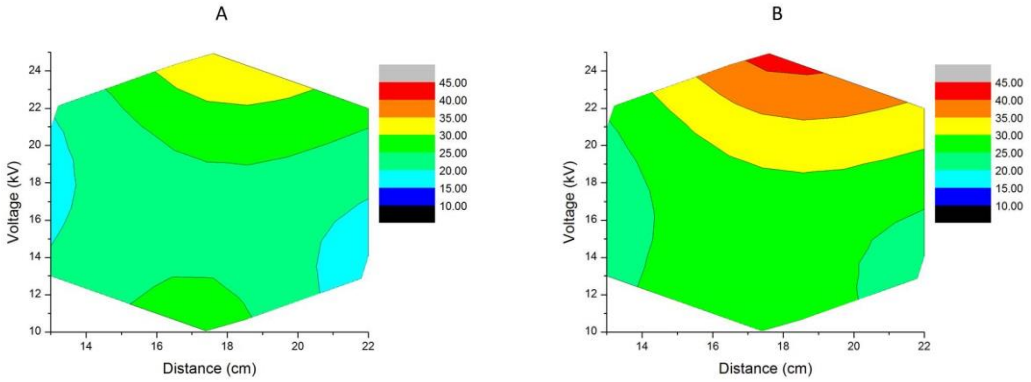

Figure 6.7. Contour plots of relative pore covered area as a function of voltage and distance at (A) Minimum flow rate, (B) Maximum flow rate.

A comparison between the plots can reveal the effect of flow rate on the fibre surface morphology. High flow rate seems to favour pore formation, since the relative pore covered area lies between 15-35% for the minimum flow rate value, whereas, the range is shifted to values between 20-45% when the flow rate is set to its maximum value. The effect is expanded to values outside the investigated region, as indicated by the morphology of the fibres obtained at a flow rate of 0.5ml/h. The interaction of the spinning distance and voltage is not affected by the value of the flow rate, as indicated by the similar curvature of the contour lines.

A minimum flow rate has to be surpassed for the induction of the thermodynamic instability of the solution. At the minimum flow rate of the experimental design (0.5 ml/h), the composition of the electrospinning jet didn't change enough as to initiate the phase separation mechanism (**Figure 6.1.16**). Above that lower limit, there is a proportional relationship between the flow rate and the RPCA due to the more intense changes of the composition of the electrospinning jet after its ejection. In addition to that, de Moel et al (1998) proved that high flow rates for linear polymer solutions can shift the critical temperature and favour demixing of the solution. High flow rates favour different polymer chain configurations in the polymer poor and polymer rich phases. Macromolecular chains in the polymer poor phase can be subjected to stretching easier compared to those in the polymer rich phase, which leads to an increase of polymer solvent contacts and, therefore, to a difference in the polymer solvent interaction energy between the two phases.

A novel method was implemented for the quantification of individual parameter effect. Values of the relative pore covered area were calculated for three cases for each individual parameter (when the other two variables were set at their minimum, medium and maximum values, respectively). In each series, the difference between the maximum and minimum value of the response (relative pore covered area) provided an indication of its dependence on the individual parameter. The parameters can be subsequently classified based on their individual responses' value difference. The investigated region is not symmetrical, therefore new coding of the independent variables was necessary, in order to achieve uniform comparison. Equation (6.5) assisted the determination of eleven equivalent values for each individual parameter, for which the relative pore covered area was calculated.

$$\mathrm{x_i} = \mathrm{x_{min}} + i\left(\frac{\mathrm{x_{max}} - \mathrm{x_{min}}}{10}\right), i = 0,1,2,\dots,10 \quad (6.5)$$

Where x_{min} and x_{max} are the minimum and maximum values of any individual parameter within the analysed region, respectively.

Values of the relative pore covered area were calculated for three cases for each individual parameter (when the other two variables were set at their minimum, medium and maximum values). In each series, the difference between the maximum and minimum value of the relative pore covered area provided an indication of its dependence on the individual parameter. The results are shown in **Figure 6.8**.

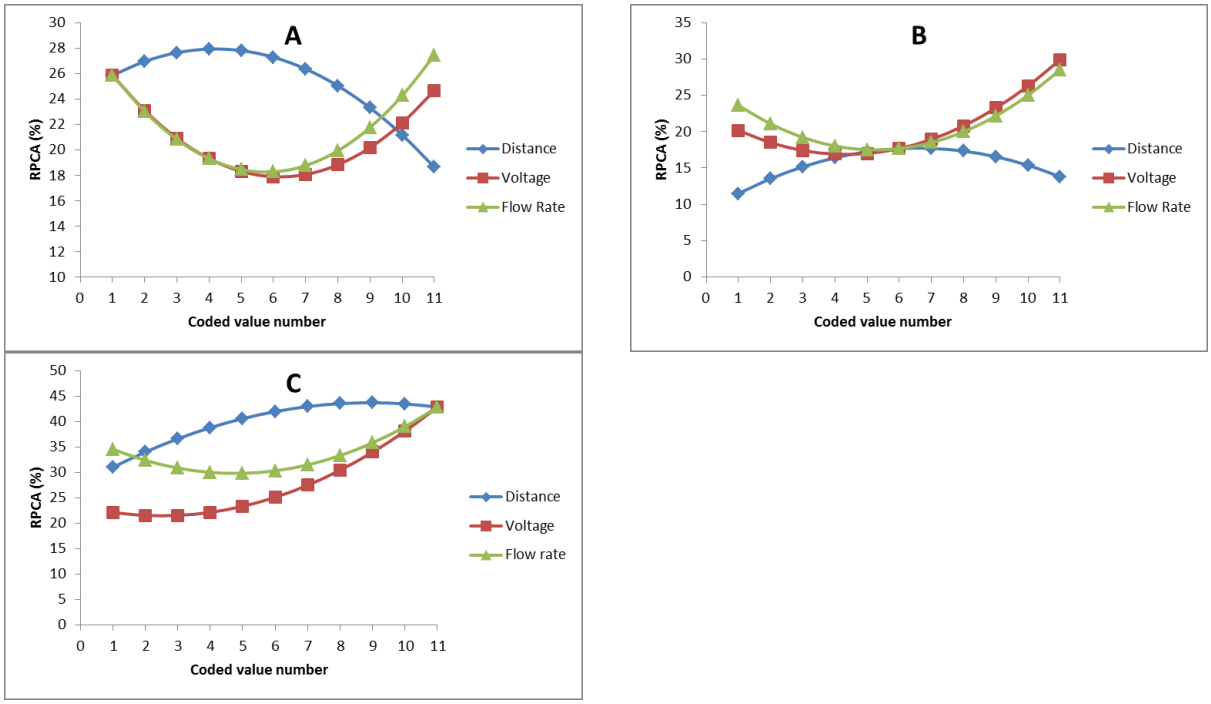

Figure 6.8. Relative pore covered area as a function of individual parameters at (A) minimum values, (B) medium values, (C) maximum values.

In the cases were the variables were set, either at their minimum, or at their medium values, all the parameters had comparable effect on the pore formation. However, when the values are set at their maximum values, voltage seems to have a stronger effect on the relative pore covered area. Variations of voltage result a change of 21.3% of relative pore covered area, instead of 13.0% for flow rate and 12.7% for distance.

The local extrema of equation (6.3) were calculated. If a maximum or minimum exists, it will be located at the point where the partial derivatives of equation (3) are equal to zero, as defined by the system of equations (6.6).

$$\frac{\partial \mathrm{RPCA}}{\partial \mathrm{x}_1} = 0, \frac{\partial \mathrm{RPCA}}{\partial \mathrm{x}_2} = 0, \frac{\partial \mathrm{RPCA}}{\partial \mathrm{x}_3} = 0 \quad (6.6)$$

The solution of system (6.6) predicted a stationary point at (x_1, x_2, x_3 = 17.4, 15.1, 2.98), which is within the investigated region. The characterization of the stationary point as a maximum, minimum or saddle point occurred by the sign of the determinants, shown in equations (6.7), (6.8) and (6.9).

$$|H_1| = \frac{\partial RPCA}{\partial x_1 \partial x_1} < 0 \quad (6.7)$$

$$|H_2| = \begin{vmatrix} \frac{\partial RPCA}{\partial x_1 \partial x_1} & \frac{\partial RPCA}{\partial x_1 \partial x_2} \\ \frac{\partial RPCA}{\partial x_2 \partial x_1} & \frac{\partial RPCA}{\partial x_2 \partial x_2} \end{vmatrix} < 0 \quad (6.8)$$

$$|H_3| = \begin{vmatrix} \frac{\partial RPCA}{\partial x_1 \partial x_1} & \frac{\partial RPCA}{\partial x_1 \partial x_2} & \frac{\partial RPCA}{\partial x_1 \partial x_3} \\ \frac{\partial RPCA}{\partial x_2 \partial x_1} & \frac{\partial RPCA}{\partial x_2 \partial x_2} & \frac{\partial RPCA}{\partial x_2 \partial x_3} \\ \frac{\partial RPCA}{\partial x_3 \partial x_1} & \frac{\partial RPCA}{\partial x_3 \partial x_2} & \frac{\partial RPCA}{\partial x_3 \partial x_3} \end{vmatrix} > 0 \quad (6.9)$$

The signs determine that the stationary point is a saddle point.

6.7. Electrospinning parameter effect on fibre average diameter

Generally, as noted in Chapter 2, a universal effect of individual electrospinning process parameter on fibre average diameter does not exist. In the current study, the overall phenomena occurring during the process are even more complicated, due to the presence of non-solvent in the electrospinning jet and the subsequent pore formation on electrospun fibres. Nonetheless, similar to the one followed in the case of RPCA methodology was implemented for the investigation of the individual process parameter effect on the fibre average diameter.

Figure 6.9 shows the contour plots of average fibre diameter as a function of voltage and distance at the minimum and maximum values of flow rate. A comparison between the plots can reveal the effect of flow rate on the fibre average diameter.

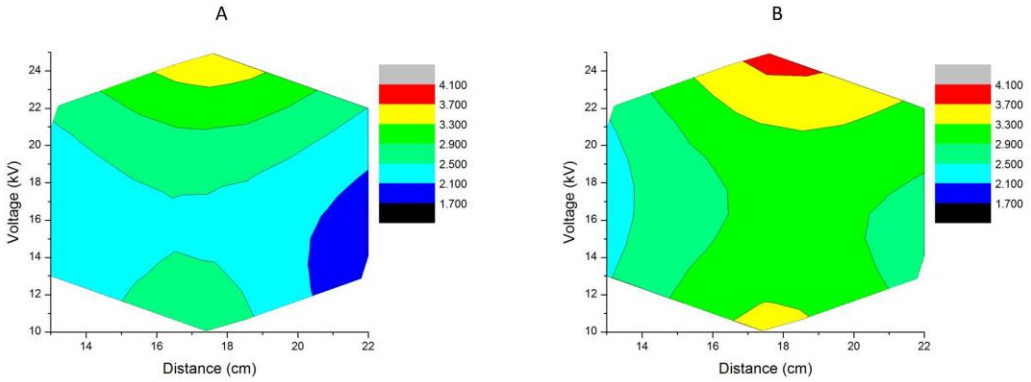

Figure 6.9. Contour plots of fibre average diameter as a function of voltage and distance at (A) Minimum flow rate, (B) Maximum flow rate.

The equation predicts an increase in the average diameter of the fibres as a result of an increase in the flow rate. The majority of the fibre average diameter lies was measured between the range of 2100-2900 nm for minimum flow rate, whereas, it increases to values above 2900 nm for maximum flow rate. The larger amount of solution, which is ejected at high flow rates, cannot be sufficiently stretched, therefore, the diameter of the fibres is relatively high.

Figure 6.10 shows the contour plots of average fibre diameter as a function of voltage and flow rate at the minimum and maximum values of distance. A comparison between the plots can reveal the effect of spinning distance on the fibre average diameter.

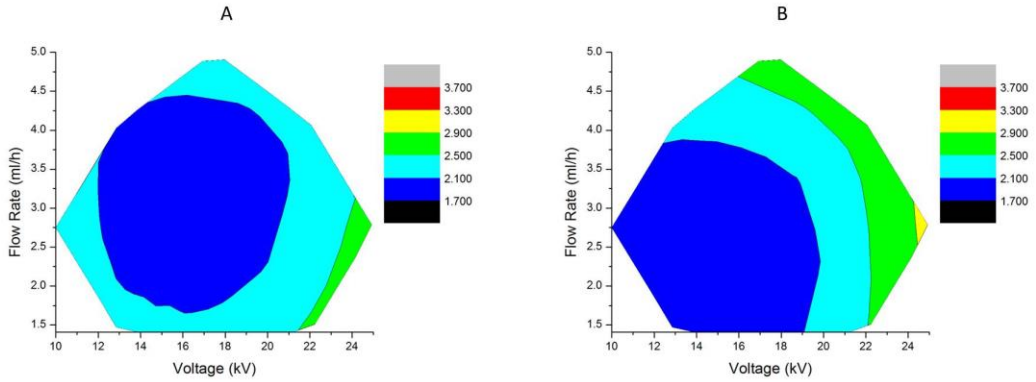

Figure 6.10. Contour plots of fibre average diameter as a function of flow rate and voltage at (A) Minimum distance, (B) Maximum distance.

Interestingly, the equation predicts a slight increase of the fibre diameter with the increase of distance. At the minimum spinning distance the majority of the fibre average diameter lies between 1700-2300 nm, and reaches up to 2900 nm, whereas, at the maximum distance the region where fibres with diameters above 2700 nm is increased and the fibres with diameters up to 3100 nm can be produced. Even though that seems to contradict the theory, one must bear in mind that longer spinning distances favour pore formation. The void generated by the pores contributes to the total measured fibre diameter, hence, the proportional relationship between spinning distance and fibre diameter is observed.

Figure 6.11 shows the contour plots of average fibre diameter as a function of flow rate and distance at the minimum and maximum values of voltage. A comparison between the plots can reveal the effect of voltage on the fibre average diameter.

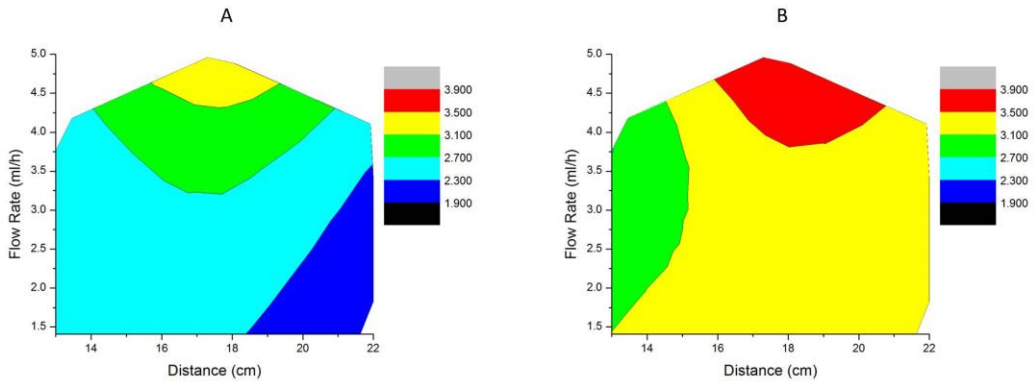

Figure 6.11. Contour plots of fibre average diameter as a function of flow rate and distance at (A) Minimum voltage, (B) Maximum voltage.

Voltage increases seem to favour the production of fibres with larger diameters. The range of fibre diameters for the minimum voltage is between 1900-3500 nm, whereas it is shifted to values between 2700-3900 for the maximum voltage. Similarly to the distance effect, the increased tendency for pore formation accompanying the voltage increase can be held responsible the observed increase of the fibre diameter.

Coded values from equation (6.5) were used to compare the effect of the individual parameters on the fibre diameter (**Figure 6.12**).

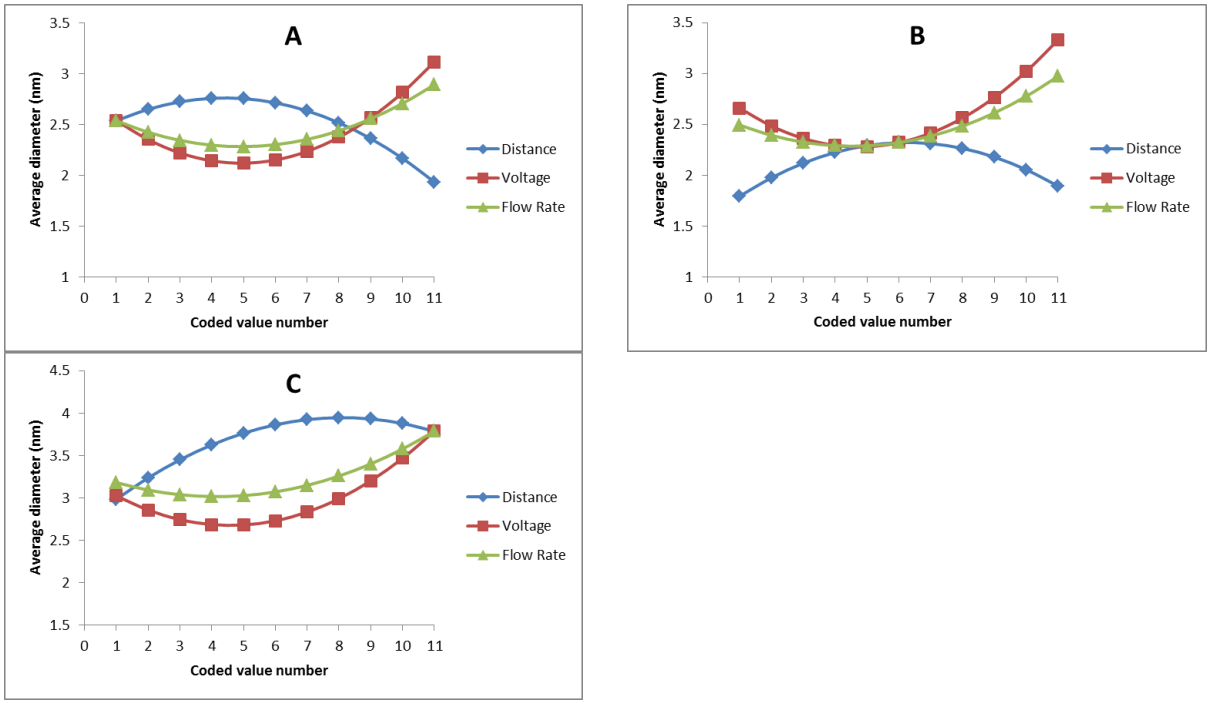

Figure 6.12. Fibre average diameter as a function of individual parameters at (A) minimum values, (B) medium values, (C) maximum values.

Voltage remains the most influential parameter, however, the average diameter seems to be more responsive at the medium range of values (diameter differences of 1050nm, compared to 530nm for distance and 680nm for flow rate).

The local extrema were calculated for equation (6.5), following a similar methodology to that of the RPCA. The solution of the system where the first derivatives of equation (5) were equal to zero predicted a stationary point at (x_1, x_2, x_3 = 17.1, 15.5, 2.71). The determinants were all negative, therefore the stationary point was characterised as saddle point.

6.8. Conclusions

The effect of individual electrospinning process parameter (applied voltage, spinning distance, and solution flow rate) on electrospun PCL fibre morphology and size, in a combined electrospinning and phase separation process, was investigated in this chapter. Electrospinning experiments, conducted at conditions determined by a

central composite design, generated the necessary data for the development of second order polynomial equations correlating the relative pore covered area and the fibre average diameter to electrospinning process parameters. The empirical models predict an increase of both relative pore covered area and fibre average diameter, with the increase of any of the process parameters within the investigated region (applied voltage between 10-25 kV, spinning distance between 13-22 cm, solution flow rate between 1.41-5 ml/h). Voltage seems to be the parameter with the strongest effect on the fibre morphology and size.

7. Conclusions – Future Work

7.1. Thesis conclusions

Nanoporosity generation on electrospun poly(ε-caprolactone) fibres through a combinative, single step process electrospinning - Non-solvent Induced Phase Separation (NIPS) was investigated in this study.

Theoretical and experimental work established the significance of pore induction on the increase of the electrospun network specific surface area (**Chapter 4**). Theoretical models, that correlated the network surface area to the material properties (density, surface tension, Young's modulus, Poisson's ratio) and network physical properties (density) and geometrical characteristics (fibre radius, fibre aspect ratio, network thickness), were developed. The models take into account fibre-to-fibre contacts based on three different contact models (Hertzian, DMT, JKR) in order to achieve more accurate scaling up of the fibre to network specific surface area. Pore induction proved to increase the network specific surface area up to 52%, compared to the maximum surface area that could be achieved by smooth surface fibre network with the same physical properties and geometrical characteristics. Considering that the JKR model can accurately predict the excluded contact area, the actual network specific surface area increase rises to 56%.

Chapter 5 investigated the good solvent effect in the fibre morphology and size. Through experimental testing of binary solvent solutions based on four different good solvents for polycaprolactone (CF, DCM, THF, FA) at various good/poor solvent ratios, general guidelines for the production of porous, bead free fibres were identified. These involve the selection of a good solvent with suitable evaporation rate, use of solution with appropriate concentration and the setting of the good/poor solvent ratio. Good solvent evaporation rate can determine whether phase separation will occur (discrete difference to the non-solvent evaporation rate is required) or the morphology of the fibres (fibres with ribbon cross section are likely to be produced by high evaporation good solvents due to limited polymer chain diffusion from jet surface to the liquid core). Low solution concentration can result the production of beaded fibres, due to insufficient polymer chain entanglements. Low good/poor solvents are required in the case of viscous solutions, such as those investigated in this study, since the presence of non-solvent in the electrospinning jet can hinder the chain diffusion and cause the production of ribbon fibres or cause the

formation of heterogeneous regions within the jet and subsequently cause the production of beaded fibres. 12.5% w/v PCL in CF/DMSO solution with good/poor solvent ratios varying from 75-90% v/v at the applied voltage of 15 kV, a spinning distance of 20 cm, and the feed flow rate of 1 ml/h was identified as a region that can result the production of porous, bead free fibres.

Response Surface Methodology was implemented for the determination of individual electrospinning process parameter (applied voltage, solution flow rate, spinning distance) effect on the fibre surface morphology and size (**Chapter 6**). Phenomena like increased time of the process (spinning distance), different polymer chain configurations (solution flow rate) and increased jet stretching (applied voltage) that accompany the increase in the value of any parameter seem to enhance either the tendency for pore generation or formed pore size within the investigated region (applied voltage between 10-25 kV, spinning distance between 13-22 cm, solution flow rate between 1.41-5 ml/h). That, subsequently, increases the average diameter of the fibres produced. Voltage was proven to be the most influential parameter on both the selected responses.

Findings from this study enhance the understanding of the combinative electrospinning - Non-solvent Induced Phase Separation technique and offer a convenient method for the production of poly(ε-caprolactone) fibres with controlled morphology and size.

7.2. Recommendations for future work

The work presented in this project can be used as foundation for further research in order to obtain an even clearer picture on the combinative electrospinning - Non-solvent Induced Phase Separation technique.

The first step towards this direction would be the implementation of the methodology developed in this study for prediction of fibrous network specific area to a wider range of networks. The use of different models for the prediction of the number of contacts could also be considered in that case. This could enable the accurate

determination of the level of contribution of individual factors in the configuration of the network specific area and offer alternative methods for increasing it.

The complete investigation of the combinative technique on other polymers could also be considered. Besides the practical advantage of increasing the number of potential applications due to expanded material properties that could be achieved, that would serve another purpose as well. This would be the provision of necessary data for investigation of parameters that were not examined in this study, such as the polymer MW or its chemical nature.

A second step could be the inclusion of humidity in the investigation of the overall process. The humidity effect wasn't investigated in this study due to the lack of appropriate equipment. However, theoretically, humidity can positively contribute in the pore generation through two different mechanisms. Neither of those contradicts the electrospinning-NIPS technique, therefore, elevated levels of humidity could further improve the results.

Appendices

Appendix A

Table A1. Surface tension measurements of polymer solutions.

Sample	Measurement 1 (mN/m)	Measurement 2 (mN/m)	Measurement 3 (mN/m)	Average (mN/m)
CF50	42.1	42.1	42.2	42.1
CF60	39.7	39.8	39.8	39.8
CF70	38.0	38.0	38.0	38.0
CF80	35.4	35.4	35.4	35.4
CF90	32.3	32.2	32.3	32.3
CF100	30.7	30.6	30.7	30.7
DCM50	42.2	42.3	42.3	42.3
DCM60	40.5	40.4	40.3	40.4
DCM70	37.8	38.1	38.0	38.0
DCM80	36.2	36.2	36.2	36.2
DCM90	34.8	34.9	34.9	34.9
DCM100	32.5	32.5	32.5	32.5
THF50	42.0	42.3	42.3	42.2
THF60	40.6	40.5	40.4	40.5
THF70	37.8	37.7	37.9	37.8
THF80	36.1	36.1	36.1	36.1
THF90	34.2	34.3	34.3	34.3
THF100	32.3	32.1	32.3	32.3

Appendix B

Table B2. Conductivity measurements of polymer solutions.

Sample	Measurement 1 (μS/cm)	Measurement 2 (μS/cm)	Measurement 3 (μS/cm)	Average (μS/cm)
CF50	1.22	1.21	1.21	1.21
CF60	0.88	0.91	0.90	0.90
CF70	0.78	0.77	0.78	0.78
CF80	0.67	0.68	0.66	0.67
CF90	0.41	0.43	0.43	0.42
CF100	0.15	0.14	0.14	0.14
DCM50	2.21	2.24	2.22	2.22
DCM60	1.93	1.93	1.93	1.93
DCM70	1.14	1.13	1.13	1.13
DCM80	0.97	0.97	0.97	0.97
DCM90	0.67	0.68	0.67	0.67
DCM100	0.06	0.05	0.06	0.06
THF50	1.63	1.61	1.62	1.62
THF60	0.94	0.94	0.95	0.94
THF70	0.83	0.83	0.82	0.83
THF80	0.71	0.70	0.71	0.71
THF90	0.59	0.58	0.58	0.58
THF100	0.01	0.01	0.01	0.01

References

Journals

Arayanarakul K, Choktaweesap N, Aht-ong D, Meechaisue C, Supaphol P. Effects of Poly(ethylene glycol), Inorganic Salt, Sodium Dodecyl Sulfate, and Solvent System on Electrospinning of Poly(ethylene oxide). *Macromolecular Materials and Engineering* **2006**, 291, 581–591.

Bae H-S, Haider A, Kamruzzaman Selim K.M, Kang D-Y, Kim E-J, Kang I-K. Fabrication of highly porous PMMA electrospun fibers and their application in the removal of phenol and iodine. *Journal of Polymer Research* **2013**, 20, 158-165.

Bagherzadeh R, Najar SS, Latifi M, Tehran MA, Kong LX. A theoretical analysis and prediction of pore size and pore size distribution in electrospun multilayer nanofibrous materials. *Journal of Biomedical Materials Research Part A* **2013**, 101A, 2107– 2117.

Barnes C.P, Sell S.A, Boland E.D, Simpson D.G, Bowlin G.L. Nanofiber technology: Designing the next generation of tissue engineering scaffolds. *Advanced Drug Delivery Reviews* **2007**, 59, 1413–1433.

Beachley V, Wen X. Effect of electrospinning parameters on the nanofiber diameter and length. *Materials Science and Engineering* **2009**, C29, 663–668.

Bhardwaj N, Kundu S.C. Electrospinning: A fascinating fiber fabrication technique. *Biotechnology Advances* **2010**, 28, 325–347.

Bognitzki M, Frese T, Steinhart M, Greiner A, Wendorff J. Preparation of Fibers With Nanoscaled Morphologies: Electrospinning of Polymer Blends. *Polymer Engineering and Science* **2001**, 41, 982-989.

Casper C.L, Stephens J.S, Tassi N. Chase D.B, Rabolt J.F. Controlling Surface Morphology of Electrospun Polystyrene Fibers: Effect of Humidity and Molecular Weight in the Electrospinning Process. *Macromolecules* **2004**, 37, 573-578.

Castro M, Jianbo Lu J, Bruzaud S, Kumar B, Feller J-F. Carbon nanotubes/poly(e-caprolactone) composite vapour sensors. Carbon **2009,** 47, 1930-1942.

Cava D, Gavara R, Lagaron J.M, Voelkel A. Surface characterization of poly(lactic acid) and polycaprolactone by inverse gas chromatography. *Journal of Chromatography A* **2007**, 1148, 86–91.

Celebioglu A, Uyar T. Electrospun porous cellulose acetate fibers from volatile solvent mixture. *Materials Letters* **2011**, 65, 2291-2294.

Chen Z.G, Wang P.W, Wei B., Mo X.M, Cui F.Z. Electrospun collagen–chitosan nanofiber: A biomimetic extracellular matrix for endothelial cell and smooth muscle cell. *Acta Biomaterialia* **2010**, 6, 372–382.

Chong E.J, Phan T.T, Lim I.J, Zhang Y.Z, Bay B.H , Ramakrishna S, Lim C.T. Evaluation of electrospun PCL/gelatin nanofibrous scaffold for wound healing and layered dermal reconstitution. *Acta Biomaterialia* **2007**, 3, 321–330.

Chowdhury M, Stylios G. Effect of Experimental Parameters on the Morphology of Electrospun Nylon 6 fibres. *International Journal of Basic & Applied Sciences* **2010**, 10, 70-78.

Cipitria A, Scelton A, Dargaville T. R, Dalton P. D, Hutmacher D. W. Design, fabrication and characterization of PCL electrospun scaffolds—a review. *Journal of Materials Chemistry* **2011**, 21, 9419–9453.

Croisier F, Duwez A-S, Jerome C, Leonard A.F, van der Werf K.O, Dijkstra P.J, Bennink M.L. Mechanical testing of electrospun PCL fibers. *Acta Biomaterialia* **2012**, 8, 218-224.

Croiser F, Jerome C. Chitosan-based biomaterials for tissue engineering. *European Polymer Journal* **2013**, 49, 780-792.

De Moel K, Flikkema E, Szleifer I, ten Brinke G. Flow-induced phase separation in polymer solutions. *Europhysics Letters* **1998**, 42, 407-412.

Deitzel J.M, Kleinmeyer J, Harris D, Beck Tan N.C. The effect of processing variables on the morphology of electrospun nanofibers and textiles. *Polymer* **2001**, 42, 261–272.

Demir MM, Yilgor I, Yilgor E, Erman B. Electrospinning of polyurethane fibers. *Polymer* **2002**, 43, 3303-3309.

Demir, M. M., Gulgun M. A., Menceloglu Y. Z., Erman B., Abramchuk S. S., Makhaeva E.E., Khokhlov A. R., Matveeva V. G., Sulman M. G. Palladium nanoparticles by electrospinning from poly(acrylonitrile-co-acrylic acid)-PdCl2 solutions. Relations between preparation conditions, particle size, and catalytic activity. *Macromolecules* **2004**, 37, 1787 – 1792.

Derjaguin BV, Muller VM, Toporov YP. Effect of contact deformations on the adhesion of particles. *Journal of Colloid and Interface Science* **1975**, 53(2), 314-326.

Dods S.R, Oliver Hardick O, Bob Stevens B, Daniel G. Bracewell D.G. Fabricating electrospun cellulose nanofibre adsorbents forion-exchange chromatography. *Journal of Chromatography A* **2015**, 1376, 74–83.

Doshi J and Reneker D.H. Electrospinning Process and Applications of Electrospun Fibers. *Journal of Electrostatics* **1995**, 35, 151-160.

Eicchorn S.J, Sampson W.W. Relationships between specific surface area and pore size in electrospun polymer fibre networks. *Journal of the Royal Society Interface* **2010**, 7, 641–649.

Eicchorn S.J, Sampson W.W. Statistical geometry of pores and statistics of porous nanofibrous assemblies. *Journal of the Royal Society Interface* **2005**, 2, 309–318.

Eshraghi S, Das S. Mechanical and Microstructural Properties of Polycaprolactone Scaffolds with 1-D, 2-D, and 3-D Orthogonally Oriented Porous Architectures Produced by Selective Laser Sintering. *Acta Biomaterialia* **2010**, 6(7), 2467–2476.

Fashandi H and Karimi M. Pore formation in polystyrene fiber by superimposing temperature and relative humidity of electrospinning atmosphere. *Polymer* **2012**, 53, 5832-5849.

Fong H, Chun I, Reneker D.H. Beaded nanofibers formed during electrospinning. *Polymer* **1999**, 40, 4585–4592.

Fridrikh S.V, Yu J.H, Brenner M.P, Rutledge G.C. Controlling the Fiber Diameter during Electrospinning. *Physical review letters* **2003**, 90, 144502.

Garg K and Bowlin G.L. Electrospinning jets and nanofibrous structures. *Biomicrofluidics* **2011**, 5, 013403.

Geng X, Kwon O-H, Jang J. Electrospinning of chitosan dissolved in concentrated acetic acid solution. *Biomaterials* **2005**, 26, 5427–5432.

Ghasemi-Mobarakeh L, Prabhakaran M.P, Morshed M, Nasr-Esfahani M-H, Ramakrishna S. Electrospun poly(3-caprolactone)/gelatin nanofibrous scaffolds for nerve tissue engineering. *Biomaterials* **2008**, 29, 4532–4539.

Gu S.Y, Ren J, Vancso G.J. Process optimization and empirical modelling for electrospun polyacrylonitrile (PAN) nanofiber precursor of carbon nanofibers. *European Polymer Journal* **2005**, 41, 2559–2568.

Gupta P, Elkins C, Long T.E, Wilkes G.L. Electrospinning of linear homopolymers of poly (methylmethacrylate): exploring relationships between fiber formation, viscosity, molecular weight and concentration in a good solvent. *Polymer* **2005**, 46, 4799–4810.

Haas D, Heinrich S, Greil P. Solvent control of cellulose acetate nanofibre felt structure produced by electrospinning. *Journal of Materials Science* **2010**, 45, 1299-1306.

Hansen C. M. The three dimensional solubility parameter—key to paint component affinities. Part I: Solvents, plasticizers, polymers, and resins. *Journal of Paint Technology* **1967**, 39, 104 – 117.

Heikkila P, Harlin A. Electrospinning of polyacrylonitrile (PAN) solution: Effect of conductive additive and filler on the process. *Express Polymer Letters* **2009**, 3, 437–445.

Hertz H. *Über die Berührung* fester *elastischer Körper* (On the *contact* of *elastic* solids). *Journal für die reine und angewandte Mathematik* **1882**, 92, 156–171 in Bhushan B. Modern Tribology Handbook Volume One, **2001**.

Heydarkhan-Hagvall S, Schenke-Layland K, Dhanasopon A.P, Rofail F, Smith H, Wu B.M, Shemin R, Beygui R.E, MacLellan W.R. Three-dimensional electrospun ECM-based hybrid scaffolds for cardiovascular tissue engineering. *Biomaterials* **2008**, 29, 2907–2914.

Hsiao H-Y, Huang C-M, Liu Y-Y, Kuo Y-C ,Chen H. Effect of air blowing on the morphology and nanofiber properties of blowing-assisted electrospun polycarbonates. *Journal of Applied Polymer Science* **2012**, 124 (6), 4904-4914.

Hsu C-M, Shivkumar S. N,N-Dimethylformamide Additions to the Solution for the Electrospinning of Poly(e-caprolactone) Nanofibers. *Macromolecular Materials and Engineering* **2004,** 289, 334-340.

Hu Y, Winn S.R, Krajbich I, Hollinger J.O. Porous polymer scaffolds surface-modified with arginine-glycine-aspartic acid enhance bone cell attachment and differentiation *in vitro. Journal of Biomedical Materials Research Part A* **2003**, 64A (3), 583-590.

Huang C, Chen S, Lai C, Reneker D.H, Qiu H, Ye Y, Hou H. Electrospun polymer nanofibres with small diameters. *Nanotechnology*, **2006**, 17, 1558–1563.

Huang L, Bui N-N, Manickam S.S, McCutcheon J.R. Controlling Electrospun Nanofiber Morphology and Mechanical Properties Using Humidity. *Journal of Polymer Science Part: Polymer Physics* **2011**, 49, 1734–1744.

Ji L, Lin Z, Medford A.J, Zhang X. Porous carbon nanofibers from electrospun polyacrylonitrile/SiO_2 composites as an energy storage material. *Carbon* **2009**, 47, 3346-3354.

Jia Y.T, Gong J, Gu X.H, Kim H.Y, Dong J, Shen X.Y. Fabrication and characterization of poly (vinyl alcohol)/chitosan blend nanofibers produced by electrospinning method. *Carbohydrate Polymers* **2007**, 67, 403–409.

Johnson K.L, K. Kendall K, Roberts A.D. Surface Energy and the Contact of Elastic Solids. *Proceedings of the Royal Society of London. Series A, Mathematical and PhysicalSciences* **1971**, 324, 301-313.

Kanani A.G, Bahrami S.G. Effect of Changing Solvents on Poly(ε-Caprolactone) Nanofibrous Webs Morphology. *Journal of Nanomaterials* **2011**, 724153.

Kim G.M, Lach R, Michler G.H, Chang Y-W. The Mechanical Deformation Process of Electrospun Polymer Nanocomposite Fibers. *Macromolecular Rapid Communications*, **2005**, 26, 728—733.

Kiselev P, Rosell-Llompart J. Highly Aligned Electrospun Nanofibers by Elimination of the Whipping Motion. *Journal of Applied Polymer Science* **2012**, 125, 2433–2441.

Kong L and Ziegler G.R. Quantitative relationship between electrospinning parameters and starch fiber diameter. *Carbohydrate Polymers* **2013**, 92, 1416– 1422.

Koombhongse S, Liu W, Reneker D.H. Flat Polymer Ribbons and Other Shapes by Electrospinning. *Journal of Polymer Science Part B: Polymer Physics* **2001**, 39, 2598–2606.

Koski A, Yim K, Shivkumar S. Effect of molecular weight on fibrous PVA produced by electrospinning. *Materials Letters* **2004**, 58, 493-497.

Kulichikhin V.G, Malkin A.Y, Semakov A.V, Skvortsov I.Y, Arinstein A. Liquid filament instability due to stretch-induced phase separation in polymer solutions. *The European Physical Journal E* **2014**, 37, 10-16.

Lavielle N, Popa A-M, de Geus M, Hébraud A, Schlatter G, Thöny-Meyer L, Rossi R.M. Controlled formation of poly(ε-caprolactone) ultrathin electrospun nanofibers in a hydrolytic degradation-assisted process. *European Polymer Journal* **2013**, 49, 1331–1336.

Laiva A.L, Venugopal J.R, Sridhar S, Rangarajan B, Navaneethan B, Ramakrishna S. Novel and simple methodology to fabricate porous and buckled fibrous structures for biomedical applications. *Polymer* **2014**, 55, 5837-5842.

Lee K.H, Kim H.Y, Bang H.J, Jung Y.H, Lee S.G. The change of bead morphology formed on electrospun polystyrene fibers. *Polymer* **2003**, 44, 4029–4034.

Li D, Xia Y. Direct fabrication of composite and ceramic hollow nanofibres by electrospinning. *Nano Letters* **2004**, 4, 933–938.

Lin T, Wang H, Wang H, Wang X. The charge effect of cationic surfactants on the elimination of fibre beads in the electrospinning of polystyrene. *Nanotechnology* **2004**, 15, 1375–1381.

Liu Y, He J-H, Yu J-Y, Zeng H-M. Controlling numbers and sizes of beads in electrospun nanofibers. *Polymer International* **2008**, 57, 632–636.

Lubasova D and Martinova L. Controlled Morphology of Porous Polyvinyl Butyral Nanofibers. *Journal of Nanomaterials* **2011**, 292516.

Luo C.J, Nangrejo M, Edirisinghe M. A novel method of selecting solvents for polymer electrospinning. *Polymer* **2010**, 51, 1654–1662.

Luo C.J, Stride E, Edirisinghe M. Mapping the Influence of Solubility and Dielectric Constant on Electrospinning Polycaprolactone Solutions. *Macromolecules* **2012**, 45, 4669−4680.

Mattheus J.A, Boland E.D, Wnek G.E, Simpson D.G, Bowlin G.L. Electrospinning of Collagen Type II: A Feasibility Study. *Journal of Bioactive and Compatible Polymers* **2003**,18, 125.

Megelski S, Stephens J.S, Chase D.B, Rabolt J.F. Micro- and Nanostructured Surface Morphology on Electrospun Polymer Fibers. *Macromolecules* **2002**, 35, 8456-8466.

Min BM, Lee G, Kim SH, Nam YS, Lee TS, Park WH. Electrospinning of silk fibroin nanofibers and its effect on the adhesion and spreading of normal by human keratinocytes and fibroblasts in vitro. *Biomaterials* **2004**, 25, 1289–97.

Mit-uppatham C, Nithitanakul M, Supaphol P. Ultrafine electrospun polyamide-6 fibers: effect of solution conditions on morphology and average fiber diameter. *Macromolecular Chemistry and Physics* **2004**, 205, 2327–2338.

Moghe A.K, R. Hufenus R, Hudson S.M, Gupta B.S. Effect of the addition of a fugitive salt on electrospinnability of poly(ε-caprolactone). *Polymer* **2009**, 50, 3311–

3318.

Morehouse J.A, Worrel L.S, Taylor D. Lloyd D.R, Freeman B.D, Lawler D.F. The effect of uni-axial orientation on macroporous membrane structure. *Journal of Porous Materials* **2006**, 13, 61–72.

Moroni L, Licht R, Boer J, Wijn J.R, Blitterswijk C.A. Fiber diameter and texture of electrospun PEOT/PBT scaffolds influence human mesenchymal stem cell proliferation and morphology, and the release of incorporated compounds. Biomaterials, **2006**, 27, 4911-4922.

Muller VM, Derjaguin BV, Toporov YP. On two methods of calculation of the force of sticking of an elastic sphere to a rigid plane. *Colloids and Surfaces* **1983**, 7, 251-259.

Munaweera I, Aliev A, Balkus K.J. Electrospun Cellulose Acetate-Garnet Nanocomposite Magnetic Fibers for Bioseparations. *ACS Applied Materials & Interfaces* **2014**, 6, 244–251.

Nayani K, Katepalli H, Sharma C.S, A. Sharma A, Patil S, Venkataraghavan R. Electrospinning combined with nonsolvent-induced phase separation to fabricate highly porous and hollow submicrometer polymer fibers. *Industrial & Engineering Chemistry Research* **2012**, 51, 1761–1766.

Nezarati R.M, Eifert M.B, and Cosgriff-Hernandez E. Effects of Humidity and Solution Viscosity on Electrospun Fiber Morphology. *Tissue Engineering : Part C* **2013**, 19, 1-10.

Ojha S.S, Afshari M, Kotek R, Gorga R.E. Morphology of Electrospun Nylon-6 Nanofibers as a Function of Molecular Weight and Processing Parameters. *Journal of Applied Polymer Science* **2008**, 108, 308-319.

Pai C-L, Boyce M.C, Rutledge G.C. Morphology of Porous and Wrinkled Fibers of Polystyrene Electrospun from Dimethylformamide. *Macromolecules* **2009**, 42, 2102-2114.

Pant H.R, Neupane M.P, Pant B, Panthi G, Oh H-J, Lee M.H, Kim H.Y. Fabrication of highly porous poly (ε-caprolactone) fibers for novel tissue scaffold via water-bath electrospinning. *Colloids and Surfaces B: Biointerfaces* **2011**, 88, 587– 592.

Park J., Lee I.H, Bea G.W. Optimization of the electrospinning conditions for preparation of nanofibers from polyvinylacetate (PVAc) in ethanol solvent. *Journal of Industrial and Engineering Chemistry* **2008**, 14, 707–713.

Piskin E, Isoglu I.A, Bolgen N, Vargel I, Griffiths S, Cavusoglu T, Korkusuz P, Guzel E, Cartmell S. *In vivo* performance of simvastatin-loaded electrospun spiral-wound polycaprolactone scaffolds in reconstruction of cranial bone defects in the rat model. *Journal of Biomedical Materials Research Part A* **2009**, 90(4), 1137–1151 in Cipitria A, Scelton A, Dargaville T. R, Dalton P. D, Hutmacher D. W. Design, fabrication and

characterization of PCL electrospun scaffolds—a review. *Journal of Materials Chemistry* **2011**, 21, 9419–9453.

Powell HM, Boyce ST. Engineered human skin fabricated using electrospun collagen–PCL blends: morphogenesis and mechanical properties. *Tissue Engineering Part A* **2009**, 15, 2177–2187.

Qi Z, Yu H, Chen Y , Zhu M. Highly porous fibers prepared by electrospinning a ternary system of nonsolvent/solvent/poly(L-lactic acid). *Materials Letters* **2009**, 63, 415-418.

Qin X-H, Yang E-L, Li N, Wang S-Y. Effect of Different Salts on Electrospinning of Polyacrylonitrile (PAN) Polymer Solution. *Journal of Applied Polymer Science* **2007**, 103, 3865–3870.

Reneker D.H and Yarin A.L. Electrospinning jets and polymer nanofibers. Polymer 2008, 49, 2387-2425.

Sampson W.W. A model for fibre contact in planar random fibre networks. *Journal of Materials Science* **2004**, 39, 2775-2781.

Schnell E, Klinkhammer K, Balzer S, Brook G, Klee D, Dalton P, Mey J. Guidance of glial cell migration and axonal growth on electrospun nanofibers of poly-e-caprolactone and a collagen/poly-e-caprolactone blend. *Biomaterials* **2007**, 28, 3012–3025.

Sencadas V, Correia D.M, Areias A, Botelho G, Fonseca A.M, Neves I.C, Gomez Ribelles J.L, Lanceros Mendez S. Determination of the parameters affecting electrospun chitosan fiber size distribution and morphology. *Carbohydrate Polymers* **2012**, 87, 1295-1301.

Seo J.M, Arumugam G.K, Khan A.S, Heiden P.A. Comparison of the Effects of an Ionic Liquid and Triethylbenzylammonium Chloride on the Properties of Electrospun Fibers,1–Poly(lactic acid). *Macromolecular Materials and Engineering* **2009**, 294, 35-44.

Seo Y-A, Pant H.R, Nirmala R, Lee J-H, Song K.G, Kim H.Y. Fabrication of highly porous poly (ε-caprolactone) microfibers via electrospinning. *Journal of Porous Materials* **2012**, 19, 217–223.

Shalumon K.T, Anulekha K.H, Girish C.M, Prasanth R, Nair S.V, Jayakumar R. Single step electrospinning of chitosan/poly(caprolactone) nanofibers using formic acid/acetone solvent mixture. *Carbohydrate Polymers* **2010**, 80, 413–419.

Shi X, Zhao Y-P. Comparison of various adhesion contact theories and the influence of dimensionless load parameter. *Journal of Adhesion Science* and *Technology* **2004**, 18, 55–68.

Shin Y.M, Hohman M.M, Brenner M.P, Rutledge G.C. Electrospinning: A whipping fluid jet generates submicron polymer fibers. Applied Physics Letters **2001**, 78, 1149-1151.

Sukigara S, Gandhi M, Ayutsede J, Micklus M, Ko F. Regeneration of *Bombyx mori* silk by electrospinning. Part 2. Process optimization and empirical modeling using response surface methodology. *Polymer* **2004**, 45, 3701–3708.

Taylor G. Electrically driven jets. Proceedings of the Royal Society **1969**, 313, 453-475.

Touny A.H and Bhaduri S.B. A reactive electrospinning approach for nanoporous PLA/monetite nanocomposite fibers. *Materials Science and Engineering C* **2010**, 30, 1304-1312.

Wannatong L, Sirivat A, Supaphol P. Effects of solvents on electrospun polymeric fibers: preliminary study on polystyrene. *Polymer International* **2004**, 53, 1851–1859.

Wei Z, Zhang Q, Wang L Wang X, Long S Yang J. Porous electrospun ultrafine fibers via a liquid–liquid phase separation method. *Colloid and Polymer Science* **2013**, 291, 1293–1296.

Wen X. T, Fan H. S, Tan Y. F, Cao H. D, Li H, Cai B, Zhang X. D. Preparation of Electrospun PLA Nanofiber Scaffold and the Evaluation in Vitro. *Key Engineering Materials* **2005**, 288-289, 139-142.

Williams J.M, Adewunmi A, Schek R.M, Flanagan C.L, Krebsbach P.H, Feinberg S.E, Hollister S.J, Das S. Bone tissue engineering using polycaprolactone scaffolds fabricated via selective laser sintering. *Biomaterials* **2005**, 26, 4817–4827.

Woodruff M.A, Hutmacher D.W. The return of a forgotten polymer-Polycaprolactone in the 21st century. *Progress in Polymer Science* **2010**, 35, 1217–1256.

Yamaguchi M, Shinbo T, Kanamori T, Wang P, Niwa M, Kawakami H, Nagaoka S, Hirakawa K, Kamiya M. Surface modification of poly(L-lactic acid) affects initial cell attachment, cell morphology, and cell growth. *Journal of Artificial Organs* **2004**, 7, 187–193.

Yao L, Haas T.W, A. Guiseppi-Elie A, G. L. Bowlin G.L, D. G. Simpson D.G, and G. E. Wnek G.E. Electrospinning and stabilization of fully hydrolyzed poly(vinyl alcohol)

fibers. *Chemistry of Materials* **2003**, 15, 1860–1864.

Yogeshwar Chakrapani V, Gnanamani A, Giridev V. R, Madhusoothanan M, Sekaran G. Electrospinning of Type I Collagen and PCL Nanofibers Using Acetic Acid. *Journal of Applied Polymer Science* **2012**, 125, 3221–3227.

Yordem O.S, Papila M, Menceloglu Y.Z. Effects of electrospinning parameters on polyacrylonitrile nanofiber diameter: An investigation by response surface methodology. *Materials and Design* **2008**, 29, 34–44.

Yoshimoto H, Shin Y.M, Terai H, Vacanti J.P. A biodegradable nanofiber scaffold by electrospinning and its potential for bone tissue engineering. Biomaterials **2003**, 24, 2077-2082.

You Y, Lee S.W, Youk J.H, Min B.M, Lee S.J, Park W.H. In vitro degradation behaviour of non-porous ultra-fine poly(glycolic acid)/poly(L-lactic acid) fibres and porous ultra-fine poly(glycolic acid) fibres. *Polymer Degradation and Stability* **2005**, 90, 441-448.

Yu X, Xiang H, Long Y, Zhao N, Zhang X, Xu J. Preparation of porous polyacrylonitrile fibers by electrospinning a ternary system of PAN/DMF/H_2O. *Materials Letters* **2010**, 64, 2407–2409.

Zargham S, Bazgir S, Tavakoli A, Rashidi A.S, Damerchely R. The Effect of Flow Rate on Morphology and Deposition Area of Electrospun Nylon 6 Nanofiber. *Journal of Engineered Fibers and Fabrics* **2012**, 7, 42-49.

Zeng J, Xu X.Y, Chen X.S, Liang Q.Z, Bian X.C, Yang L.X, Jing X.B. Biodegradable electrospun fibers for drug delivery. *Journal of Controlled Release* **2003**, 92, 227–231.

Zhang C, Yuan X, Wu L, Han Y, Sheng J. Study on morphology of electrospun poly(vinyl alcohol) mats. *European Polymer Journal* **2005**, 41, 423–432.

Zheng J-Y, Zhuang M-F, Yu Z-J, Zheng G-F, Zhao Y, Wang H, Sun D-H. The Effect of Surfactants on the Diameter and Morphology of Electrospun Ultrafine Nanofiber. *Journal of Nanomaterials* **2014**, doi:10.1155/2014/689298.

Zuo W, Zhu M, Yang W, Yu H, Chen Y, Zhang Y. Experimental study on relationship between jet instability and formation of beaded fibers during electrospinning. *Polymer Engineering & Science* **2005**, 45, 704-709.

Books

Bhushan B. Modern Tribology Handbook Volume One, **2001**.

Box G.E.P, Draper N.R. Response Surfaces, Mixtures, and Ridge Analyses, **2007**.